FORSCHUNGSZENTRUM ROSSENDORF FZR

FZR-166

Archiv-Ex.:

Institute of Ion Beam Physics and Materials Research

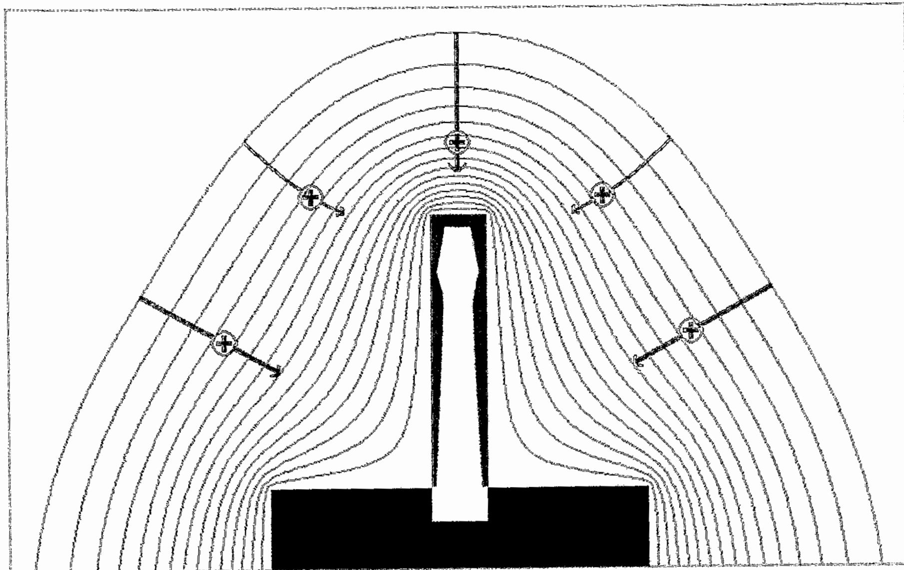

Annual Report 1996

Postfach 510119
D-01314 Dresden, Germany
Tel. +49-351-260-22 45
Fax +49-351-260-32 85

FORSCHUNGSZENTRUM ROSSENDORF
INSTITUT FÜR IONENSTRAHLPHYSIK UND MATERIALFORSCHUNG

Annual Report 1996

Editors:
J. von Borany, H.-U. Jäger, W. Möller, E. Wieser

FZR-166
März 1997

For further information on the research projects described in the present annual report, please address the director or one of the authors at the institute.

Front cover:
Lateral dose uniformity is a crucial question for three-dimensional applications of plasma immersion ion implantation. The figure shows the ion-emitting plasma boundary and equipotential surfaces around a cylindrical object (representing, e.g., a drill) on a substrate holder, as derived from a simplified model (see p. 43). From subsequent calculations of the ion trajectories, the locally implanted ion dose can be calculated, which is indicated by the read contour along the surface. Apparently, the dose uniformity is satisfactory for tribological purposes.

Director: Prof. Dr. Wolfhard Möller

P. O. B. 51 01 19
D-01314 Dresden
Germany

Tel.: +49 351 260 2245
Fax: +49 351 260 3285
E-mail: moellerw@fz-rossendorf.de

Preface

The Research Center Rossendorf (Forschungszentrum Fossendorf, FZR) represents the largest governmental research institution in the "new" states of the Federal Republic of Germany. Its presently about 600 employees, organized in five institutes, study problems of basic and applied science in the fields of biomedicine, environmental research and materials science. The FZR is a member of the so-called "Blue List" organization (recently renamed as "Gottfried Wilhelm Leibniz Society"), with the federal government and the state of Saxony each providing 50 % of the basic funding.

The Institute of Ion Beam Physics and Materials Research (IIM) has 78 permanent positions of scientists (28), technicians and engineers (48) and administration personnel (2). In average about 40 additional employees are funded from PhD student and PostDoc programs, guest funds, and governmental and industrial projects. The central task of the institute is to combine basic research and application-oriented studies in the fields of ion surface modification and ion surface analysis. According to the German Science Council, the institute shall represent a national ion beam center, which, in addition to its own scientific knowledge, offers services and transfers know-how with ion beam techniques to universities, other research institutes, and industry.

For these aims, a broad range of ion-related equipment is available, delivering ion energies from about 10 eV (plasma treatment) to several 10 MeV (electrostatic accelerators). For the diagnostics of ion-treated surfaces, standard analytical techniques are available such as transmission electron microscopy, X-ray diffraction, Auger and photoelectron spectroscopy, and a number of chemical, optical, electrical, and mechanical diagnostics. Sample preparation is available for a large number of different materials including standard silicon processing.

In the beginning of 1996, the main research areas and the organization of the institute have been redefined. As project activities related to non ion-based sensor systems were transferred to a small company in the Rossendorf Technology Center in 1995, sensors development was no longer maintained as a main research task. Instead, nanoclusters formed by ion implantation with their different applications in optoelectronics, microelectronics and mechanics constitute a major new task. The main R&D activities of the institute may now be subdivided into the fields of New Materials (Hard Coatings, Phases and Defects, Nanoclusters) and New Processes (Focused Ion Beam, Plasma Immersion Implantation, MeV Ion Beam Analysis) as shown in the figure.

Another main aim of reorganization was to intensify the relations to industry. For this purpose, one of the leading scientists is now responsible for steering the industrial contacts of the individual departments, representing the institute on fairs, preparing material for advertising the capabilities of the institute, and knitting new relations with possible industrial partners. We are aware of the fact that technology transfer is a slow process in particular in periods when money is short. Nevertheless, we expect that at least a small percentage of our present contacts to more than 70 different small, medium sized and large companies will result in extended tasks of ion beam service or common R&D projects, and add to our present successful, but still few activities in this area.

The development of the research activities of the institute in 1996 is documented by an increasing number of scientific publications, in particular in renowned international journals, many continued and new collaborations through visits of IIM members at external institutions

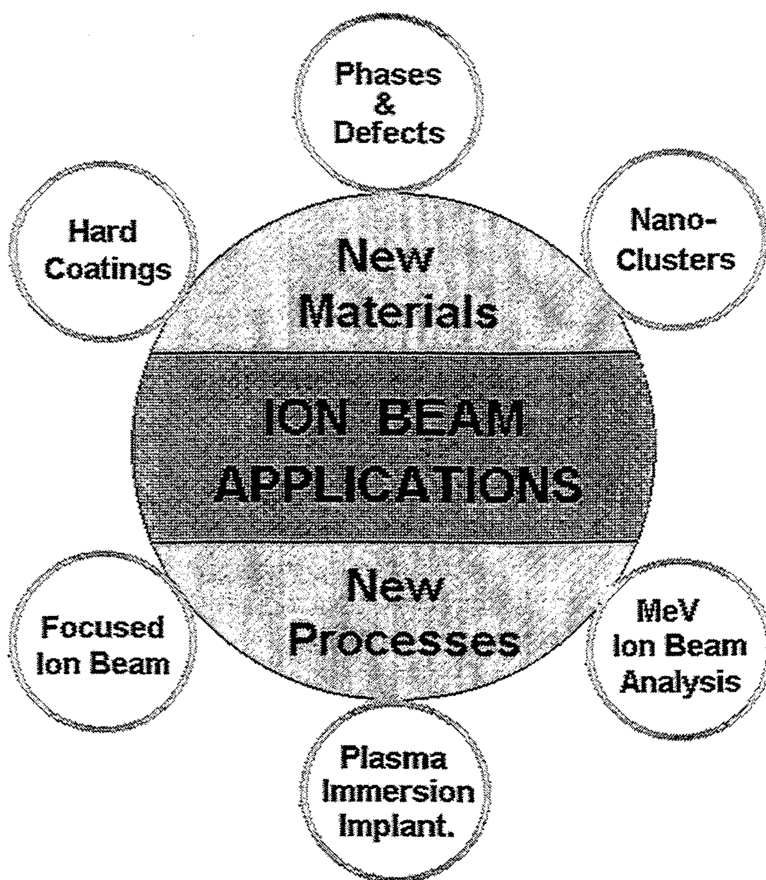

and national and international guests in Rossendorf, and numerous invitations of IIM members to conferences and lectures. Four PhD students received their degree with considerable success both of the theses and in the examinations.

The role of the institute in the international scientific community was also documented by a chairmanship at the world's largest conference in materials science, the fall meeting of the U.S. Materials Research Society. Several meetings were organized at the institute. An unexpectedly large number of around 100 participants from 20 different countries met in Rossendorf for the Third International Workshop on Plasma Based Ion Implantation.

A number of new projects have been acquired, funded by the federal and local governments, the Deutsche Forschungsgemeinschaft, and directly from industry. In contrast, the results of actions with the European Union remained largely disappointing.

The installation of additional major experimental equipment has gradually reached an intermediate state of saturation. Nevertheless, some new equipment has been commissioned in 1996. A new and unique experiment was commissioned combining low-pressure plasma processing with ellipsometry and high-energy ion beam analysis, thus constituting a new and powerful in-situ facility. Further, the design and construction of the Rossendorf Beam Line at the ESRF (ROBL), which is now being installed, continued to be a major task of the institute, which is responsible for the setup of the beam optics and a thin film diffractometer.

Many improvements and replacements were and are still necessary with older equipment, in particular with the 5 MV tandem accelerator. Similarly, the renovation of building and supply facilities required the active participation of staff of the institute, and sometimes considerable patience of the scientists. We appreciate that the construction of the new accelerator building, which will allow further combinations for in-situ diagnostics, has commenced in autumn 1996, with fast progress being clearly visible!

The present report will first describe the most important scientific results achieved in 1996, in the form of letter contributions. Subsequently, a complete list of results of the individual research tasks will be given, followed by a statistical section.

The institute would like to thank all friends and organisations who supported its progress in 1996. Special thanks are due to the directors of the Research Center Rossendorf, the minister of science and arts of the Free State of Saxony, the minister of research and technology of the Federal Government of Germany, and our partners from industry. Last but not least, the director would like to thank all members and guests of the institute for their active and partly excellent contributions to a successful development in 1996.

Prof. Wolfhard Möller

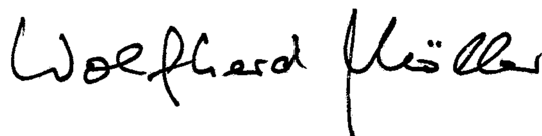

Contents

Page

Highlights

Computer Simulation Studies on Structure and Growth of c-BN 9

Investigations on Structure and Growth Mechanisms of Boron Nitride Thin Films 13

Formation, Microstructure and Gettering Ability of Helium Induced Cavities in Silicon 16

Ion Beam Synthesis by Tungsten Implantation into 6H-Silicon Carbide 19

Implantation and Columnar Growth of Large ß-$FeSi_2$ Precipitates and α-$FeSi_2$ Network Structures in Silicon 23

Ion Beam Synthesis of Nanoclusters and Buried Layers Studied by Kinetic 3D Lattice Monte Carlo Simulations 28

Evolution of Nanocluster Bands in Ge-Implanted Silicon Dioxide Films 33

Acoustic Waves Induced by a Focused Ion Beam 38

Dose Distribution for Plasma Immersion Ion Implantation into 3D-Objects 42

In-situ ERDA Studies of Nitrogen Implantation into Amorphous Carbon 46

Short Contributions

Abbreviations 51

Hard Coatings 52

Phases and Defects 53

Nanoclusters 62

Focused Ion Beam 65

Plasma Immersion Ion Implantation 66

Ion Beam Analysis 68

Equipment 70

Other Activities 71

Statistics

Publications	73
Conference Contributions	81
Lectures	92
Reports	95
Laboratory Visits	97
Guests	99
Awards	102
PhD Theses	103
Diploma Thesis	103
Meetings Organized by the Institute	103
Patents	103
Departments of the Institute	105
Experimental Equipment	106
List of Personnel	107

Highlights

Computer Simulation Studies on Structure and Growth of *c*-BN

K. Albe

In materials science there is a considerable interest in the high density zinc blende modification of boron nitride (*c*-BN), which has many useful physical properties, such as extreme hardness, chemical inertness with respect to iron, high melting temperature, wide band-gap and low dielectric constant. For this reason in the last years there has been a renewed interest in this compound system as thin films of *c*-BN became more and more available. At present a wide range of synthesis methods is being used successfully, but the cubic phase of boron nitride is still hard to grow and the processes which are relevant for growth and stability of *c*-BN are scarcely understood. Here computer simulation on atomic scale can be a helpful tool for identifying high and low energy processes occuring during deposition.

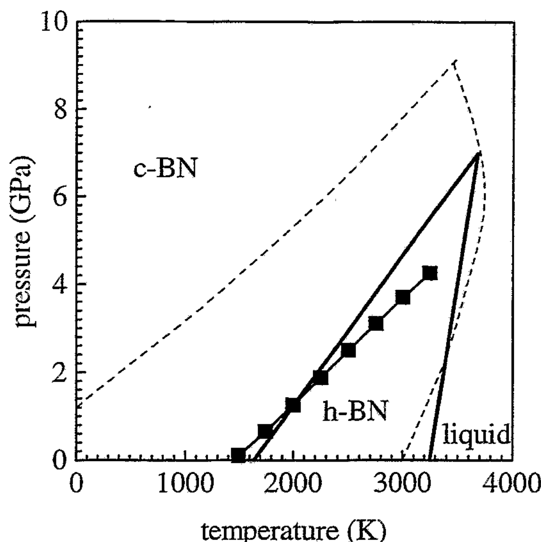

Fig. 1: Phase diagram of boron nitride: Dashed line represents the proposal of Corrigan & Bundy [3]. The thick solid line is Solozhenko's diagram [4]. The solid squares represent the theoretical result of this work [1].

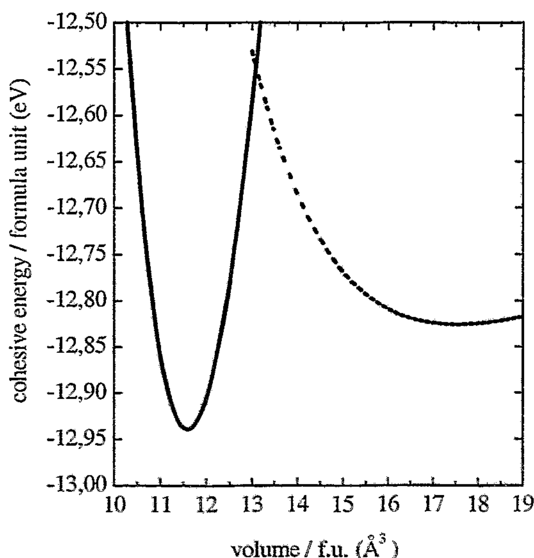

Fig. 2: *Ab initio*-calculation of cohesive energies of hexagonal (dashed line) and cubic boron nitride (solid line) as function of volume. Cell parameters were optimised systematically [1].

This contribution reports computer simulation studies of boron nitride using *ab initio* and empirical methods. First, results of density-functional calculations are shown, which were performed in order to characterise structural ground-state properties [1]. Second, a classical empirical potential is presented, which was parametrized by *ab inito* data and allows molecular dynamics simulations of B_nN_m clusters and solids [2].

Boron nitride exhibits four different crystal structures similar to carbon: The graphite-like hexagonal (*h*-BN) and rhombohedral (*r*-BN) structures with AaAa... and ABCABC... stacking sequence, respectively, and the dense zinc blende (*c*-BN) and wurtzite structure (*w*-BN), which are the analogues to cubic and hexagonal diamond. While *w*-BN and *r*-BN are

metastable modifications, it is controversial discussed in literature (see Fig. 1) if the cubic or hexagonal phase, which occur both in BN thin films, is thermodynamically stable at standard conditions. Therefore, most accurate total energy calculations were done using density-functional theory within the local density approximation (LDA). A plane-wave expansion for the pseudo-potentials and wave functions as well as the Ceperley-Alder exchange-correlation functional were used and norm-conserving pseudo-potentials were generated following the Troullier and Martins generation scheme [1,5,6]. The energy cut-off for the electronic wave functions (1630 eV) and the number of k-points were chosen to reach full convergence.

	E_{coh}/f.u. (eV)	a (Å)	c/a	B (GPa)	B'
c-BN	-12.94	3.593		395	3.65
w-BN	-12.92	2.532	0.826	394	3.68
h-BN	-12.83	2.496	1.300	30.1	10.1
r-BN	-12.83	2.493	1.296	32.3	10.3

Tab. 1: Calculated properties of BN: Cohesive energy E_{coh}, lattice constant a, ratio of interlayer distance to lattice constant a/c, bulk modulus B, pressure derivative of bulk modulus B'.

For all structures the bulk moduli, their pressure derivatives, minimum energies and volumes were obtained by fitting energy-volume data to the Birch-equation of state [1]. For the anisotropic sp^2-bonded structures energies were calculated over a mesh of a-c lattice constants. Thereafter for each volume the corresponding minimum energy was found by a twofold fitting procedure [1]. In Fig. 2 the energy-volume data are shown, corresponding numerical results are presented in Tab. 1. The zinc blende structure has the lowest static lattice energy. The calculated bulk modulus is 395 GPa at T=0 K. The cohesive energy per formula unit was determined as 12.94 eV/f.u. and agrees with estimations from experimental data [1].

The energy minimum for h-BN is determined to 0.1 eV/f.u. above the minimum of c-BN. The calculated bulk modulus of the layered structures is more than 10 times smaller than the bulk modulus of c-BN. The c-axis length which is determined by weak van der Waals interaction varies strongly under hydrostatic pressure, whereas the a-axis length, which is determined by the extremely short and strong ionic-covalent sp^2-bondings, changes only a little (see Fig. 3). Up to 12 GPa the relative compression of the a-axis is insignificant, while the c-axis is compressed to about 85% of its uncompressed length. The calculated energies for h-BN and r-BN are nearly equal. This is due to the fact, that the LDA is inadequate to distinguish between different stacking of sp^2-bonded planes. The shape of the energy-volume curves in Fig. 2 shows, that a Gibbs-construction, which allows the determination of the

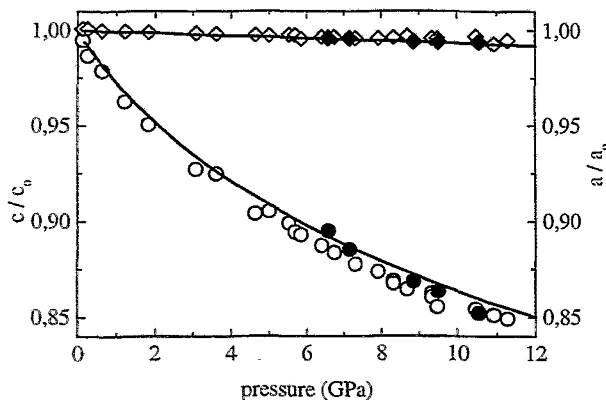

Fig. 3: Relative compression of h-BN cell parameters as function of hydrostatic pressure. Dots (c-axis) and diamonds (a-axis) are measurements by Solozhenko *et al.* [7], the solid line is the theoretical result.

transition pressure at T=0 K, is impossible. Even if contributions from zero point vibrations are taken into account, the energy differences change only by a few hundredths eV [1]. Hence a p-T equilibrium line, which cuts the pressure axis, is impossible.

In a further step the well known Debye-Grüneisen model was used in order to calculate vibrational and entropical energy contributions to the free energy of c-BN and h-BN, respectively, and to estimate the full thermodynamic potential of the coexisting phases in terms of a first-order phase transition [1]. The result is shown in Fig. 1. c-BN is predicted as the stable phase at standard conditions. The equilibrium line corresponds strongly to one of the experimental proposals and has nearly the same shape. The intersection point with the temperature axis is somewhat lower at 1400-1500 K, which depends on the choice of anharmonic contributions for h-BN.

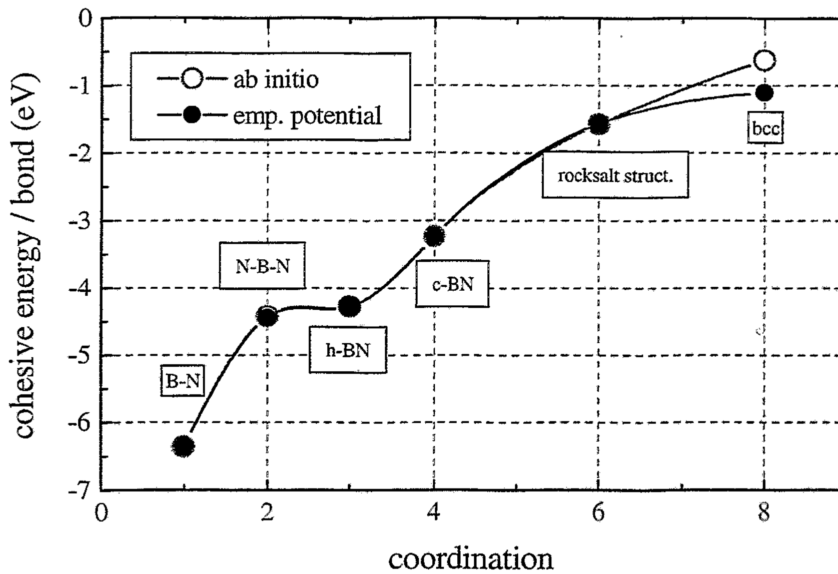

Fig. 4: Cohesive energy per bond versus local coordination: Comparison of results obtained by the empirical potential and by *ab initio* calculations [2] (The lines are drawn to guide the eye).

Nowadays, there are numerous *ab initio* methods which allow MD-simulations of small systems on time scales up to a few picosecond [6]. On the other hand computer simulations of processes which lie within the scope of this work, i.e. thin film growth, require time scales in the range of hundreds of picoseconds and system sizes of many thousand atoms. Here the fast calculation of force fields is the crucial point. Classical interatomic potentials have tremendous practical advantages, because the energy and consequently the force fields are calculated simply as function of atomic coordinates. Therefore an empirical potential was developed following the bond order approach of Abell, which was introduced by Tersoff for SiC [8] and used in a similar fashion for GaAs by Smith [9]:

$$\Phi = \frac{1}{2}\sum_{i \neq j} f_{cut}(r_{ij})[f_{repulsive}(r_{ij}) - b_{ij}(z) f_{attractive}(r_{ij})].$$

Here the lattice energy is a sum over attractive and repulsive Morse-like pair functions of the

distances r_{ij}, where the first is weighted by a factor depending in principle on the local atomic arrangement and coordination z. All parameters were fitted by the nonlinear Levenberg-Marquardt method to structural data of B_n, N_m, B_nN_m, so that different molecules and solid polymorphs can be described with reliable accuracy [2] by one set of parameters. Fig. 4 shows the cohesive energy per bond of different BN modification calculated by the empirical function in comparison to *ab initio* results.

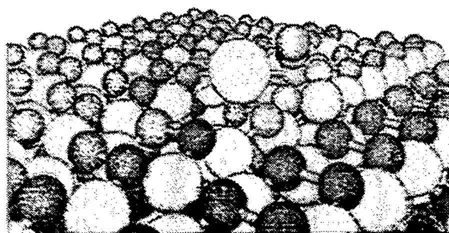

Fig. 5: 400 eV argon impact at low angle on a boron terminated and 2x1-reconstructed *c*-BN surface. Several boron atoms are sputtered.

Future potential applications of this empirical potential for MD-simulations are shown in the following. In Fig. 5 the simulation of 400 eV argon impact on a boron terminated, and dimer-reconstructed *c*-BN (100)-surface is depicted. Due to the flat impact angle several boron atoms are sputtered directly.

In TEM-micrographs it is generally observed, that cubic boron nitride occurs only on top of a sp^2-bonded intralayer. Next to the substrate the *c*-axes of this graphitelike modification are randomly oriented, while they are aligned parallel to the substrate plane near the cubic top layer [10]. Therefore the impact of a N_2 molecule on an ideal non-reconstructed (1000) *h*-BN surface has been simulated. The impact is in normal direction with a projectile energy of 400 eV and a molecule axis perpendicular to the surface. The molecule is destroyed in the surface region of the target and the atoms can channel through the target. If the kinetic energy is low enough they are trapped between the layers and build defect configurations stable over several picoseconds. This involves a local densification and could be the origin for the *h*-BN to *c*-BN transition (see Fig. 6).

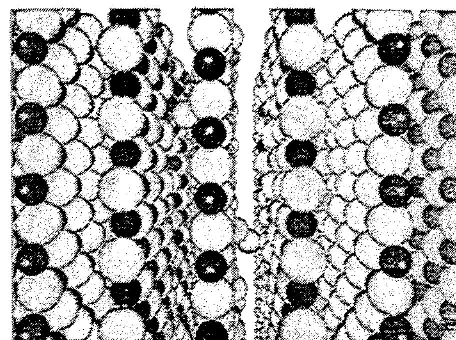

Fig. 6: Impact of a 400 eV N_2-molecule on a *h*-BN layer after 100 fs.

Acknowledgements

This work was supported by a project of SMWK.

References

[1] K. Albe, Phys. Rev. B (in print)

[2] K. Albe, W. Möller, K.-H. Heinig, Rad. Eff. Def. Sol. (in print)

[3] F.R. Corrigan, F.P. Bundy, J. Chem. Phys. 63 (1975) 3812

[4] V.L. Solozhenko, Diamond Rel. Mat. 4 (1994) 1

[5] Computational results were obtained using the codes `Plane_Wave` and `Dsolid` of Molecular Simulations, San Diego

[6] M. Payne *et al.,* Rev. Mod. Phys. 64 (1992) 1045

[7] V.L. Solozhenko *et al.,* Solid State Comm. 91 (1995) 1

[8] J. Tersoff, Phys. Rev. B 39 (1989) 5566

[9] R. Smith, Nucl. Instr. Meth. B 67 (1992) 335

[10] D.J. Kester, K.S. Ailey, D.J. Lichtenwalner, R.F. Davis, J. Vac. Sci. Technology A12 (1994) 3074

Investigations on Structure and Growth Mechanisms of Boron Nitride Thin Films

W. Fukarek, O. Kruse, M.F. Plass, A. Kolitsch and A. Mücklich

Cubic boron nitride (cBN) has remarkable properties, like high hardness, good thermal conductivity, chemical inertness, and a large band gap. Thin cBN containing films are mostly reported to exhibit a layered structure. A few nanometers thick amorphous layer is found in cross sectional high-resolution transmission electron microscopy (HREM) micrographs as a first layer on crystalline silicon substrate material. This layer has been assigned as an amorphous boron nitride (aBN) layer [1,2]. On top of this layer a highly textured hexagonal (hBN) or turbostratic (tBN) layer is found with the c-axis oriented parallel to the substrate surface. On this layer nanocrystalline cBN starts growing that contains only a small volume fraction of sp^2-bonded grain boundary material [3]. The transition from hexagonal to cubic growth has been described as a quasi-thermodynamic phase transition attributed to compressive stress [4], or as a nucleation and growth process, in which cBN nucleates on the prism edges of hBN [5,6].

In recent publications we have shown, that the double-layered structure (cBN on top of hBN) can also be detected with Rutherford backscattering spectrometry (RBS) [7] and polarized infrared reflection spectroscopy (PIRR) [8]. In RBS spectra the cBN layer can be identified by its Ar incorporation which is significantly lower than in the hBN material [7]. PIRR in combination with optical multilayer analysis taking into account the anisotropy and orientation of hBN allows of a quantitative layer analysis. The thicknesses of hBN and cBN layers, oscillator strengths and peak positions, the volume fraction of sp^2 bonded BN within the cBN material, and also preferential orientation of the c-axis of hBN within the film plane can be determined [8]. In this communication we report on experimental results that indicate the necessity to re-examine established models for the growth mechanisms of boron nitride films.

Cubic boron nitride films have been prepared with ion beam assisted deposition (IBAD) using an electron beam evaporator and a Kaufman ion source. The films were analyzed with *in situ* elastic recoil detection (ERD) and *in situ* ellipsometry simultaneously during a SF_6/O_2 plasma etching process. In the ERD experiment a 35 MeV Cl^{7+} ion beam and an angular resolved ionization chamber (ΔE, E_{REST}) are employed allowing of a repetition rate of up to 6 spectra per minute. A 30 minute ion beam irradiation of a BN film using measurement conditions did not cause detectable alterations of the ERD signals. The technique can be considered to be non-destructive under these conditions. The detection limit for boron and nitrogen is about $2*10^{16}$ at/cm^2 corresponding to a BN film thickness of about 10 monolayers. Dynamic ERD provides time dependent area densities of light elements like boron and nitrogen simultaneously and allows of atomic etch rates (at/cm^{2}s) to be calculated. *In situ* ellipsometry measures the change in the state of polarization caused by reflection at the sample surface in dependence on the process time. From these data refractive indices and etch rates can be calculated based on optical multilayer models. The analysis of ellipsometric data is difficult for very thin films of some nanometers only in case the optical properties are not exactly known. However, the endpoint of the etch process when the crystalline silicon substrate is reached can be determined accurately. Amorphous or heavily damaged silicon layers can be measured with ellipsometry due to different dielectric functions in comparison with crystalline silicon. However, a thin amorphous silicon layer is not detectable with ERD and it appears as an amorphous structure similar to glue or other amorphous matter in HREM micrographs.

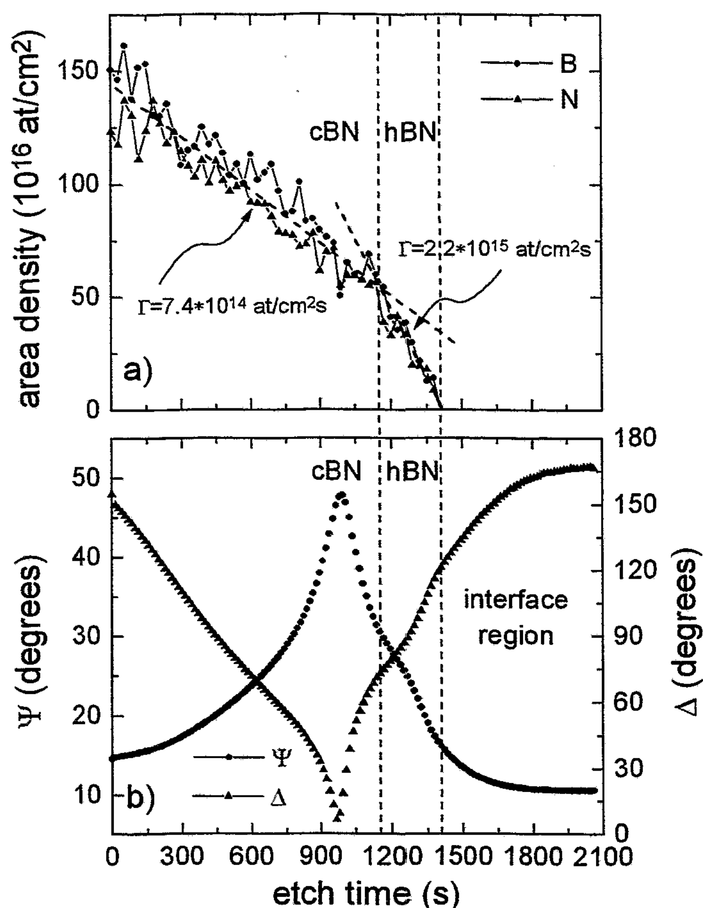

Fig. 1: Time dependent area density of B and N from ERD data (a) and dynamic ellipsometric angles (b) measured simultaneously during plasma etching of a cBN film.

In Fig. 1a the time dependent area density of B and N during plasma etching of a BN film is shown. The typical layered structure of this film was confirmed with PIRR analysis. During the first 1150 s of the etch process an etch rate of $7.4*10^{14}$ at/cm^{2}s is found. From 1150 s to 1410 s the atomic etch rate is increased by a factor of about three. In comparison with PIRR and XTEM micrographs it is concluded that these two regions correspond to the cBN on hBN structure. The higher etch rate of hBN compared to that of cBN in the SF_6/O_2 plasma used indicates the possibility to find a CVD growth regime for cBN in halogen plasmas similar to that for diamond in hydrogen plasmas. In Fig. 1b the ellipsometric data measured simultaneously during the etch process are shown. A change in the curvature and data spacing in the range from 1150 s to 1410 s can be seen in accordance with the ERD data. However, a significant change in the ellipsometric data (about 40° in delta) becomes apparent during the proceeded etch process after reaching the detection limit in the ERD signal. This further change in the ellipsometric angles would correspond to an amorphous BN film of about 20nm thickness and would be clearly detected with ERD. From the vanishing boron and nitrogen ERD signals we conclude that the amorphous interlayer visible in HREM micrographs does not consist of aBN. This amorphous layer is probably a mixture of amorphous silicon, nitrogen, oxygen, and boron that is formed by implantation of ions from the ion source in the beginning of the deposition process and perhaps by diffusion or migration of defects. The composition of this amorphous layer still has to be investigated with other techniques. Single wavelength *in situ* ellipsometry is not capable of an unambiguous characterization of this layer.

It has been shown recently [9] that textured hBN films with the c-axis oriented parallel to the substrate surface can also be grown at very low ion energies of only a few tens of eV by radio frequency plasma-assisted chemical vapor deposition. These films have been grown without the need of high compressive stress and show the textured microstructure throughout the film of 150 nm thickness. No amorphous interlayer to the Si substrate was found in TEM micrographs of these films, although the native Si oxide layer was not removed before deposition. This could be explained by the cleaning effect of the hydrogen rich plasma and is also in agreement

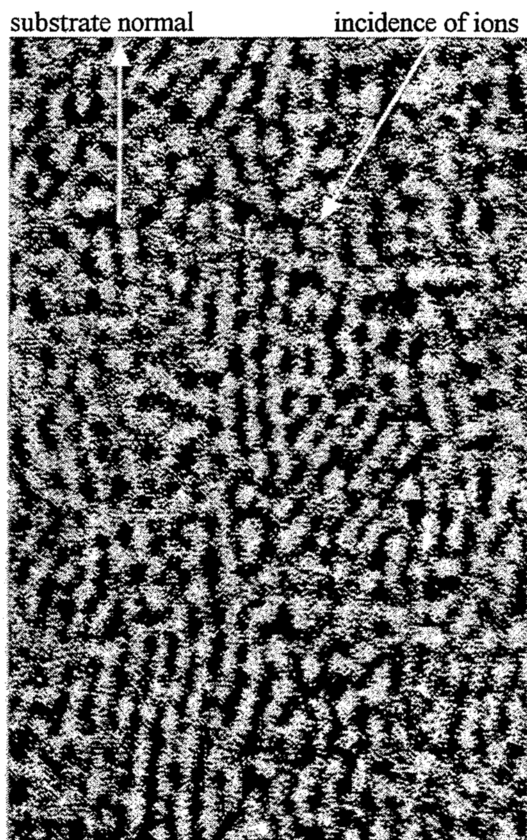

Fig. 2: HREM micrograph of a hBN film grown with ions incident at 30° relative to the substrate normal.

with the assumption of ion induced formation of the amorphous interlayer. These results are indicative of another mechanism being active in this structure formation process apart from compressive stress.

We have grown BN films with the ions incident at 30° relative to the substrate normal and at low ion/atom arrival ratios to form hexagonal material. Samples were cut in the ion plane of incidence for XTEM sample preparation. Fig. 2 shows hBN basal planes oriented around normal to the substrate surface as well as about 30° off normal. This result is indicative of an ion beam induced orientation of the basal planes besides stress induced orientation. This experimental finding has to be carefully verified with other techniques as it is in contradiction to reports claiming that there is no influence of the angle of incidence of the ion beam on the orientation of hBN basal planes.

In conclusion, we assume that ion bombardment and resulting compressive stress do not cause the formation of textured hBN layers with the c-axis oriented parallel to the substrate surface, but are essential in altering this structure and thereby originating the transition to cBN growth.

References

[1] D.J. Kester, K.S. Ailey, R.F. Davis, K.L. More, J. Mater. Res. 8 (1993) 1213
[2] S. Watanabe, S. Miyake, W. Zhou, Y. Ikuhara, T. Suzuki, M. Murakawa, Appl. Phys. Lett. 66 (1995) 1478
[3] W.-L. Zhou, Y. Ikuhara, M. Murakawa, S. Watanabe, T. Suzuki, Appl. Phys. Lett. 66 (1995) 2490
[4] D.R. McKenzie, W.D. McFall, W.G. Sainty, C.A. Davis, R.E. Collins, Diamond Related Mats. 2 (1993) 970
[5] W.-L. Zhou, Y. Ikuhara, T. Suzuki, Appl. Phys. Lett. 67 (1995) 3551
[6] J. Robertson, Diamond Related Mats. 5 (1996) 519
[7] M.F. Plass, W. Fukarek, A. Kolitsch, M. Mäder, W. Möller, phys. stat. sol. 155 (1996) K1
[8] M.F. Plass, W. Fukarek, S. Mändl, W. Möller, Appl. Phys. Lett. 69 (1996) 46
[9] J.L. Andujar, E. Bertran, Y. Maniette, J. Appl. Phys. 80 (1996) 6553

Formation, Microstructure and Gettering Ability of Helium Induced Cavities in Silicon

J.R. Kaschny*, P.F.P. Fichtner+, A. Mücklich, U. Kreißig, R.A. Yankov, R. Kögler, A.B. Danilin✦ and W. Skorupa
* On leave from Instituto de Fisica - UFRGS, Porto Alegre, Brazil
+ On leave from Depto. de Metalurgia - UFRGS, Porto Alegre, Brazil
✦ Centre for Analysis of Substances, Moscow, Russia

Cavity microstructures formed in Si by He ion implantation and annealing have been found to getter efficiently transition-metal impurities such as Cu and Au. This is a novel concept which holds great technological promise for front-side gettering in the proximity of an active device region [1]. Most of the studies in the field have concentrated on high-dose He implants (typically 2×10^{17} cm^{-2}) producing a high number density of cavities. For advanced submicron devices, however, not only very low levels of contamination, but also low defect densities are required. This implies that, from the viewpoint of device processing optimization, it would be desirable to reduce the He dose necessary to create a local gettering cavity system. Therefore, the emphasis of our present study [2] has been placed on Si implanted with relatively low He doses where, after annealing, a rather low number density of cavities is formed.

In our experiments (100)-oriented Si wafers have been implanted with He^+ ions at room temperature using energies of 10 and 40 keV and doses of 1×10^{15}, 1×10^{16} and 5×10^{16} cm^{-2}. After implantation the wafers have been furnace annealed at 800 °C for 10 min in an N_2 ambient. Cross-sectional (XTEM) and plan-view (TEM) specimens have been conventionally prepared and examined on a Philips CM 300 electron microscope. Elastic recoil detection (ERD) measurements have been performed using a primary beam of 35 MeV Cl^{+7} ions at an angle of 15° as described elsewhere [3]. The ability of cavity microstructures to act as gettering centers has been tested for the least favorable case of Fe. The metal impurity has been controllably introduced into the Si substrates using implantation at an energy of 50 keV to a dose of 1×10^{12} cm^{-2} and subsequent annealing. The resulting depth profiles of Fe have been evaluated by secondary-ion-mass spectrometry (SIMS).

For the low He dose of 1×10^{15} cm^{-2} (peak He concentration of ~ 4×10^{19} cm^{-3}), no cavities are seen in either the as-implanted or the annealed samples. This is consistent with previous work [4] where the minimum He concentration required to form He cavities after annealing has been estimated to be 3.5×10^{20} cm^{-3}. For the high dose of 5×10^{16} cm^{-2}, a dense array of small cavities is already observed in the as-implanted samples. Upon annealing the cavities grow and cluster in a well-defined buried layer, in agreement with what is known about the cavity structures produced in a similar manner. The He content in the as-implanted and annealed samples has been experimentally determined by ERD for both implantation energies and it has accordingly been found that ~ 4% and 20% of the implanted He is still present within the cavity-containing layers for the 10 keV and 40 keV implants, respectively. These values are much larger than that of the respective amount of residual He assessed on the basis of the first-order gas-release model [5]. Such a discrepancy arises possibly from the use of incorrect values of the activation energy and permeation rate which have been obtained under different experimental conditions and within the temperature range of 950 - 1200 °C. Indeed, recent He-diffusion studies [6] have shown that at sufficiently high He concentrations the diffusivity of He is largely reduced, especially for temperatures below 800 °C.

Fig. 1: Plan view TEM micrograph showing a cavity system resulting from the 40 keV, 1×10^{16} cm^{-2} He implant after a 10 min, 800 °C anneal in N_2 ambient. (a) General appearance of the cavities along with dislocation loops. Analysis conditions: dynamic bright field image with electron beam parallel to the <100> axis, multibeam, underfocus. (b) A typical large cavity surrounded by a ring of smaller ones. Analysis conditions: kinematics bright field image, underfocus. (c) A strain field contrast around the cavities and dislocation loops (marked with an arrow) emerging from the strained structure. Analysis conditions: dynamic bright field with electron beam close to <100> lattice direction, g=400, underfocus.

For the medium dose of 1×10^{16} cm^{-2} there is no clear evidence for the presence of cavities in the as-implanted state. After annealing, however, a diluted system of large cavities surrounded by a strong strain field is observed. It is worth pointing out that the dimensions and morphology of the cavity arrangements may vary with implantation energy. Fig. 1a is a plan view micrograph from the 40 keV implant showing a general appearance of the cavity system together with a network of extended defects (dislocation loops). A typical arrangement observed in an enlarged micrograph from the same implant is shown in Fig. 1b. The large central cavities are always surrounded by a number of smaller ones forming "planetary-like" configurations. Fig. 1c shows the presence of a strong strain field around these configurations, and dislocation loops running from the cavities. Such features have been previously observed in the case of overpressured bubbles, i.e. when the gas pressure inside the bubbles exceeds the thermodynamic equilibrium conditions. Clearly, in our case neither strain fields nor dislocation loops can originate from voids or even from equilibrium bubbles (here equilibrium means that the gas pressure inside the bubble is balanced by the surface tension of the matrix). Thus, it is logical to consider that the observed cavities for the 1×10^{16} cm^{-2} He implantation are not empty, but are rather filled with He gas, or in another words, these are bubbles in an overpressurized state.

SIMS analyses of the Si samples implanted with 40 keV, 1×10^{16} cm^{-2} He and then contaminated intentionally with Fe reveal that about 7% of the metal impurity is gettered by the cavities. At the same time our recent studies [1] of the gettering behavior of Fe in He-implanted SIMOX wafers have demonstrated that no detectable trapping of Fe occurs to the cavity-containing layers formed below the buried oxide. Further investigations are in progress to clarify the observed difference in the gettering behavior of Fe.

Acknowledgements

Three of us (P.F.P.F, J.R.K. and R.A.Y.) would like to acknowledge support from Alexander von Humboldt Foundation, National Research Council (CNPq) - Brazil and Deutsche Forschungsgemeinschaft, respectively.

References

[1] W. Skorupa, N. Hatzopoulos, R.A. Yankov, A.B. Danilin, Appl. Phys. Lett. 67 (1995) 2292
[2] P.F.P. Fichtner, J.R. Kaschny, R.A. Yankov, A. Mücklich, U. Kreißig, W. Skorupa, Appl. Phys. Lett. 70 (1997), in press
[3] U. Kreißig, R. Grötzschel, R. Behrisch, Nucl. Instr. and Meth. B85 (1994) 71
[4] S.M. Myers, D.M. Follstaedt, J. Appl. Phys. 79 (1996) 1337
[5] C.C. Griffioen, J.H. Evans, P.C. de Jong, A. van Veen, Nucl. Instr. and Meth. B27 (1987) 417
[6] P. Jung, Nucl. Instr. and Meth. B91 (1994) 362

Ion Beam Synthesis by Tungsten Implantation into 6H-Silicon Carbide

H. Weishart, W. Matz and W. Skorupa

Silicon carbide is an auspicious material for high-temperature semiconductor devices because of its superior properties such as high thermal conductivity, high electron velocity and wide bandgap [1, 2]. High-temperature devices, however, are in need of reliable metallization since their working temperature can be as high as 700 °C. A proper ohmic contact should have a low resistivity, good adhesion to the underlying SiC, as well as high chemical stability at elevated temperatures for more than 1000 hours. Contacts that could meet all of the above-mentioned requirements are either layered structures consisting of a reactive metal to ensure adhesion, a diffusion barrier and a low resistivity metal, or high temperature stability, low resistivity materials. Promising materials of the latter class are tungsten silicide and tungsten carbide. Fabrication of W-based contact layers has been achieved up to now by (i) deposition of pure tungsten on SiC and subsequent annealing [3, 4] or (ii) sputter deposition, subsequent ion beam mixing and final annealing of W/Si multilayers [5]. However, the first technique requires annealing temperatures in excess of 1000 °C and produces an inhomogenous mixture of polycrystalline tungsten silicide, tungsten carbide and tungsten. The latter needs much expenditure to form a homogeneous layer of tungsten silicide. The reaction of a deposited W layer with crystalline SiC was investigated earlier [6, 7] using Auger electron spectroscopy. Already after deposition, little amounts of tungsten carbide and silicide were found, which formed at defects within the W/SiC-interfacial region. It was also shown that annealing at 950 °C is necessary to maintain further the reaction between SiC and W [4]. We showed earlier that synthesis of tungsten carbide and silicide in SiC is possible at low temperatures by using ion implantation of W into SiC [8, 9]. This technique introduces at the same time defects and tungsten into SiC and thus facilitates the formation of tungsten compounds in the implanted region. However, annealing temperatures of 1500 °C would be necessary to recrystallize the amorphized SiC after room-temperature (RT) implantation [10, 11]. High temperature implantation may reduce the damage introduced into SiC.

The present work reports results on high-dose ion implantation of W^+ performed at an elevated substrate temperature. These results are compared to those obtained earlier by RT implantation [8]. The objective of the investigation is to gain an insight into the influence of both implantation and annealing temperatures on the depth distribution of the elements, the phase formation as well as the properties of W-implanted 6H-SiC.

W^+ ions were implanted into wafers of single crystal n-type 6H-SiC (Cree Research, Inc.) at a dose of 1×10^{17} cm^{-2} using an energy of 200 keV. The mean projected range for this energy, according to TRIM91, is 50 nm. The substrates were held at 500 °C during implantation and subsequently underwent an anneal for 30 min in Ar at either 950 °C or 1100 °C. The W profile and the stoichiometry of the synthesized layers were analyzed by Rutherford backscattering spectrometry (RBS) of 1.2 MeV $^4He^+$. Auger electron spectroscopy (AES) in combination with sputter depth profiling during sample rotation was performed using a 3 keV Ar^+ beam. The AES spectra of crystalline Si, 6H-SiC, WC, W_5Si_3 and WSi_2 were taken as references to characterize the chemical state of the elements. X-ray diffraction (XRD) with gracing incidence was employed to determine the crystalline phases.

X-ray diffraction performed on the RT implanted samples indicates that in the as-implanted state no crystalline phase exists in the near-surface region. Annealing at 950 °C causes crystallization of W_2C. No evidence for crystalline WC, WSi_2 or W_5Si_3 is found. Fig. 1a shows

an X-ray diffraction spectrum of the sample implanted at 500 °C in the as-implanted state. Two distinct SiC peaks originating from Umweganregung as well as a broad peak around 40° are evident. Annealing at 950 °C results in crystallization of W_2C and W_5Si_3 as can be seen from the peaks between 30° and 46° in Fig. 1b. Samples annealed at 1100 °C contain crystallites of W_5Si_3 only; the corresponding peaks in Fig. 1c are marked with arrows.

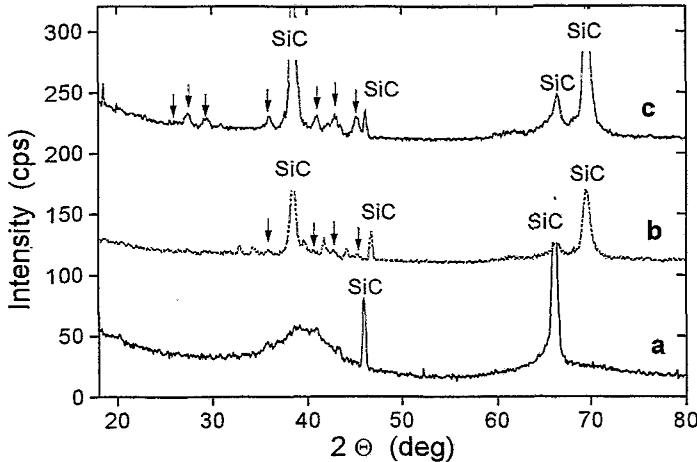

Fig. 1: X ray diffraction pattern of 6H-SiC implanted with 1×10^{17} W^+ cm^{-2} at 500 °C.
(a) The sample shows in the as-implanted state a broad peak around 40° indicating first phase formation.
(b) The sample annealed at 950 °C shows peaks of crystalline W_5Si_3 and W_2C.
(c) The sample annealed at 1100 °C exhibits only peaks due to crystalline W_5Si_3.
The observed SiC peaks are not due to direct Bragg reflection but due to Umweganregung. The W_5Si_3 peaks are marked with arrows.

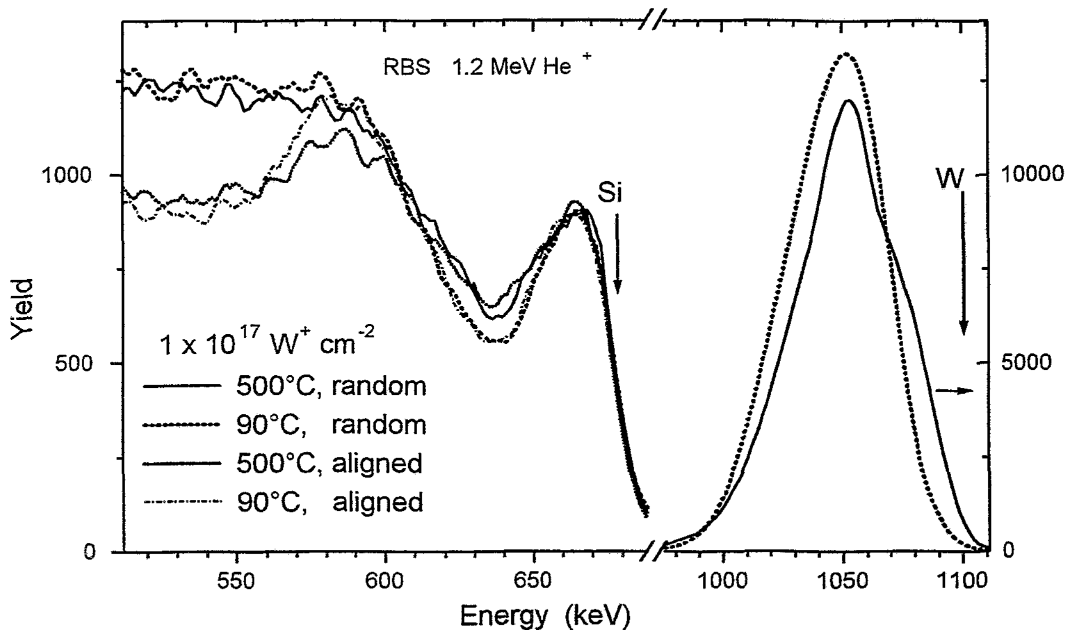

Fig. 2: Channeled and random RBS spectra of SiC samples implanted with 1×10^{17} W^+ cm^{-2} at 200 keV. The implantation temperatures are 90 °C and 500 °C. The surface edges of Si and W are marked with arrows. The aligned spectra indicate that implantation at 500 °C produces less damage in the SiC.

The RBS channeled and random spectra of the as-implanted samples for the implantation temperatures of 90 °C and 500 °C are depicted in Fig. 2. A comparison of the aligned spectra at an energy of 570 keV reveals that the sample implanted at 90 °C is amorphized beyond the W-rich layer and has a sharp crystalline/amorphous interface in the SiC. The difference between aligned and random yields indicates a less pronounced damage in this region for the sample implanted at 500 °C. Implanting at higher temperatures, therefore, reduces the damage

introduced into SiC. The W peak for the lower implantation temperature is higher and more narrow. The W peak for the 500 °C implant shows a small shoulder on its right edge, i.e. in direction to the surface, which indicates the presence of a small additional W peak.

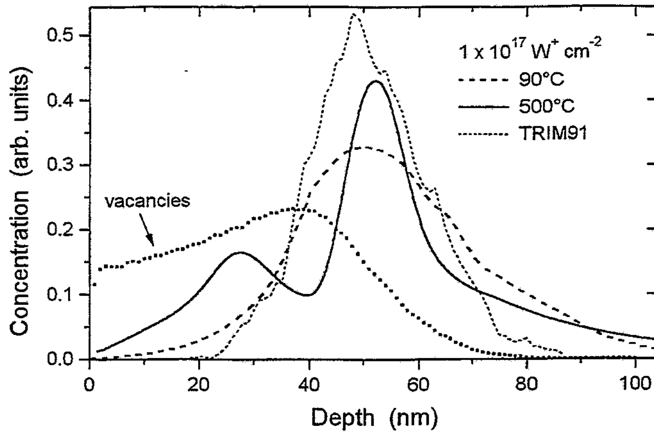

Fig. 3: Tungsten concentration profiles of SiC samples implanted with W^+ at 200 keV.
The profile of the high temperature implant is obtained by AES, while that of the 90 °C implant originates from RBS. TRIM calculations predict a Gaussian peak with a mean projected range of 50 nm. The W distribution of the 90 °C implant shows good agreement with the TRIM profile. The sample implanted at 500 °C has a bimodal W distribution, the second peak being at the mean projected range.

Auger depth profiling confirms the bimodal tungsten distribution in the sample implanted at 500 °C. The double peak is clearly seen in Fig. 3, which shows the tungsten profiles of the as-implanted samples as a function of the implantation temperature. For comparison, both the W and the vacancy profiles, as predicted by TRIM, are also included. The W profile of the 90 °C implant displays a broad single peak which, taking into account the detector resolution, shows rather good agreement with TRIM. However, the W profile of the 500 °C implantation has two peaks, with the second peek being much more pronounced. An enhanced mobility of atoms at elevated implantation temperatures may be the reason for the development of two W peaks instead of a single Gaussian peak; however, as yet the basic driving force cannot be reasonably accounted for. We believe that the W profile originates from an initially Gaussian distribution, which during implantation transforms to a double peak structure. From Fig. 3 it is evident that the minimum between the two W peaks is located at the depth of maximum energy deposited into the SiC by nuclear stopping during implantation as calculated by TRIM. We suppose that a large number of tungsten silicide and carbide precipitates are destroyed within this region during implantation. The enhanced atom mobility at elevated implantation temperatures enables an Ostwald ripening process. Thus, the destroyed precipitates in the region of maximum energy deposition shrink and disappear during implantation. Consequently, two W peaks appear, whereby the higher one is located a few nanometers beyond R_p and the lower one is positioned at a depth of 0.56 R_p. Evidence for this ripening process are the narrow structure of the second W peak as well as the XRD spectrum of the as-implanted sample. The broad peak centered around 40° is more pronounced for the 500 °C implant than for the 90 °C implant [8]. This fact indicates the presence of a larger number of microcrystallites or larger sized crystallites in the sample.

Analysis of the Auger energy spectra demonstrates clearly the depth dependent chemical states of Si, W and C. A comparison of the C and Si line shapes with the reference spectra of 6H-SiC, W_5Si_3, WSi_2 and WC proves that formation of tungsten carbide and tungsten silicide occurs already in the as-implanted state within the implantation zone. Both the C and the Si line shapes indicate a preferential bonding of W with C and Si at the expense of SiC within the two W-rich layers. According to Ref. [6], the abundance of defects generated by the implantation is responsible for this enhanced spontaneous formation of tungsten silicide and tungsten carbide. Annealing the samples leads to the formation of crystalline W_2C and W_5Si_3 at 950 °C and at 1100 °C of W_5Si_3 only, as confirmed by the XRD results. However, the Auger

line shapes indicate the presence of tungsten silicide as well as tungsten carbide in all the samples. The crystalline phases, therefore, are mixed with amorphous phases.

Taking into account the fact that crystallization of phases in Ti-implanted and annealed SiC is temperature- and composition-dependent [12], we believe W_2C to be the energetically more favored phase to crystallize during annealing at 950 °C under sufficiently high carbon supersaturation in the matrix. The critical radius for W_2C nuclei in such a matrix is much smaller than for nuclei which form in a matrix of low carbon supersaturation. The carbon concentration of the sample implanted at 90 °C never drops below 40 at% [8], we therefore anticipate a sufficiently high carbon supersaturation in the implanted region. The AES depth profiles show that the sample implanted at 500 °C exhibits a loss of carbon in the W-rich regions at a depth of 20 nm and 50 nm [13]. Thus, formation of W_5Si_3 during annealing appears to be favored.

Resistance measurements using the four-point probe technique on the sample implanted at 500 °C and annealed at 1100 °C yield a mean value of 125 Ω/□ for the sheet resistance. Using a thickness of 54 nm for the W containing layer, we calculate a resistivity of 675 μΩcm, which is only by one order of magnitude higher than that for single crystalline tungsten silicide [14].

ACKNOWLEDGMENTS

The authors would like to thank Dr. J. Schöneich for the implantation, Mrs. E. Quaritsch and Dr. H. Reuther for the AES and Dr. M. Voelskow and Dr. M. Mäder for the RBS measurements. We are especially indebted to Mrs. A. Scholz for the XRD analysis and Dr. R.A. Yankov for fruitful discussions.

REFERENCES

[1] W.E. Nelson, F.A. Halden, A. Rosengreen, J. Appl. Phys. 37 (1966) 333
[2] G. Pensl, R. Helbig, Festkörperprobleme/Advances in Solid State Physics 30 (1990) 133
[3] M.M. Anikin, M.R. Rastegaeva, A.L. Syrkin, I.V. Chuiko, Springer Proceedings in Physics 56 (1992) 183
[4] L. Baud, C. Jaussaud, R. Madar, C. Bernard, J.S. Chen, M.A. Nicolet, Mat. Sci. Eng. B29 (1995) 126
[5] H. Zhang, PhD thesis, Friedrich Alexander Universität Erlangen, 1990
[6] K.M. Geib, C. Wilson, R.G. Long, C.W. Wilmsen, J. Appl. Phys. 68 (1990) 2796
[7] C. Jacob, S. Nishino, M. Mehregany, P. Pirouz, in: Silicon Carbide, Related Materials (Institute of Physics Publishing, Bristol, Philadelphia, 1994) ch.3 p.247
[8] H. Weishart, J. Schöneich, H.-J. Steffen, W. Matz, W. Skorupa, Mater. Res. Soc. Symp. Proc. 354 (1995) 177
[9] H. Weishart, H.-J. Steffen, W. Matz, M. Voelskow, W. Skorupa, Nucl. Instr. Meth. B112 (1996) 338
[10] C.J. McHargue, J.M. Williams, Nucl. Instr. Meth. B80/81 (1993) 889
[11] V. Heera, R. Kögler, W. Skorupa, J. Stoemenos, Appl. Phys. Lett. 67 (1995) 1999
[12] R.G. Vardiman, Mater. Science Eng. A177 (1994) 209
[13] H. Weishart, W. Matz, W. Skorupa, Mater. Res. Soc. Symp. Proc. 423 (1996) 999.
[14] S.P. Murarka, in: Silicides for VLSI Applications (Academic Press, Orlando, 1983) p. 30

Implantation and Columnar Growth of Large $\beta-FeSi_2$ Precipitates and $\alpha-FeSi_2$ Network Structures in Silicon

H. Reuther and M. Dobler

Iron silicides of different stoichiometry and structure may be formed by ion beam synthesis (IBS) [1]. The semiconducting $\beta-FeSi_2$ is very interesting for possible applications, e.g. in optoelectronic, photo- and thermovoltaic devices [2]. In recent years, therefore most attention has been devoted to this phase [3]. It is stoichiometric and stable below 960 °C for bulk materials, while the high temperature α–phase is metallic and understoichiometric due to iron vacancies [4]. Investigations of α–phase layers produced by IBS [5] show that this phase can be stabilized also below the phase transition temperature of 960 °C. The phase formation process during ion implantation and phase transitions induced by annealing are connected to many fundamental processes like supersaturation, nucleation, diffusion, Ostwald ripening and coalescence of precipitates [6].

Phase formation after iron implantation into silicon was successfully studied by conversion electron Mössbauer spectroscopy (CEMS) while Auger electron spectroscopy (AES) depth profiling was used to determine the element concentration profiles [7]. Phase analysis indicated a mixture of ε-FeSi, α- and $\beta-FeSi_2$ with fractions depending on the implanted dose, however depth profiling gave maximum iron concentrations less than the required stoichiometric value, which might be due to the formation of silicide precipitates within the silicon matrix. Therefore, in the present investigation scanning AES was utilized in combination with CEMS to identify such precipitates and their morphology. It will be demonstrated that the shape of the $FeSi_2$ precipitates depends on the phase type α or β.

A wafer of n–type Si(111) (resistivity: 1 – 10 Ωcm) was implanted with 200 keV Fe^+ ions at 350 °C. First, $2.3x10^{17}$ cm^{-2} ^{56}Fe was implanted followed by the implantation with $7x10^{16}$ cm^{-2} of the ^{57}Fe Mössbauer probe nuclei to reach the total nominal iron dose of $3x10^{17}$ cm^{-2}. The implantation temperature of 350 °C was chosen to avoid amorphization of the implanted layer. After the implantation, the sample was cut into three pieces. One was annealed in Ar atmosphere for 18 h at 900 °C and a second one for 1 h at 1150 °C. The temperatures were chosen to induce the formation and crystallization of pure β– and $\alpha-FeSi_2$ phases.

Phase analysis with CEMS was performed as described in Ref. [7]. Sputter depth profiling and scanning AES were executed with the scanning Auger electron spectrometer MICROLAB 310F. Sputtering was performed while sample rotating with a 3 keV Ar^+ ion beam at a current density of about 1 $\mu A/mm^2$. Both for depth profiling and for scanning AES the Auger peaks Si(KLL) at 1616 eV, Fe(LMM) at 703 eV and O(KLL) at 507 eV were used. The primary electron beam had an energy of 10 keV, the sample current was about 30 nA for the depth profiling and 2–3 nA for the element mapping. In the first case the analyzing electron beam had a diameter of about 1 μm, in the second it was focused to about 25 nm which enables to resolve lateral structures of less than 50 nm extension. For element mapping the image field was divided into 256 x 256 pixels. At every position the intensities of the O(KLL), the Fe(LMM) and the Si(KLL) peak were detected and corrected for the background. The measurements were performed at different depths of the profiles after removing sample material by sputtering. The size of the sputtered area (1 mm in diameter) was much larger than the investigated area (several μm^2). The depths of the sputtered craters were measured with a profilometer (DEKTAK 8000).

The CEM spectra of the as–implanted and annealed samples are displayed in Fig. 1. The phase analysis was performed under the assumption that a mixture of α–and β– $FeSi_2$ and ε–FeSi can be formed as a result of the implantation. The evaluation of the spectra was performed with the well known values of the hyperfine parameters for the different phases from literature [8–10]. A detailed description of the fitting procedure is reported elsewhere [11,12]. In the as–implanted sample α–$FeSi_2$ (44 %) and β–$FeSi_2$ (56 %) and no ε–FeSi were found while in the sample annealed at 900 °C only β–$FeSi_2$ and in the sample annealed at 1050 °C only α–$FeSi_2$ were detected.

The iron concentration profiles measured by AES are displayed in Fig. 2. The as–implanted sample shows a nearly Gaussian profile with a maximum iron concentration of 23 at.% at 130 nm depth. Annealing changes the profiles significantly. The sample annealed at 900 °C shows a broad plateau–like profile with an average iron concentration of 12 at.%. The plateau is about 200 nm long and starts already close to the surface. The sample annealed at 1050 °C shows only a weak broadening of the profile with an average iron concentration of about 15 at.% and a thickness of about 170 nm at half maximum. Strong iron concentration fluctuations in the profile (up to 10 at.% for sample annealed at 1050 °C) are obvious.

At both annealed samples a grown SiO_2 layer can be detected. While the thin SiO_2 layer at the surface of the sample annealed at 900 °C is removed after the first sputtering step, on the sample annealed at 1050 °C a thick SiO_2 layer (about 40 – 50 nm) is found extending from the surface up to the iron silicide layer. In both cases the oxygen concentration drops to zero when the iron concentration begins to raise.

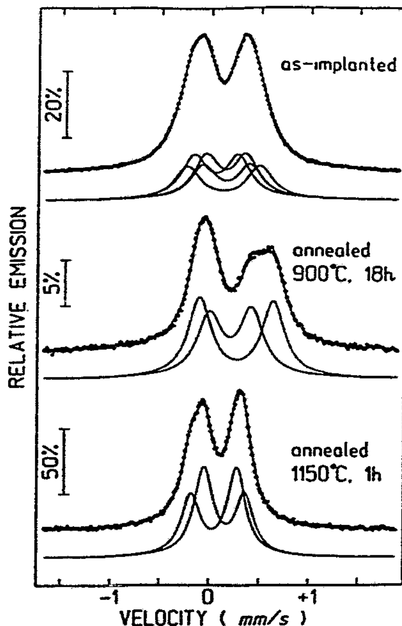

Fig. 1:
CEM spectra of the as–implanted and annealed samples.

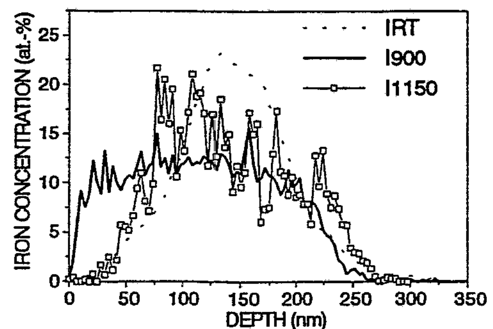

Fig. 2:
AES iron concentration depth profiles of the as–implanted and annealed samples.

Secondary electron microscopic (SEM) and scanning Auger microscopic (SAM) images of the as–implanted sample were taken in a depth of about 130 nm corresponding to the maximum iron concentration. SEM and Si–SAM viewgraphs are structureless while the Fe–SAM viewgraph shows only weak intensity fluctuations corresponding to relative concentration variations of less than ± 10 %.

Fig. 3 shows images of the annealed samples. The images of the sample annealed at 900 °C were recorded after a short sputtering to remove completely the thin SiO_2 layer in a depth of about 10 nm. At the SEM viewgraph circular bright structures with diameters of about 500 nm down to less than 50 nm can be detected within a dark matrix. Si– (not shown) and Fe–SAM viewgraphs prove that they are iron rich precipitates in a nearly iron free matrix. A quantitative AES point analysis gives the result of up to 30 at.% Fe in the precipitates and less than 2 at.% Fe in the matrix.

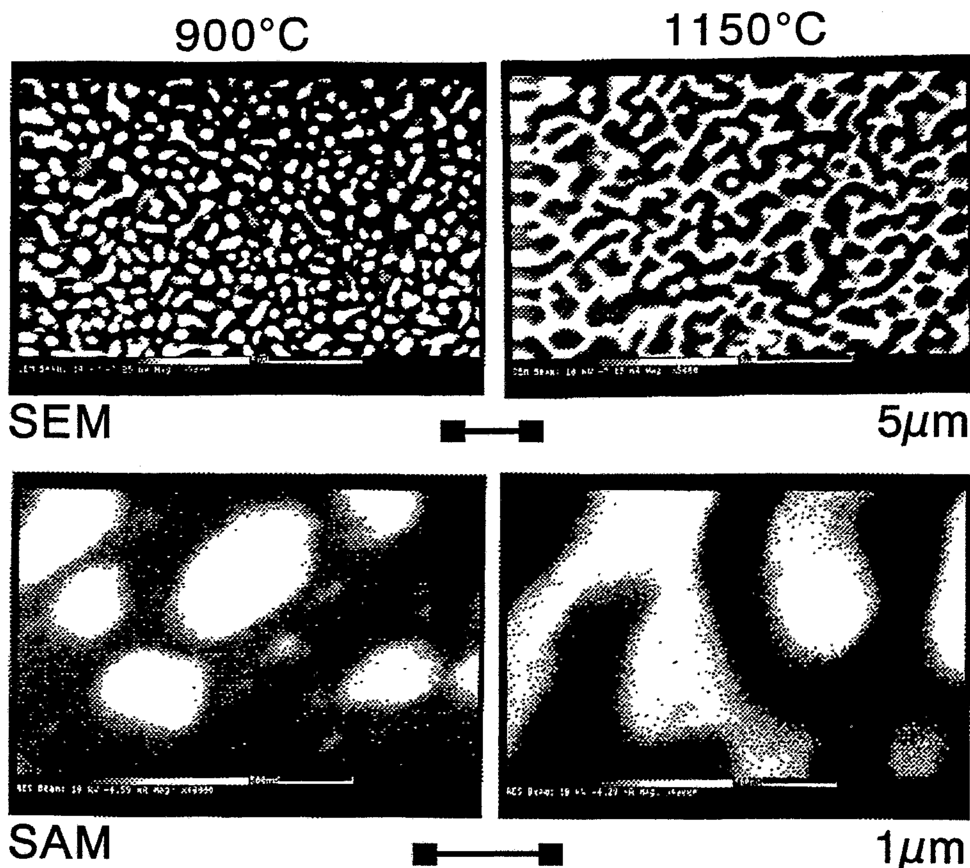

Fig. 3:
Top: SEM micrographs, bottom: Fe–SAM micrographs.
Left: Images of the sample annealed at 900 °C, right: images of the sample implanted at 1150 °C.
The contrast in the SEM image is produced both due to topographic and composition variations. The contrast in SAM images is calculated for each of the 256 x 256 pixels from the difference between the Auger signal at 703 eV for iron and the background signal far from the Auger peak. Bright areas indicate high concentrations, dark areas indicate low concentrations. The magnification of the SAM micrographs is 8 x higher than that of the SEM micrographs.

The images of the sample annealed at 1050 °C were recorded in a depth of about 100 nm within the plateau of the iron concentration profile. A connected penetration structure is seen in the SEM viewgraph. The comparison of the Fe–SAM and Si–SAM viewgraphs shows an iron rich connected penetration structure alternating with iron poor regions and vice versa. The structure resembles those known from spinodal decomposition in alloys and glasses with a miscibility gap [13], however such a miscibility gap is unknown in the Fe–Si equilibrium phase diagram up to now. The quantitative AES point analysis gives again the result of about

30 at.% Fe in the precipitates and less than 2 at.% Fe in the matrix. In both cases, oxygen cannot be detected neither in the matrix nor in the precipitates.

To determine the 3–dimensional shape of the structures detected in the annealed samples, additional SEM and SAM viewgraphs were taken at different positions of the depth profiles (for the sample annealed at 1050 °C see Fig. 4). Surprisingly, the geometrical shape of the structures is maintained over the whole extension of the profiles. Only at the bottom the structures vanish. The disilicide structures are not flat, ball–like or snake–like, but are columnar structures. They are disk–like for the sample annealed at 900 °C (ß–$FeSi_2$) and wall–like for the sample annealed at 1050 °C (α–$FeSi_2$) reaching a length of 200 to 250 nm with lateral dimensions of up to 1000 nm. From element mappings performed at the same positions as the SEM viewgraphs of Fig. 4, it is obvious that the silicide forming columns do not contain iron and less oxygen just below the surface. The surrounding matrix is formed by silicon oxide. Only after going deeper when the oxygen is removed completely the columns are composed by the iron disilicide surrounded by the silicon matrix.

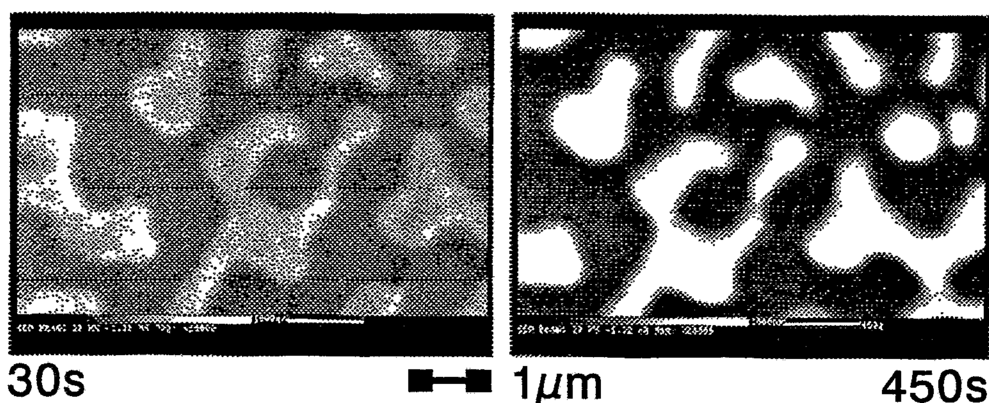

Fig. 4
SEM viewgraphs of the sample annealed at 1050 °C taken after different sputtering times (sputtering rate about 0.22 nm/s).

For the first time, growth of large silicide precipitate structures after ion implantation and subsequent annealing is shown by scanning AES. Taking into consideration the CEMS results the conclusion has to be drawn that during annealing large separated β–$FeSi_2$ precipitates and a penetration α–$FeSi_2$ network structure are grown. Before annealing silicide precipitates may exist too, however if so their size must be below 25 nm which is the minimum instrumental lateral resolution of the used experimental setup.

During annealing, depending on the temperature an $\alpha \rightarrow \beta$ and $\beta \rightarrow \alpha$ phase transition, respectively, and a growth of precipitates take place. Long time annealing at 900 °C, according to the Fe–Si phase diagram a value below the formation temperature of α–$FeSi_2$ (960 °C) and within the existence range of ß–$FeSi_2$, let transform the whole mixture to ß–$FeSi_2$. Annealing above the formation temperature of α–$FeSi_2$ at 1150 °C results in a complete $\beta \rightarrow \alpha$ phase transition. The shape of the precipitates of the two disilicide phases is different, separated structures for the ß–phase, a connected penetration structure for the α–phase. Analogous to the spinodal decomposition, phase separation in a metastable region may be responsible for the formation of both kinds.

Due to the annealing, the concentration depth profiles are changed significantly. Oxygen is absorbed and, in dependence of the annealing temperature, a fast oxidation of the surface takes place. The silicide layer acts as diffusion barrier for the oxygen. Oxygen does not penetrate into the silicide structure. Regarding the iron concentration profiles, the oscillating behaviour of the annealed samples can be explained by the produced lateral silicide structures. The size of the electron beam at the depth profiling (about 1 μm) is in the order of magnitude of the structures detected after the annealing. The iron concentration is high or low depending on that if the electron beam hits an iron silicide structure or not. Due to the sample rotation during sputtering such small shifts of the measuring position may be possible.

In conclusion, we have reported about the formation of iron disilicide structures by iron implantation into silicon. Implantation induced first the formation of a mixture of α– and ß–$FeSi_2$. Due to special annealing the mixture could be transformed to pure α– and ß–$FeSi_2$, respectively. There was no homogenous distribution of the silicides but columns formed by connected penetration networks or large precipitates. CEMS in combination with AES was very suitable to watch the processes of phase transformation and precipitate formation. For the first time, the formation of such large precipitate structures was observed. Moreover, scanning AES was successfully applied to detect structures of less than 50 nm.

References

[1] T.B. Massalski, in: Binary Alloy Phase Diagrams (American Society for Metals, Metal Park, OH) 1986

[2] R.W. Fathauer, S. Mantl, L.J. Schowalter, K.N. Tu (eds.), Silicides, Germanides and their Interfaces, Mat. Res. Soc. Symp. Proc. 320 (1994)

[3] N.E. Christensen, Phys. Rev. B42 (1990) 7148

[4] C. Le Corre, J.M. Genin, Phys. Stat. Sol. (b) 51 (1972) K85

[5] K. Radermacher, Thesis, KFA Jülich, 1993

[6] S. Mantl, Materials Science Report 8 (1992) 1

[7] H. Reuther, M. Dobler, Surface and Interface Analysis 24 (1996) 411

[8] R. Wandji, C. Le Corre, J.M. Genin, B. Roques, Phys. Stat. Sol. (b) 45 (1971) K123

[9] G.K. Wertheim, J.H. Wernick, D.N.E. Buchanan, J.Appl. Phys. 37 (1966) 3333

[10] T.I Sigfusson, O. Helgason, Hyperfine Interactions 54 (1990) 861

[11] M. Dobler, H. Reuther, N.P. Barradas, Hyperfine Interactions (C) 1 (1996) 266

[12] M. Dobler, H. Reuther, M. Betzl, M. Mäder, W. Möller, Nucl. Instr. Meth. B117 (1996) 117

[13] R.W. Cahn, R.J. Charles, Phys. Chem. Glasses 6 (1965) 181

Ion Beam Synthesis of Nanoclusters and Buried Layers Studied by Kinetic 3D Lattice Monte Carlo Simulations

K.-H. Heinig and M. Strobel

New materials are required in advanced silicon technologies for the integration of more and more MOS field effect transistors in one circuit and for the integration of micro- and opto-electronic devices on the same silicon substrate. Some of these new, advanced materials can be produced by high-dose ion implantation, i.e. by Ion Beam Synthesis (IBS) [1]. For instance, the Separation by IMplanted OXygen (SIMOX) technology allows the electronical separation (isolation) of a sub-micrometer thick Si layer from the silicon wafer [2]. Here, the implanted oxygen ions form with Si substrate atoms a buried SiO_2 layer. Another example is the high-dose Co^+ implantation in silicon, which results in the synthesis of (buried) $CoSi_2$ layers or wires having a very low electrical resistance [3]. If silicon or germanium ions are implanted into SiO_2 quantum-size precipitates of these indirect bandgap semiconductors can be synthesised. The recently demonstrated effect of light emission from such nanoclusters [4] opens a promising way to the fabrication of truly integrated opto-electronic microchips.

The nucleation and coarsening of nanosize precipitates in solids during ion implantation and post-implantation heat treatment are the crucial processes for both the synthesis of nanoclusters and buried layer formation (see Fig. 1). Some general features of IBS can be

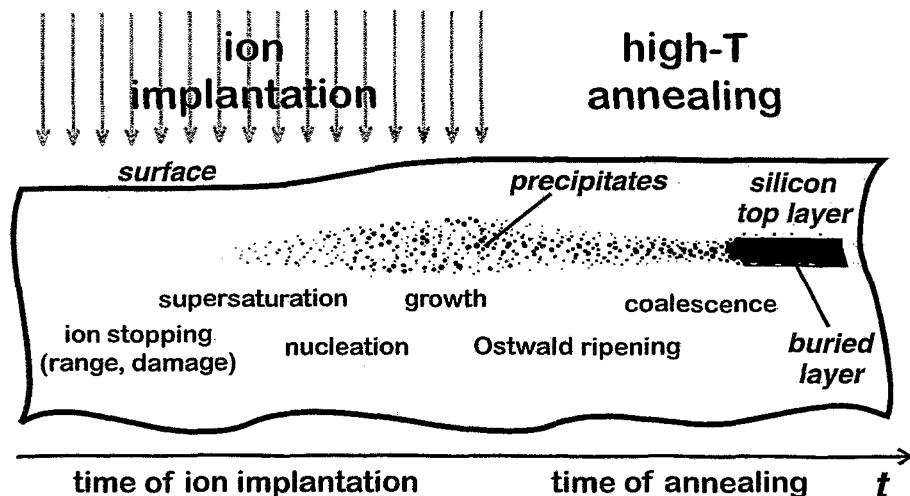

Fig. 1: Scheme of IBS which shows the physical processes occurring during ion implantation and post-implantation annealing.

found: (i) At the initial stage of ion implantation the substrate becomes supersaturated by the implanted species. (ii) If the implanted atoms are sufficiently mobile during ion implantation, tiny precipitates of implanted atoms or of their compound with matrix atoms can nucleate; if they are not mobile during ion implantation, this process occurs during post-implantation annealing. (iii) The precipitates grow at the expense of the accumu-

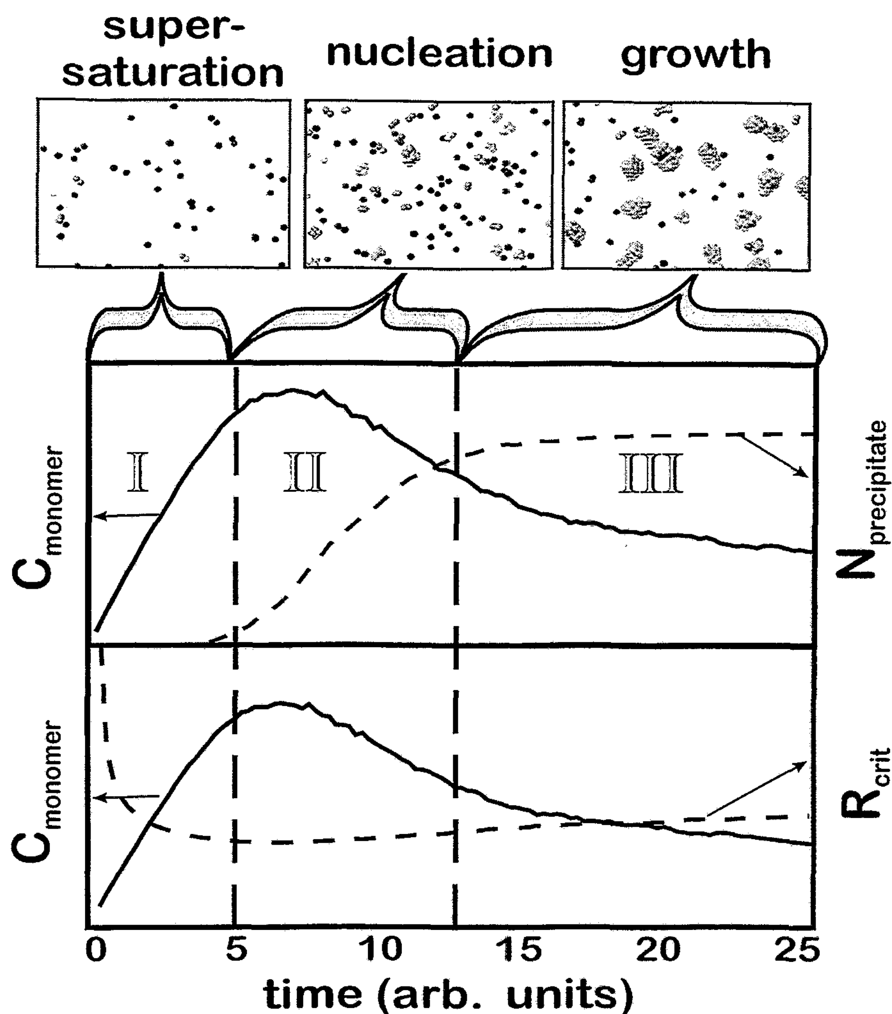

Fig. 2: Principle behaviour of impurity atoms continuously incorporated into a solid by ion implantation at high temperature. The kinetic 3D lattice MC simulation of the evolution of characteristic physical quantities allows the definition of three stages of precipitate formation, namely (i) supersaturation, (ii) nucleation and (iii) growth. In the upper and lower plots the density of precipitates and the critical radius of cluster nucleation (according to Eq. (1)), respectively, are shown together with the monomer concentration. The simulation cell can be thought to be small compared to the implanted layer thickness, i.e. spatially homogeneous ion deposition is assumed. The top row shows snapshots of the configurations of the implanted atoms. For the sake of clarity, atoms of the host lattice are not shown.

lated supersaturation and the continuously implanted ions. (iv) At post-implantation annealing coarsening of nanoclusters occurs due to Ostwald ripening. (v) With increasing nanocluster sizes coalescence processes contribute to coarsening. (vi) If the fluence was sufficiently high, the coalescence of precipitates may result in the formation of a buried layer.

A kinetic 3D lattice Monte Carlo method has been developed which provides an appropriate simulation tool for the simultaneous investigation of all stages of IBS (Figs. 2,3). A very efficient and fast treatment of interatomic many-body interactions has been achieved

by the construction of a code based on a special cellular automaton. The kinetics (diffusion, nucleation,...) of up to 10^6 implanted atoms in a fcc lattice of up to 10^8 lattice sites, i.e. volumes being larger than $(100 \text{ nm})^3$, can be described. So far we assume a host matrix free of defects, which implies homogeneous diffusion of impurity atoms and excludes inhomogeneous nucleation. The nanocrystals are embedded coherently into the host lattice, i.e. no lattice mismatch is considered, which would cause strain fields. Though the model has been optimized for the simulation of nanocrystalline materials having fcc structure, e.g. the Co sublattice in $CoSi_2$, the physical behavior of other systems is supposed to behave at least qualitatively in the same manner.

In the computer simulations of Fig. 2 atoms are deposited into the simulation cell with a constant rate at random positions, a procedure which simulates ion implantation. Immediately after deposition each atom is allowed to diffuse and to react with other implanted atoms. The stages supersaturation, nucleation of precipitates and growth of them can be defined because only in stage II (see Fig.2) a remarkable increase in precipitate density has been found. However it should be mentioned that there is a complex interaction where statistical and dynamical processes as volume diffusion of impurity atoms, nucleation and interface kinetics interfere. For the (homogeneous) nucleation of a new precipitate a minimum level of supersaturation is needed in its vicinity, since the formation of dimers, trimers, ..., depends on the monomer concentration. According to classical nucleation theory small nanoclusters have to reach a critical size in order to become stable against dissolution [5]. This size corresponds to the maximum of their free energy to which bulk and surface atoms give different contributions. This means, that clusters being smaller than the critical size lower their energy by detachment events, while those being larger lower the energy by attaching additional monomers. The free energy associated with this critical size has, therefore, the meaning of an energy barrier for nucleation.

In order to see qualitatively during ion implantation the evolution of the critical radius of cluster nucleation, the Gibbs-Thomson relation for the equilibrium monomer concentration at the precipitate/matrix interface $c(R) = c_\infty \exp\{R_{\text{cap}}/R\}$ has to be considered. Here, R denotes the radius of the precipitate, R_{cap} is the capillarity length and c_∞ is the solidus concentration (i.e. the equilibrium concentration at a flat interface). Thus, the (smallest) size of a precipitate being in equilibrium with an averaged concentration $\bar{c}(t)$ is given by

$$R(t) = R_{\text{cap}} \ln\left\{\frac{c_\infty}{\bar{c}(t)}\right\}. \tag{1}$$

At the initial stage of IBS there is an increase of supersaturation (see Fig. 2) due to the continuous flux of implanted ions which causes the critical radius of stable clusters to decrease (stage I). At a sufficient level of supersaturation a random agglomeration of a few impurity atoms may reach the critical radius, i.e. stable nanoclusters can form (stage II). This newly formed clusters act as sinks for impurity atoms and lower, therefore, supersaturation (stage III). The lower plot of Fig. 2 shows the evolution of the critical radius obtained by Eq. (1). The formation of new clusters is strongly dependent on the monomer concentration and ceases during the late stage of implantation, when the monomer concentration is again below the nucleation threshold.

For the specific case of Co implantation into silicon the sequence of steps of buried layer formation is shown in Fig. 3. The six pictures, which correspond roughly to the scheme

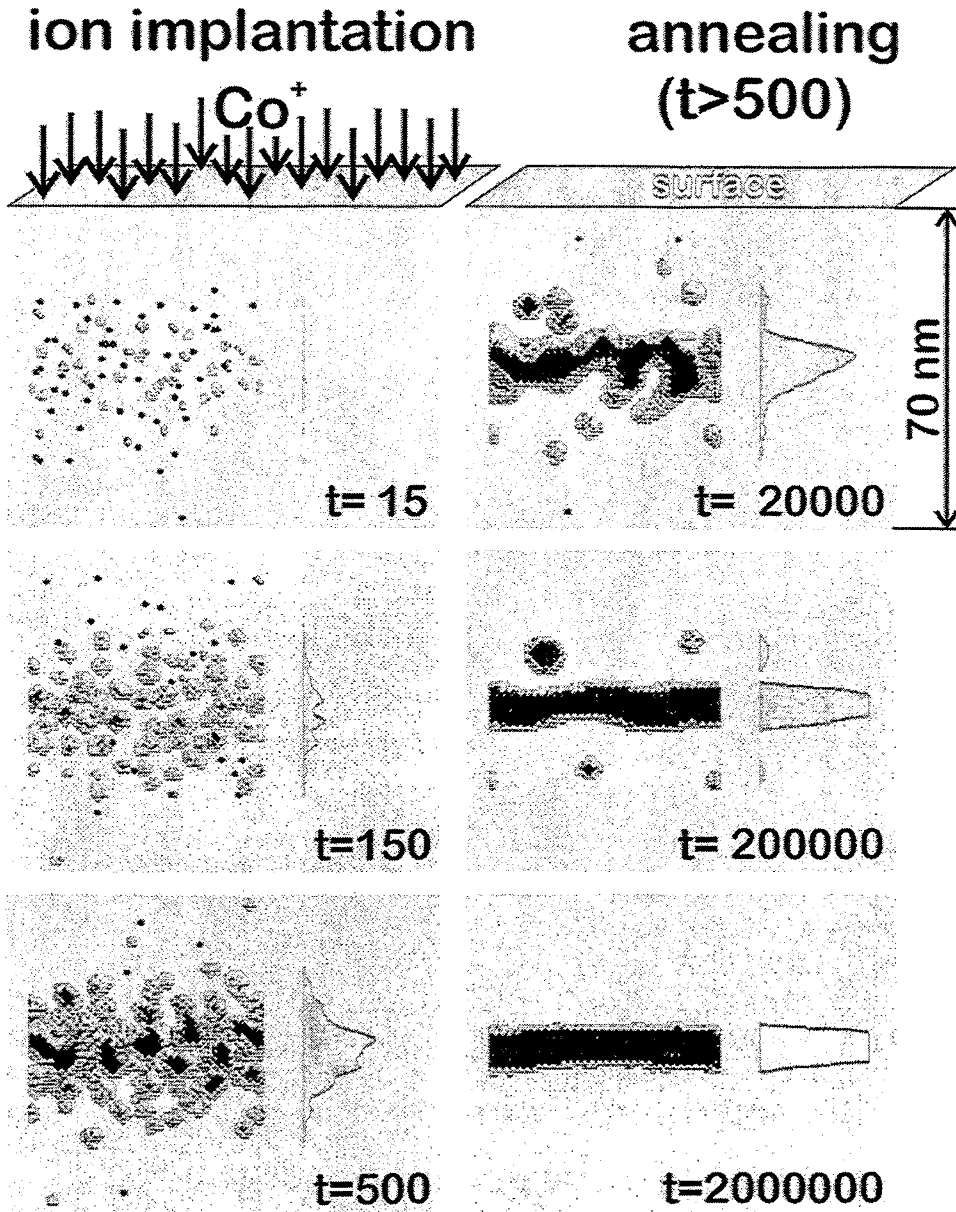

Fig. 3: Kinetic 3D MC simulation of IBS of a buried $CoSi_2$ layer in Si. Snapshots of the layer formation are given for different times (in arbitrary units). Only the Co atoms are made visible, the Si atoms are not shown for the sake of clarity. Additionally shown is the depth profile of the Co concentration which corresponds to an experimental SIMS profile. While the left column shows the formation and growth of the nanoclusters during ion implantation, the three pictures on the right illustrate coalescence and layer formation during annealing. Note, that a very smooth interface has formed.

of IBS given above, show the atomistic configurations in the simulation volume. Though models based on the numerical integration of diffusion-reaction equations describe Ostwald ripening more efficiently than MC simulations, they usually lack the possibility to handle nucleation and coalescence processes. Our new kinetic 3D lattice MC program allows for the first time a unified computer simulation of the whole process of ion beam

synthesis (ion implantation and annealing) including buried layer formation.

References

[1] S. Mantl, Mater. Sci. Rep. 8 (1992) 1
[2] M.A. Guerra, The status of SIMOX technology, Solid State Technol. 75 (1990)
[3] A.E. White, K.T. Short, R.C. Dynes, J.P.Gerno, J.M. Gibson, Appl. Phys. Lett. 50 (1987) 95
[4] T. Shimizu-Iwayama, K. Fujita, J. Appl. Phys. 75 (1994) 7779;
C.M. Yang, K.V. Shcheglov, M.L. Brongersma, A. Polman, H.A. Atwater, Mat. Res. Soc. Symp. Proc. 358 (1995) 181
[5] J.S. Langer, Solids far from equilibrium, edited by C. Godrèche (Cambridge University Press, 1992) p. 297

Evolution of Nanocluster Bands in Ge-Implanted Silicon Dioxide Films

J. von Borany, V. Borodin*, R. Grötzschel, K.H. Heinig, W. Matz, A. Mücklich, P. Nitzsche, L. Rebohle, B. Schmidt, W. Skorupa, M. Strobel, R.Yankov and I. Tyschenko**
* Kurchatov Institute Moscow, Russia
** Institute of Semiconductor Physics Novosibirsk, Russia

Light emission of semiconductors is one of the most widely investigated topics in advanced materials research due to its enormous potential for optoelectronic applications. For light emitting diodes, laser diodes or displays with high luminosity doped semiconductors based on III-V-group (GaAs, GaP, GaN) or II-VI-group (ZnS, SrS, $SrGa_2S_4$) materials are preferred because of the high probability for direct radiative transitions. Another challenge is the finding of a direct link between microelectronics and optoelectronics technology. As in the near future the development of microelectronics will rely on the use of silicon, materials and device structures will be favoured that are compatible with silicon processing. The discovery of visible photoluminescence (PL) from porous silicon has considerably stimulated the research in this field [1]. The emission of light in the red wavelength region is correlated with the properties of nanocrystalline silicon and can be explained by the quantum confinement model [2,3]. This model predicts an increased probability of radiative transitions in nanometer sized semiconductors and an emission wavelength maximum, which is inversely proportional to the nanocrystal size. PL and transmission electron microscopy (TEM) results confirm this correlation [4].

The thermal and chemical instability of porous silicon has led to the application of various alternative methods for the fabrication of nanocrystalline semiconductors. Among them the formation of silicon or germanium nanoclusters embedded in a silicon dioxide matrix is of particular interest, as SiO_2 is the standard insulating and passivating material in microelectronics technology. Two preparation methods are favoured: ion implantation into thermally grown SiO_2-layers [5,6] or sputtering of Si- or Ge- enriched silicon dioxide [7,8]. Recent studies have demonstrated the possibility of achieving strong blue and violet photoluminescence from silicon- or germanium-rich SiO_2-layers produced by ion beam synthesis [9,10].

For the purpose of electroluminescense the microstructure of ion beam synthesized Si- and Ge-rich SiO_2 layers has to be considered in detail. The electrooptical properties of electroluminescing device structures are expected to be a function of the depth distribution of the embedded nanoclusters, but from previous cross-section TEM investigations no significant information is available. Therefore, we have performed experiments to investigate the microstructure of Ge nanoclusters in SiO_2 after implantation and annealing using X-ray diffraction (XRD), transmission electron microscopy (TEM) and Rutherford backscattering spectrometry (RBS). Germanium has been used to obtain a better resolution contrast with respect to the surrounding SiO_2 matrix.

Thermally grown, 120 nm or 500 nm thick SiO_2 films on (100) oriented 2" silicon wafers (5 -10 Ωcm) have been implanted with $^{74}Ge^+$ ions to achieve an atomic Ge fraction of about 4 at% at the maximum of the implanted profile. Different implantation conditions have been used depending on the oxide thickness d_{ox} . A single implantation step at 110 keV to a dose of $2x10^{16}$ cm^{-2} has been employed for samples with d_{ox} =120 nm. In order to obtain a broader implant region in samples with d_{ox} =500 nm, double-step implantation has been carried out

at 350 keV, 2.8×10^{16} cm^{-2} and then at 200 keV, 1.8×10^{16} cm^{-2}. The substrate temperature has been maintained at about -140 °C to avoid any redistribution of the implanted species. After implantation different samples have been furnace annealed between temperatures of 400 °C and 1100 °C for 60 min in a dry nitrogen ambient.

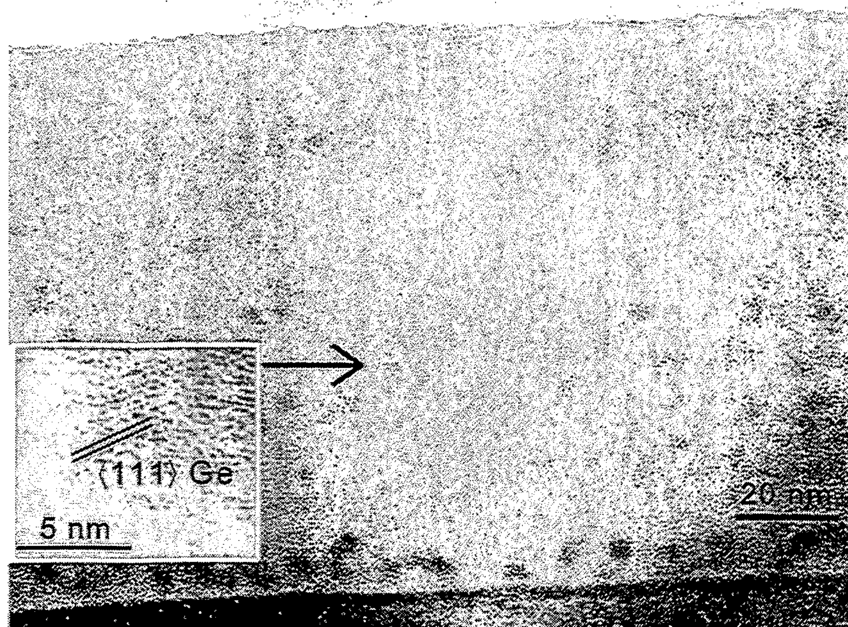

Fig. 1: Cross-sectional TEM micrograph of the SiO_2 layer (d_{ox}=120 nm) after implantation with ^{74}Ge, 110 keV, 2×10^{16} cm^{-2} and annealing at 1000 °C, 60 min. The Ge clusters are characterized by the dark spots. The SiO_2/substrate interface is at the bottom.
Inset: a high resolution TEM micrograph showing the crystal structure of one Ge nanocluster.

Fig. 1 shows a cross-sectional TEM micrograph of the Ge-implanted sample with d_{ox}=120 nm annealed at 1000°C for 60 min. The dark areas in the image are related to Ge clusters. The presence of additional Ge atoms "dissolved" in the matrix cannot be ruled out, as TEM-contrast imaging requires a minimum cluster size of $\geq$ 2 nm. The cluster depth distribution does not follow the initial Gaussian-like implantation profile ($R_p \approx$ 75 nm). Additional bands of Ge-precipitates are clearly observed on both sides of the implanted profile near the surface and the SiO_2/Si interface. The presence of Ge inside these bands has been confirmed by EDX. The mean cluster diameter in the band near the Si/SiO_2 interface is about 6 nm. The cluster-containing band in the region of the initial implantation maximum can either be interpreted as a region of lower density of larger clusters or as a stack of clusters located at different depths. The evolution of Ge cluster bands is an unexpected result as the diffusivity of both Si and Ge in thermally grown SiO_2 is assumed to be very low. Therefore, no significant redistribution of the implanted species in the oxide layer is expected. Using the high resolution mode of the microscope (HRTEM) the crystalline structure of single clusters has been confirmed. The inset to Fig.1 shows a HRTEM image of an isolated Ge cluster where the Ge (111) lattice planes are seen. The distance between these planes is determined to be 3.45 Å, which is by 6% larger than that of bulk germanium (3.23 Å).

More precise information about the mean cluster size has been obtained from XRD measu-

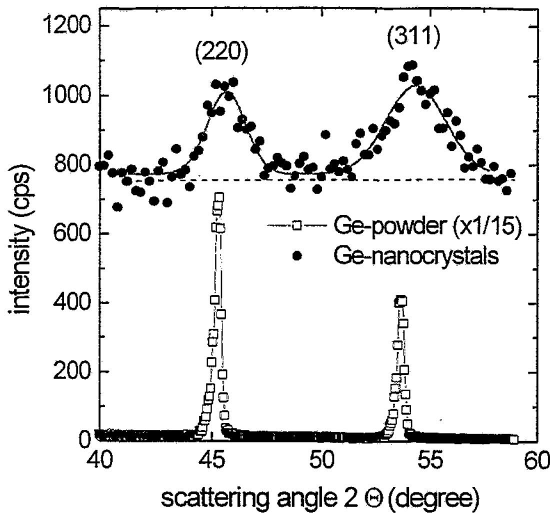

Fig. 2: XRD pattern of Ge nanocrystals in the region of the (220) and (311) Bragg reflections, compared with the pattern of pure Ge powder.

rements on annealed samples (1000 °C,60 min) with an oxide thickness of 500 nm (Fig. 2). The (111) Ge, (220) Ge and (311) Ge Bragg reflections are clearly detectable (Fig. 2). The observation of the Bragg reflections indicates that germanium exists in a single crystalline state and the crystals are randomly oriented. From the peak width the mean nanocrystal size has been estimated to be (6±1) nm neglecting the stress related peak broadening. The measured mean cluster diameter is in good agreement with the values reported in the work of Yang *et al.*[4]. The lattice constant of Ge using the peak centroid position has been found to be 5.63 Å, which deviates by less than 1% from the tabulated value for Ge powder. This closer aggreement compared to HRTEM may be due to the averaging procedure of XRD analysis which collects representative information from the whole Ge-containing layer.

RBS measurements using 1.2 MeV He^+ ions have been performed for as-implanted and annealed samples to follow the redistribution process as a function of annealing temperature. The results for both systems with d_{ox} =120 and d_{ox} =500 nm are shown in Figs. 3a and b, respectively. For the depth calibration of the RBS spectra a constant atomic density of 6.8×10^{22} cm^{-3} in the SiO_2 matrix is assumed. The stoichiometry deviation due to the implanted germanium is less than 3%.

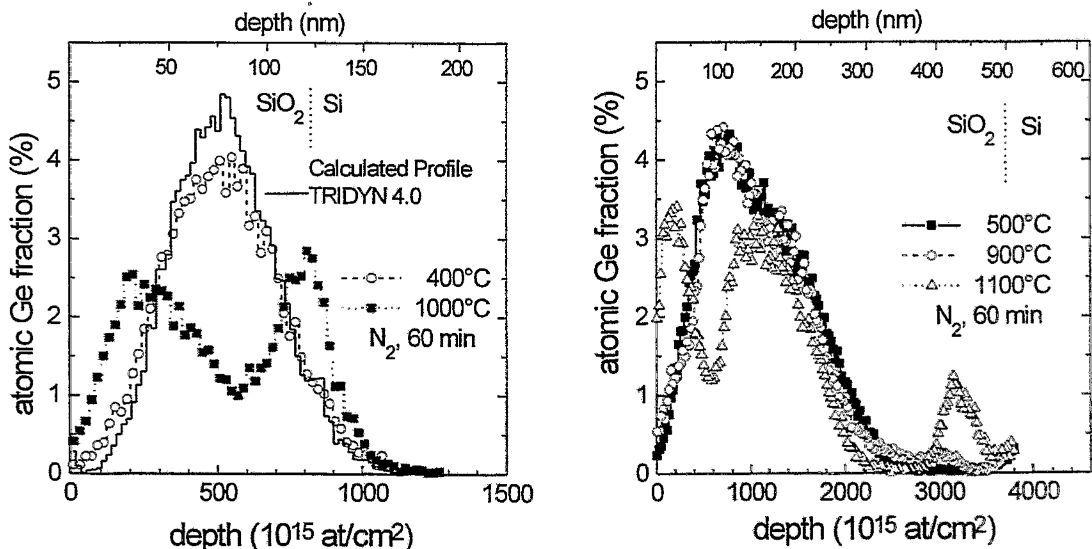

Fig. 3: Depth profiles of the atomic Ge fraction in Ge-implanted SiO_2-layers measured by RBS:
(i) $^{74}Ge^+$, 110 keV, 2×10^{16} cm^{-2}, d_{ox} =120 nm (left),
(ii) $^{74}Ge^+$, 350 keV, 2.8×10^{16} cm^{-2} + 200 keV, 1.8×10^{16} cm^{-2}, d_{ox} =500 nm (right).
The samples were finally furnace annealed between 400 °C and 1100 °C, 60 min in a dry nitrogen ambient.

The measured as-implanted Ge distribution is in good agreement with the profile calculated using the *TRIDYN* code. No Ge redistribution is observed for annealing temperatures up to 800 °C, while at 900 °C first changes occur in the Ge profile (Fig. 3b). At higher temperatures the enhanced redistribution of Ge leads to the development of new peaks in the Ge depth profile in the vicinity of the SiO_2/Si-interface and the surface (Figs. 3a, b). This process is thermally driven, whereby the evolution of the Ge profile seems to be also a function of the distance between the as-implanted peak and the above mentioned boundaries. The redistribution towards the boundary with the smaller distance to the initial implantation maximum is favoured.

A first attempt of a quantitative theoretical study will be presented to explain the observed Ge redistribution. The tendency of implanted Ge atoms to form a multimodal depth distribution rules out that pure diffusion is the driving force. Our approach follows comprehensive simulations of nucleation, growth and Ostwald ripening which have been recently applied to describe the evolution or precipitates during ion beam synthesis of buried layers in silicon [11].

Under conditions similar to the current experiment it was found for an oxygen implantation into silicon, that, despite of the strong depth variation of the oxygen concentration, the mean size of SiO_2 pricipitates is constant across the implantation profile [12]. Recent kinetic 3D lattice Monte Carlo simulations have proven that the formation of precipitates having a mean size independent of the level of supersaturation is a rather general behaviour of nucleation and growth [13]. This result can be illustrated by a simple consideration: Since the nucleation rate I_n increases with supersaturation c_s , more tiny precipitates are formed in the center of the implantation profile than in the tails. Assuming a linear relation $I_n \sim c_s$ we estimate for the density of nucleated precipitates $N_{pr} \sim c_s$. The tiny precipitates act as sinks for the supersaturation and have to share the available supersaturated momomers among themselves. The mean volume V_a from which a precipitate can absorb supersaturated momomers is larger in the tails than in the center region where N_s is higher. More precisely, $V_a \sim 1/N_{pr}$ and, therefore, $V_a \sim 1/c_s$. The average number of monomers n_m absorbed by a precipitate is $n_m = V_a \; x \; c_s = const.$ Thus, the mean nanocluster size should be independent of supersaturation and constant across the implantation profile. If I_s increases nonlinearly with c_s (as predicted by classical nucleation theory), the mean nanocluster radius should be even larger in the tail regions.

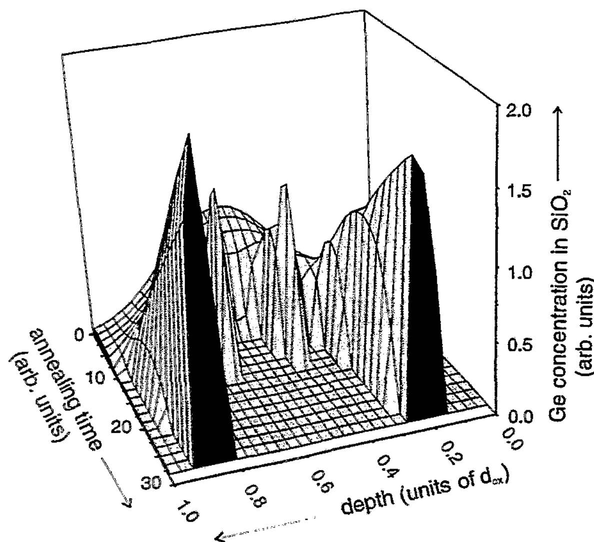

Fig. 4: Evolution of a bimodal Ge depth distribution due to Ostwald ripening from a Gaussian-shaped implantation profile assuming 5% larger precipitates in the tails of the profile (0 - surface; 1 - SiO_2/Si interface)

Let us assume that the radius in the tail regions is only 5 % larger than in the center of the profile. Such a nanocluster size distribution has a tremendous consequence for the Ostwald ripening process which follows nucleation and growth at the initial stage of annealing. Fig. 4 shows the dependence of the concentrati-

on of Ge in SiO_2 on annealing time and depth predicted by a rate equation based modelling of Ostwald ripening [14]. Due to the strong similarity to this calculation, the bimodal Ge depth distribution in the 120 nm thick SiO_2 layer (Fig. 3a) could result from an initial nanocluster size distribution as it has been used for the calculation of Fig. 4.

The Ge redistribution in the 500 nm thick SiO_2 layer (Fig. 3b) seems to be more complex, especially the evolution of the Ge peak at the inner Si/SiO_2-interface outside the implantation profile requires additional driving force mechanism. As the evolution of equal-sized precipitates depends very sensitive on any inhomogeneity, regions of preferred nucleation (e.g. due to defects) or interfaces/surfaces acting as Ge sinks could induce strong Ge redistributions too.

The first direct evidence for the appearance of bands containing nanocrystalline germanium clusters within a SiO_2-matrix is of significant importance for the optimized design of electro-luminescing layers. The results obtained are also important from a fundamental point of view as they demonstrate that Ostwald ripening can occur in materials with low diffusion rates.

References

[1] L. Canham, Appl. Phys. Lett. 57 (1990) 1046

[2] L.E. Brus, IEEE J. Quantum Electronics QE-22 (1986) 1909

[3] T. Takagahara, K. Takeda, Phys. Rev. B46 (1992) 15578

[4] C.M. Yang, K.V. Sheglov, M.L. Brongersma, A. Polman, H.A. Atwater, Mat. Res. Soc. Symp. Proc. 358 (1995) 181

[5] H.A. Atwater, K.V. Sheglov, S.S. Wong, K.J. Vahala, R.C. Flagan, M.L.Brongersma, A. Polman, Mat. Res. Soc. Symp. Proc. 283 (1994) 409

[6] J.B. Khurgin, E.W. Forsythe, S.I. Kim, B.S. Sywe, B.A. Khan, G.S. Tompa, Mat. Res. Soc. Symp. Proc. 358 (1995) 193

[7] K. Kohno, Y. Osaka, F. Toyomura, H. Katayamas, Jpn. J. Appl. Phys. 33 (1994) 6616

[8] S. Yoshida, T. Hanada, S. Tanabe, N. Soga, Jpn. J. Appl. Phys. 35 (1996) 2694

[9] W. Skorupa, R.A. Yankov, I.E. Tyschenko, H. Fröb, T. Böhme, K. Leo, Appl. Phys. Lett. 68 (1996) 2410

[10] L. Rebohle, I.E. Tyschenko, H. Fröb, K. Leo, R.A. Yankov, J. von Borany, G.A. Kachurin, W. Skorupa, submitted to Microelectr. Eng.

[11] S. Reiss, K.H. Heinig, Nucl. Instr. and Meth. B84 (1994) 229, ibid. B102 (1995) 226, ibid. B112 (1996) 223

[12] R. Weber, R. Yankov, R. Müller, W. Skorupa, S. Reiss, K.H. Heinig, Mat. Res. Soc. Symp. Proc. 316 (1994) 729

[13] M. Strobel, K.H. Heinig, to be published

[14] V. Borodin, K.H. Heinig, S. Reiss, submitted to Phys. Rev. B

Acoustic Waves Induced by a Focused Ion Beam

J. Teichert, L. Bischoff and B. Köhler*
*Fraunhofer-Institute for Nondestructive Testing, Branch Lab Dresden, Germany

Intensity-modulated beams of electrons, ions, or photons incident on a solid may produce acoustic waves. Scanning electron acoustic microscopy [1], scanning laser acoustic microscopy [2], and scanned photoacoustic microscopy [3] have become widely used characterization techniques. The application of ions for that purpose is rather rare and the ion-acoustic effect (IAE) has been less investigated so far. Studies of this effect were performed with MeV protons by Sieger and Lefevre [4,5], with keV ions in a SIMS device by Satkieviez *et al.* [6,7], and with keV ions in an ion implanter by Kimura *et al.* [8] and by Rose *et al.* [9]. More recently, investigations with pulsed ion beams in the MeV and keV energy range were performed by Deemer *et al.* [10,11].

The IAE is an attractive method for in situ characterization during ion beam processes. Especially the utilization of the IAE in focused ion beam (FIB) systems would increase the amount of information from the examined specimen [12]. Systems with ion beam spot sizes of some tens of nanometers have now attained a high standard in performance and they are widely applied to analyse, repair, and modify device patterns in microelectronic circuits. For analysis, currently used FIB systems with secondary electron or ion detection systems allow a near surface imaging only. An alternative ion-acoustic imaging system would be of great advantage to provide information on subsurface structures. Nevertheless, acoustic wave generation using FIBs has not been examined so far. The main reason is the small ion current. Therefore, the aim of the experiments presented in this paper was to investigate the generation of acoustic wave signals and their possible use for imaging or material characterization in future.

The main generation mechanism of elastic waves in metals and semiconductors is the so-called thermal wave coupling. A schematic picture of this process is given in Fig. 1. The intensity-modulated ion beam which strikes the solid surface causes a periodic temperature change in the volume in which the beam energy is dissipated. This region is the source of a thermal wave.The thermal wave is exponentially damped within a scale characterized by the diffusion length μ. Local thermal expansion and stress are the source of the elastic wave generated in this volume. The spatial resolution of the method is determined by the thermal diffusion length μ being a function of thermal properties and the modulation frequency f. At f=1 MHz typical values of μ are in the range of some μm.

The experiments were carried out with the FIB system IMSA-100 at the Research Center Rossendorf [13]. A schematic view of the experimental setup is shown in Fig. 2. The ion optical column was used without further modification, only an additional intensity modulation of the beam was necessary. In the experiments the existing blanking unit allows frequencies up to 10 MHz with a duty cycle of about 1:1. The essential supplement consists of an ultrasonic sensor and the attached electronics, using a lock-in amplifier. For the investigations, a 35 keV gallium ion beam of 3 nA with a spot size of about 300 nm has been applied.

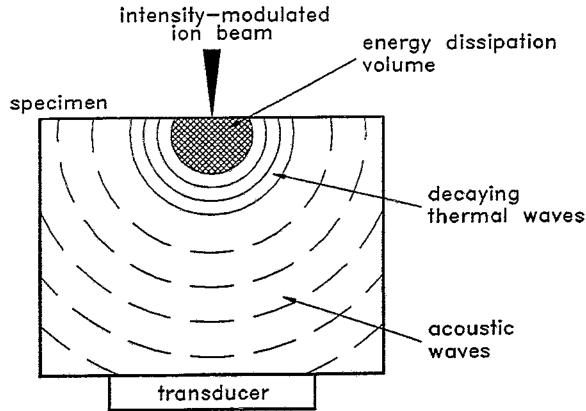

Fig. 1: Schematic picture of the ion-acoustic effect.

A special piezoelectric sensor with an integrated pre-amplifier, which also acts as a band-pass filter, was developed. Its transmission maximum is at about 100 kHz with a 3 dB band width of 100 kHz. The amplification factor is 25.000. A plate of lead zirconium titanate (PZT) with a diameter of 24 mm and a thickness of 1mm serves as transducer. Pre-amplifier and transducer are mounted inside a cylindrical box of stainless steel. This sensor was attached to an aluminium target for the ion beam irradiation.

Acoustic wave signals were detected when the ion beam was incident on the sensor housing as well as on the Al strip. The maximum input signal amplitude measured at the pre-amplifier was 120 nV. Typical values were in the range of 20 nV. In spite of proper shielding a background signal of about 4 nV was present due to electric crosstalk. The integration time of the lock-in amplifier was chosen between 1 and 60 s. For integration times below 1 s the noise level was excessively high.

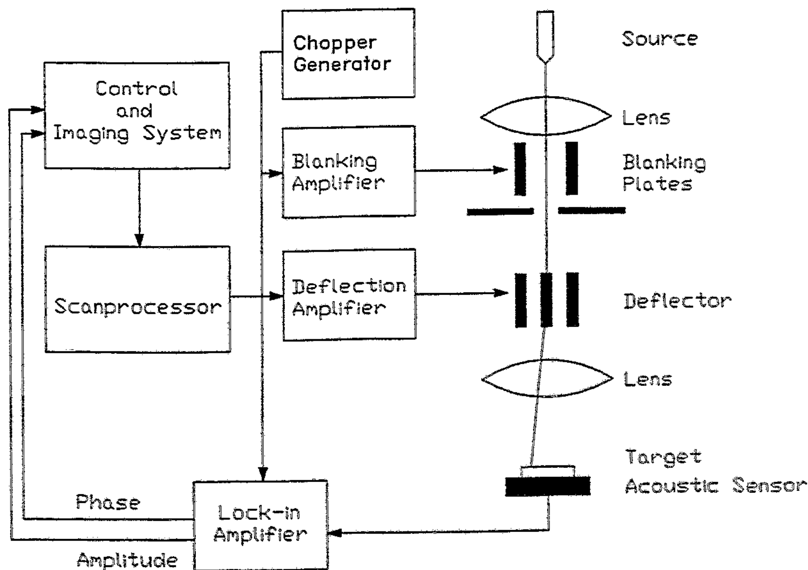

Fig. 2: Schematic view of the experimental arrangement.

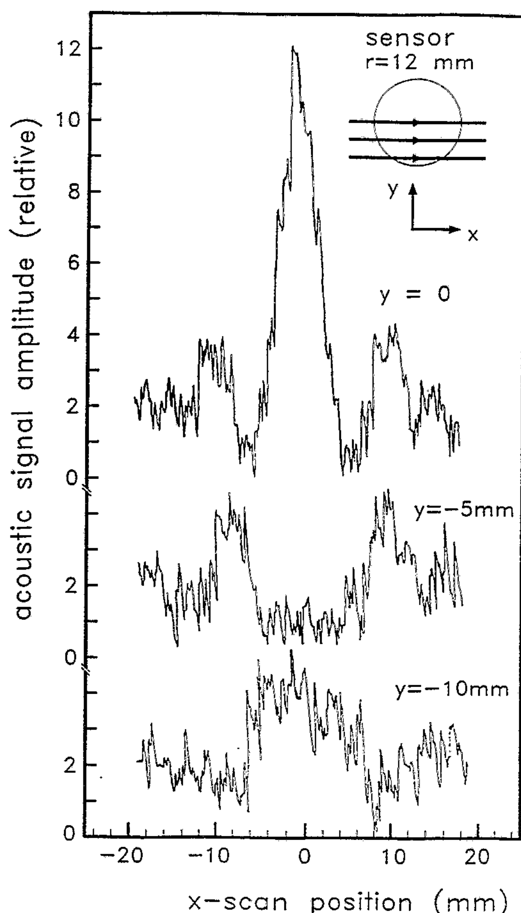

Fig. 3:
Amplitude signal of the ion-acoustic response vs FIB position for line scans across the sensor. The position of the line scans with respect to the sensor is shown in the inset. The sensor center corresponds to the origin of the scan coordinate system.

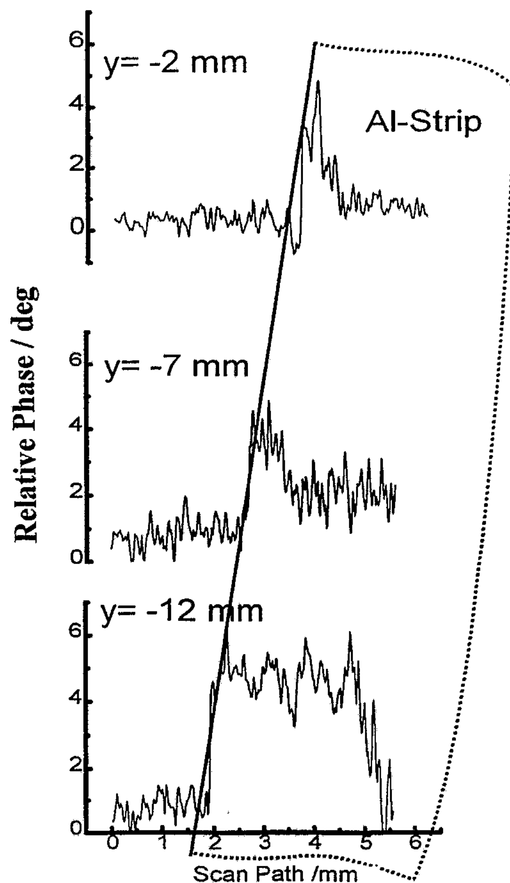

Fig. 4:
Phase signal of the acoustic response as a function of FIB position . Line scans across the Al stripe edge.

The main attention was focused on the question whether the measured signals are of ultrasonic origin or an electrical effect of the ion beam induced current itself. Possible reasons are a direct electrical crosstalk due to an imperfect shielding of the sensor housing or an electric stimulation of the piezoelectric transducer. Results which allow to distinguish between an electric stimulation of the piezoelectric transducer and an ion acoustic response are shown in Fig. 3. The ion beam was scanned along lines across the sensor surface without a sample on it. The detector signals were measured as a function of beam position at a frequency of 61 kHz which is the resonance frequency of a bending oscillation of the transducer plate. The measurement reveals distinct peaks in the signal amplitude demonstrating the position dependence of the excitation efficiency of the transducer. Bending oscillations of the transducer form circular standing waves with coaxial rings of nodes and waists. When the ion irradiation is located at a node this resonance is not excited. The vibration attains its maximum when the stimulation takes place at a waist. This locally varying excitation efficiency of the coaxial elastic standing wave is clearly visible in the experimental result. The maxima are located at the centre and at a circle with about

10 mm radius whereas a node is at about 5 mm radius. Therefore the curve measured at y = 0 shows three peaks and two minima. In good agreement the second curve at y = -5 mm has two peaks and a minimum around x = 0 corresponding to the node at r = 5 mm. The third curve at y = -10 mm shows one peak caused by the outer vibration ring. This observed position dependence of the excitation can only occur if the transducer is mechanically stimulated by an elastic wave.

Fig. 4 presents the results of three line scans crossing the edge of the Al stripe which is glued on the stainless-steel surface of the detector housing. The edge position is clearly visible in the presented phase signal by a phase jump of about 4 degree. We assume that this phase jump is caused by surface topology rather than by a change of the material properties. The width of the Al stripe is 3 mm as it is also visible in the lowest curve (y = - 12mm). The smaller width observed in the phase signal of the other two line scans cannot be explained so far. The measured phase jumps are another proof that the measured signals are of ion acoustic nature.

More systematic studies are required in order to understand in which way sample material and structure affect phase and amplitude of the acoustic signal. At present, the limit for such investigations is the long integration time of the lock-in amplifier due to the low detector signals. One line scan requires several minutes. Therefore the piezoelectric sensor, amplifier and registration electronics must be improved. Stronger signals and a better signal-to-noise ratio would allow full 2D-imaging with high lateral resolution as well as more extensive studies of the influence of material properties on the acoustic signal.

References

[1] L.J. Balk, Adv. Electron. Electron Phys. 71 (1988) 1
[2] L.W. Kessler, D.E. Yuhas, Proc. IEEE 67 (1979) 526
[3] Y.H. Wong, R.L. Thomas, G.F. Hawkins, Appl. Phys. Lett. 32 (1978) 538
[4] G. E. Sieger, H.W. Lefevre, Appl. Phys. Lett. 44 (1984) 28
[5] G. E. Sieger, H.W. Lefevre, Phys. Rev. 31 (1985) 3929
[6] F.G. Satkiewicz, J.C. Murphy, L.C. Aamodt, J.W. Maclachlan, Rev. of Prog. on QNDE 5A (1986) 455
[7] F.G. Satkiewicz, J.C. Murphy, J.W. Maclachlan, L.C. Aamodt, Rev. of Prog. on QNDE 6A (1986) 759
[8] K. Kimura, K. Nakanishi, A. Nishimura, M. Mannami, Jpn. J. Appl. Phys. 24 (1985) L449
[9] D.N. Rose, H. Turner, K.O. Legg, Can. J. Phys. 64 (1986) 284
[10] B.C. Deemer, J.C. Murphy, T.N. Claytor, J.R. Tesmer, Rev. of Prog. on QNDE 11 (1992) 2147
[11] B.C. Deemer, J.C. Murphy, T.N. Claytor, J.R. Tesmer, J.B. Spicer, Rev. of Prog. on QNDE 12 (1993) 995
[12] J. Teichert, L. Bischoff, B. Köhler, Appl. Phys. Lett. 69 (1996) 1544
[13] L. Bischoff, J. Teichert, E. Hesse, D. Panknin, W. Skorupa, J. Vac. Sci. Technol. B12 (1994) 3523

Dose Distribution for Plasma Immersion Ion Implantation into 3D-Objects

S. Mändl, H. Reuther, J. Brutscher and R. Günzel

Plasma immersion ion implantation (PIII) is a viable alternative technique to conventional beam line implantation where the whole surface of complex shaped objects is implanted simultaneously [1], thereby circumventing a target manipulation system and reducing costs. Negative high voltage pulses are applied to a target immersed in a plasma. During these pulses the plasma sheath, separating the plasma and the workpiece, is expanding and the implanted ions are accelerated through this sheath to the target. Applications for semiconductor processes [2] and, especially, hardening of austenitic stainless steels by nitrogen implantation [3] have been demonstrated. The dose distribution for non-planar tools can be determined after the implantation by analytical methods [4] or by self-consistent computer simulations calculations [5]. However, these calculations are prohibitively time consuming and have limitations in predicting the flux distribution for pulse lengths larger than a few microseconds.

Therefore, a method was developed which allows the calculation of the dose distribution on standard PCs, using two approximations for reducing the computing time [6]. The continuous plasma sheath evolution was replaced with snapshots of the sheath edge at discrete times and, additionally, a homogeneous charge density in the sheath was assumed.

For comparison with the calculation, three cylinders – representing drills – were treated with nitrogen PIII and subsequently analyzed with Auger electron spectroscopy (AES) sputtering depth profiling. The dose was determined from the relative intensities of the Al(KLL) and N(KLL) Auger peaks. No oxygen or carbon contaminations were found. The cylinders with a height of 37 mm and a diameter of 4, 6, and 8 mm were attached with good thermal and electrical contact onto the copper target holder with a diameter of 52 mm and a height of some 20 cm, positioning the samples in the center of the spherical 40 cm chamber. Aluminum foil with a thickness of 0.25 mm, cleaned in an ultrasonic bath with acetone and ethanol, was fastened around the cylinders. Nitrogen gas was used at a working pressure of 2×10^{-3} mbar in the UHV chamber (base pressure better than 10^{-6} mbar). The plasma was generated with an electron cyclotron resonance (ECR) source at 360 W mounted at the top of the chamber. Using a Langmuir probe, a plasma density $n_o = 6\times10^9$ cm^{-3} and an electron temperature kT_e = 2 eV were measured just above the target holder. The high voltage U_o = 30 kV was pulsed with a tetrode hard tube switch [7], resulting in a rise time of less than 1 µs and a total pulse length of 10 µs. The exponential decay time of the pulse was 2 µs, resulting in a negligible flux contribution.

Instead of a self-consistent three-dimensional sheath evolution, the sheath evolution was calculated for a one-dimensional cylindrical symmetry, thereby reducing the computing time substantially. Then the potential distribution was approximated for the three-dimensional plasma sheath with rotational symmetry for three discrete times during the pulse. With the obtained electric field, representative ion trajectories were calculated and used for determining the ion dose distribution at the samples.

The time evolution of the sheath edge x at a given voltage $-U_o$ assuming the validity of the Child-Langmuir law [8], i.e. a collisionless ion transit through the sheath, can be described [9] by the equation

$$\frac{dx}{dt} = \frac{4\varepsilon_o U_o^{3/2}}{\mu(t) n_o \cdot 9\beta^2 x^2}\sqrt{\frac{2}{eM}} - \nu(t) v_B, \qquad (1)$$

where M, e, ε_o, and $v_B=(kT_e/M)^{1/2}$, are the ion mass, the elementary charge, the free-space permittivity, and the ion acoustic sound velocity, respectively. $\beta(x)$ is a factor which must be

included for the cylindrical Child-Langmuir law [10]. $\mu(t)$ and $\nu(t)$ are dimensionless coefficients between 0.6 and 1, describing the response of the presheath. During the pulse, the value of $\mu(t)$ decreases to 0.6 and $\nu(t)$ increases to 1 as a new presheath is established.

The three-dimensional potential distribution with rotational symmetry was then calculated with a constant charge density n_c in the sheath by solving Poisson's equation using a set of finite-difference equations solved with the successive over-relaxation method [11]. The charge density was adjusted using the sheath widths at $t = 0^+$ (i.e. at the end of the voltage pulse rise), 3.5, and 8 μs from eqn. (1) at the bottom of the sample holder, truncated in the calculation at 2 cm, where a one-dimensional cylindrical approximation is allowed. This theoretical width is indicated in Fig. 1 with the arrow. Furthermore, the distorted spherical sheath around the 8 × 37 mm cylinder on the sample holder is shown for $t = 0^+$ μs. The distortion is more distinct near the surface, as can be seen from the equipotential lines plotted at a distance of 2 kV. Near the convex edges of the cylinder and sample holder large electric fields are present, limiting the maximum plasma density or the voltage to avoid electric breakdown and subsequent arcing [12].

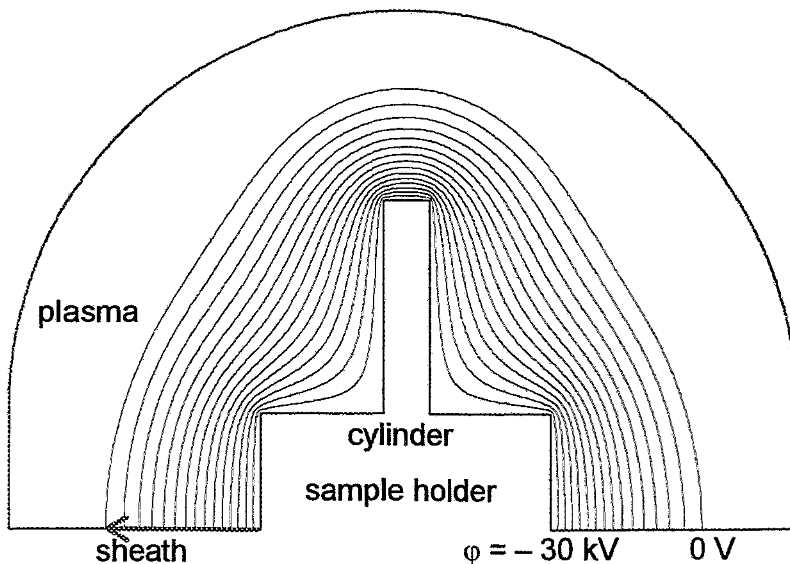

Fig. 1: Potential distribution in the plasma sheath calculated for the 8 mm cylinder. The distance between the equipotential lines is 2 kV. The arrow indicates the sheath width determined with a one dimensional model [9] for cylindrical symmetry, which was used for adjusting the charge density in the sheath.

Selected ion trajectories were calculated by integrating the equation of motion. The time step used in this procedure was adjusted inversely to the ion speed, thereby reducing the computing time. The final energy was within 1% of the expected energy of 30 keV, limited by the finite grid size of 0.5 mm in the potential and field calculations and the finite time step. Finally the dose distribution, composed of the ions uncovered by the expanding sheath and the ions entering the sheath from the presheath, is obtained by mapping the areas onto the target surface.

The calculated sheath contours for the three cylinders are shown in Fig. 2 for three different times (0^+, 3.5, and 8 μs). As can be seen, the sheath is nearly stationary after 3.5 μs, with a width, increasing for the larger cylinders, between 3 and 4 cm in the center. As the radius of the target holder with 26 mm is larger than that of the samples, the sheath edge follows not the side wall of the cylinder. Instead, it recedes at an angle of nearly 45° from the top.

The total ion dose for all the cylinders is shown in Fig. 3. The agreement between the calculated and measured dose is good. Some common features can be observed in all figures.

The dose exhibits always a maximum on the top, with a pronounced drop for position 2 and gradual decease for the last three positions. This decrease can be explained by the opposite consequence of a larger sheath, leading to more ion flux, and a smaller area of the sheath edge projected onto the target. The maximum on the top is due to the large curvature of the sheath edge in the center, focusing the ions onto the top and depleting the upper side wall.

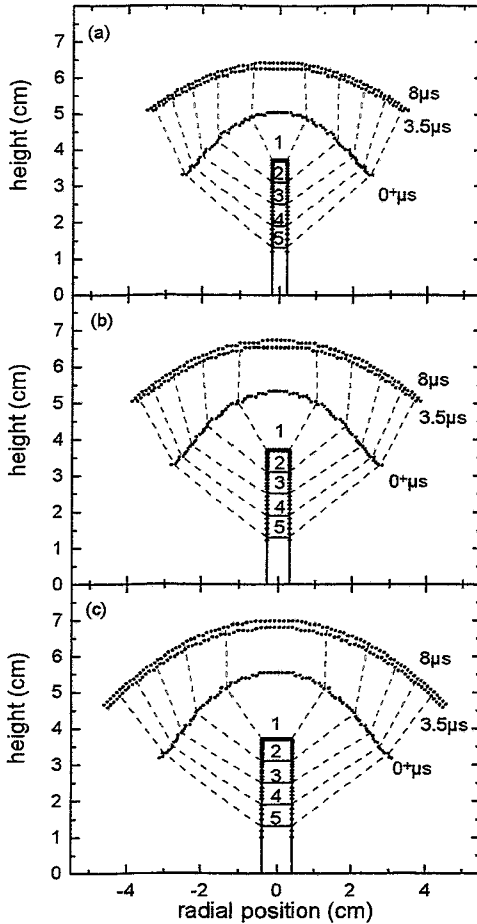

Fig. 2:
Sheath contours around the three cylinders at three different times 0^+, 3.5, and 8 µs after the start of the pulse. The numbers 1 to 5 indicate the positions where the dose was measured with 1 at the top and 2 – 5 at the side wall. The dashed lines separate the regions from which the ions are implanted in the numbered positions; (a) 4 mm, (b) 6 mm, and (c) 8 mm diameter.

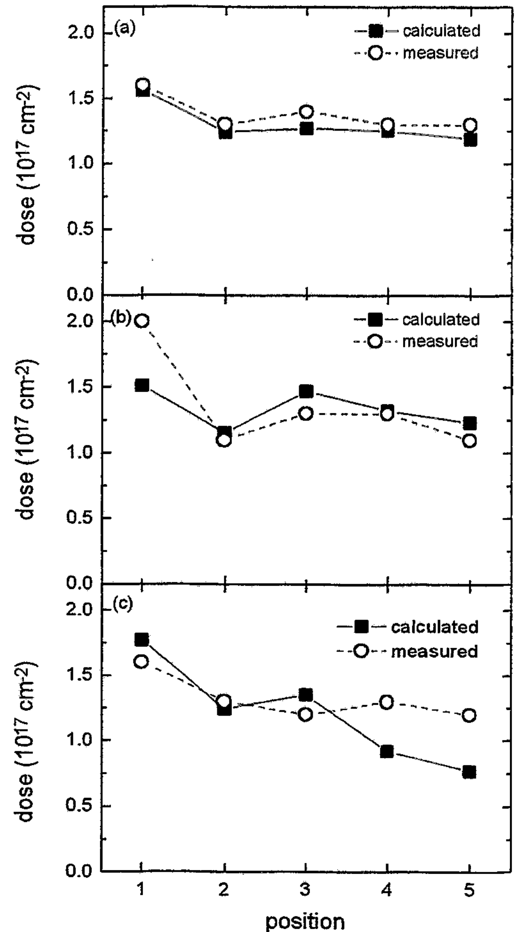

Fig. 3:
Comparison of the calculated dose and the dose as measured with AES for different points along the surface of the (a) 4 mm, (b) 6 mm, and (c) 8 mm diameter cylinder. The numbers correspond to the positions indicated in Fig. 2.

A method, approximating the continuous sheath evolution with snapshots of the contour at discrete times, was used for calculating the spatially varying ion dose for plasma immersion ion implantation in small cylinders, representing drills. Good agreement was found when comparing the calculated doses and the distribution measured with AES depth profiling. Using this method, it is possible to substantially reduce the computing time, thereby allowing several test runs for different geometries of the target holder or plasma parameters to optimize the dose distribution for the specific applications.

Acknowledgments

S. Mändl is supported by Bundesministerium für Forschung und Technologie Research Contract No. 13N6443. E. Quaritsch and C. Schönjahn are acknowledged for technical assistance.

References

[1] J. Conrad, J.L. Radtke, R.A. Dodd, F.J. Worzala, N.C. Tran, J. Appl. Phys. 62 (1987) 4591
[2] N.W. Cheung, W. En, E.C. Jones, C. Yu, Mat. Res. Soc. Symp. Proc. 279 (1993) 297
[3] M. Samandi, B.A. Shedden, O.I. Smith, G.A. Collins, R. Hutchings, J. Tendys, Surf. Coat. Technol. 59 (1993) 261
[4] J. Hartmann, W.Ensinger, R.W. Thomae, H. Bender, A. Königer, B. Stritzker, B. Rauschenbach, Nucl. Instrum. Meth. B112 (1996) 255
[5] M.W. Kissick, M.P. Hong, M.M. Shamin, J.D. Callen, J.R. Conrad, G.A. Emmert, J. Appl. Phys. 76 (1994) 7616
[6] S. Mändl, H. Reuther, J. Brutscher, R. Günzel, W. Möller, Surf. Coat. Technol. (in press)
[7] J. Brutscher, Rev. Sci. Instrum. 67 (1996) 2621
[8] C.D. Child, Phys. Rev. 32 (1911) 492
[9] S. Mändl, J. Brutscher, R. Günzel, W. Möller, to be published
[10] I. Langmuir and K.B. Blodgett, Phys. Rev. 22 (1923) 347
[11] Los Alamos Accelerator Code Group, The Poisson/Superfish group of codes, LA-UR-96-1834, LANL (1996)
[12] S. Mändl, J. Brutscher, R. Günzel, W. Möller, J. Vac. Sci. Tech. B14 (1996) 2701

In-situ ERDA Studies of Nitrogen Implantation into Amorphous Carbon

S. Grigull *, D. Henke, C. Spaeth ** and A. Mücklich
* Also at Max-Planck-Institut für Plasmaphysik, Garching bei München
** Institut für Physik, TU Chemnitz-Zwickau

A crossed-beam experiment is reported allowing *in-situ* depth profiling of light elements during the implantation of keV ions into different materials. The novel setup is used for investigations of the nitrogen-inventory buildup and saturation in nitrogen-implanted carbon films. In the context of the possible formation of the hypothetical carbon-nitride phase $\beta-C_3N_4$ [1], recent implantation experiments showed that maximum [N]/[C] ratios of 0.3 ...0.35 are achieved through nitrogen implantation into different forms of carbon [2, 3]. The focus of the present work is on the mechanism leading to the nitrogen reemission and saturation observed at large implantation fluences.

A sketch of the experiment is given in Fig. 1. Mass-analyzed 20 keV N^+ ions from an ECR ion source [4] are directed at a slightly off-normal angle onto the sample mounted on a heatable target holder. Ion fluxes of typically $1x10^{14} N^+ cm^{-2}s^{-1}$ are provided by the defocussed beam, the irradiated area being of the order of 1 cm^2. Due to the high stability of the ECR ion source, no online current monitoring is necessary during the crossed-beam measurements. The target chamber is connected to a beam line of the Rossendorf 5 MV tandem accelerator, supplying 35 MeV Cl^{7+} projectile ions for *in-situ* **E**lastic **R**ecoil **D**etection **A**nalysis (**ERDA**) of the implanted samples [5]. A small angle of incidence of $\alpha = 6.5°$ is chosen for the MeV ions, to achieve an optimum depth resolution. Using a Bragg ionization chamber mounted under a

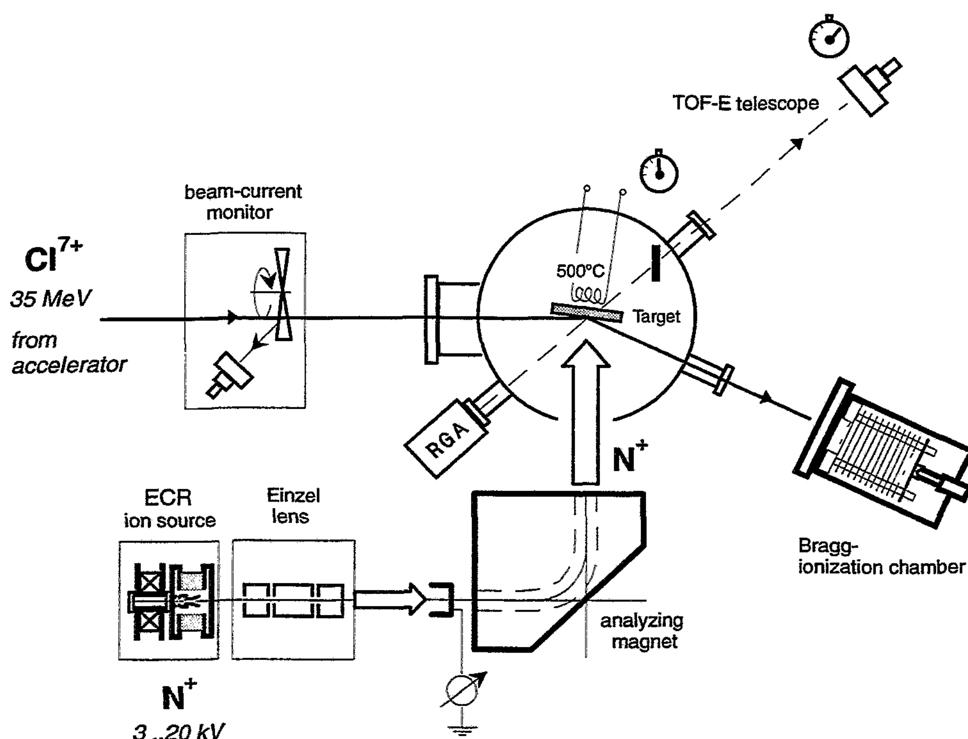

Fig. 1: Setup of the novel crossed-beam experiment combining a keV-ion beam for target modification and a MeV-analyzing beam for *in-situ* compositional analysis of the implanted near-surface region, using the **ERDA** technique.

forward-scattering angle of $\theta = 30°$ relative to the MeV beam, element resolved elastic-recoil spectra are recorded for C, N and possible impurities in the N^+-irradiated area of the carbon films at different stages of the implantation process. Following the measurement sequences, time-resolved [N]/[C] depth profiles are obtained from the spectra through a computer-based conversion technique. Alternatively to the ionization chamber, a time-of-flight system (*TOF–E telescope*) can be used for recoil detection which offers the advantage of being mass sensitive in cases when $^{14}N/^{15}N$-double implantations are carried out [6].

It is important to notice that fluxes associated with the analyzing beam are of the order of $10^{11} cm^{-2} s^{-1}$ which is small compared to the N^+ flux. As a consequence, it is reasonable to assume that the implantation process is not affected by the *in-situ* analysis. On the other hand, a sufficient sensitivity is obtained using the **ERDA** method to resolve fluence intervals of $0.2 \times 10^{17} N^+/cm^2$, corresponding to a recording time of 3 min per [N]/[C]- depth profile. Modifications of the microstructure of the implanted films are studied by cross-section transmission electron microscopy (XTEM) using a Philips CM 300 electron microscope, at an operating voltage of 300 kV. Hard amorphous carbon (ta-C) films, vacuum-arc deposited on Si [7], are used for the implantation, mainly because of their high sp^3–C contents and negligible hydrogen inventory.

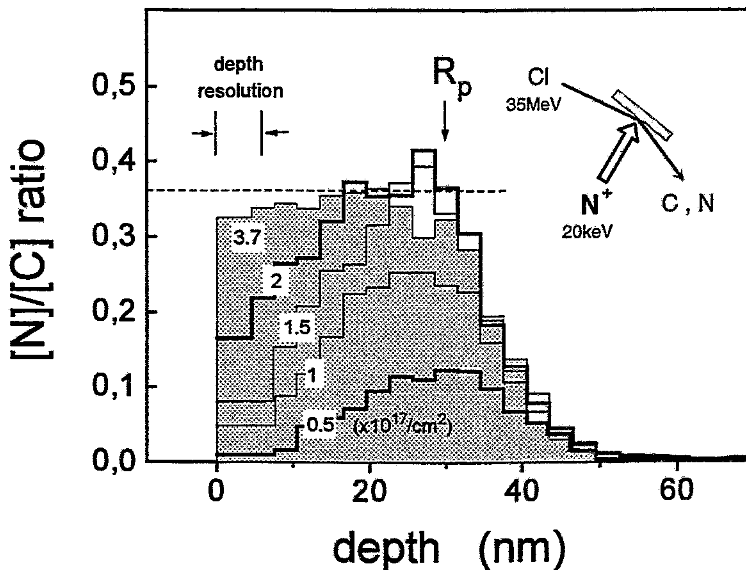

Fig. 2: *In-situ* nitrogen depth profiles obtained during room-temperature implantation into a ta-C film. The different profiles are attributed to the respective N^+ fluences specified in units of $10^{17}/cm^2$. A carbon density of 3.0 g/cm^3 is used to obtain the "nm" depth scale. The mean projected range R_p of the N^+ ions, as obtained from TRIM, is indicated for comparison.

In Fig. 2, dynamic [N]/[C] depth profiles are given, obtained from a crossed-beam measurement series, with the implanted film held at room temperature. At the smallest fluence of $0.5 \times 10^{17} N^+/cm^2$, the profile has a nearly-gaussian shape and is in fair agreement with TRIM calculations [8]. The peak concentration appears at a depth of 30 nm. Above $1.5 \times 10^{17} N^+/cm^2$, a local saturation of the N concentration is observed at $[N]/[C] = 0.35 \pm 0.03$, while in the near-surface region corresponding to depths in the range of 0 ... 10 nm nitrogen is accumulated at a much higher rate, compared to the implantation at small fluences. Simultaneously, the nitrogen retention inside the film falls below 100%. At fluences $\geq 3 \times 10^{17} N^+/cm^2$, saturation is

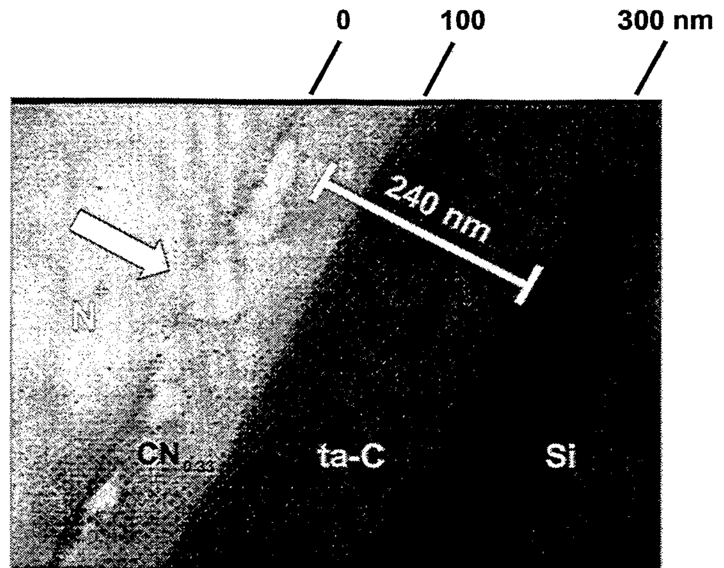

Fig. 3: XTEM micrograph of an N^+ implanted ta-C film. Clearly visible is a modified sublayer with a reduced density, due to the implantation process. The original film thickness prior to the implantation is indicated as a white bar. N_2-gas bubbles are found in the near-surface region.

observed at implantation temperatures > 150°C. The saturation goes along with 100% loss of the implanted species, since no nitrogen accumulation is found in larger depths up to the film-Si interface at 240 nm.

XTEM analysis of a sample implanted up to saturation gives an indication of the mechanism leading to the nitrogen outdiffusion. The micrograph in Fig. 3 shows large elliptical structures in the near-surface region of the film. From comparison with Raman- and XPS measurements, these structures are identified as remnants of N_2-containing gas bubbles forming during the implantation process [9]. From thermal effusion measurements, it is concluded that up to 50% of the total nitrogen inventory in the room-temparature implanted films must be attributed to N_2 rather than to covalent C–N bonds. Mass-spectrometric investigations of the species reemitted from the target (see residual-gas analyzer "RGA" in Fig. 1) show that the [N]/[C] saturation occurs due to the outdiffusion of N_2 molecules that form *inside* the films at fluences above 1 ...$2x10^{17} N^+/cm^2$ [6]. The bubbles are found in the top half of a sharp-edged modified sublayer of 100 nm thickness which appears brighter than the underlying nitrogen-free ta-C layer, indicating a structural modification of the implanted region, with a reduction of the density as a result. Due to the smaller density, the extension of the sublayer is larger by a factor of two than the maximum range of the N^+ ions in Fig. 2, because the depth scale of the **ERDA** profiles is related to the density of 3.0 g/cm^3 of the unimplanted film. Note that no information on the target density can be obtained from **ERDA** measurements.

In conclusion, the potential of the novel crossed-beam setup combining a keV-ion beam for target modification and a MeV-analyzing beam for *in-situ* compositional analysis of the modified depth region, has been demonstrated for the carbon-nitrogen system. As a suggestion, the technique may be applied to different materials problems related to ion implantation of light elements.

Acknowledgements

As an ion-beam analyst, the first author is greatly indebted to Dr. A. Kolitsch for continuous support in all carbon-nitride related matters.

References

[1] A.Y. Liu, M. Cohen, Science 245 (1989) 841

[2] A. Hoffmann, R. Brener, I. Gouzman, C. Cytermann, H. Geller, L. Levin, M. Kenny, Diamond Relat. Mater. 4 (1995) 292

[3] F. Link, H. Baumann, A. Markwitz, E.F. Krimmel, K. Bethge, Nucl. Instr. Meth. B113 (1996) 235

[4] D. Henke, R. Hentschel, Rev. Sci. Instrum. 63 (1992) 2538

[5] U. Kreissig, R. Grötzschel, R. Behrisch, S. Grigull, Institute of Ion Beam Physics and Materials Research, Annual Report 1993

[6] S. Grigull, *Transport und Strukturmodifikation bei der Stickstoff-Implantation in amorphen Kohlenstoff*, PhD thesis, submitted to TU Dresden, Feb. 1997

[7] M. Kühn, P. Meja, F. Richter, Diamond Relat. Mater. 2 (1993) 1350

[8] TRIM code, version 95; J.P. Biersack, L.G. Haggmark, Nucl. Instr. Meth. 174 (1980) 257

[9] S. Grigull, W. Jacob, D. Henke, C. Spaeth, A. Mücklich, L. Sümmchen, to be published in Appl. Phys. Lett. 70, 11 (1997)

Short Contributions

Abbreviations for analytical techniques often used in the short reports:

AES	Auger Electron Spectroscopy
AFM	Atomic Force Microscopy
EELS	Electron Energy Loss Spectroscopy
ERDA	Elastic Recoil Detection Analysis
HRTEM	High Resolution Transmission Electron Microscopy
PIXE	Proton Induced X-ray Emission
RBS	Rutherford Backscattering Spectroscopy
RBS/C	Rutherford Backscattering Spectroscopy under Channeling Conditions
SEM	Scanning Electron Microscopy
SIMS	Secondary Ion Mass Spectroscopy
STM	Scanning Tunnel Microscopy
TEM	Transmission Electron Microscopy
XRD	X-ray Diffraction
XPS	X-ray excited Photoelectron Spectroscopy

Hard Coatings

A. Kolitsch
U. Kreißig

Synthesis of carbon nitride containing films by IBAD

Synthesis of super hard predicted β-C_3N_4 has recently been claimed worldwide with a lot of different methods of thin film deposition, but in all cases the obtained film composition is not stoichiometric and β-C_3N_4 was not reliably identified. We have investigated the C_xN_y film formation by nitrogen ion beam assisted deposition of carbon. The investigation of the influence of the deposition temperature (20 °C - 1000 °C) on the resulting film stoichiometry and the chemical binding energies of the film components has shown a nitrogen maximum at 33 at.% in the films deposited at 200 °C and increasing graphitic structure with a low nitrogen content in the films deposited above 600 °C (Raman, XPS, ERDA). The variation of the nitrogen ion energy ranging from 200 eV to 1200 eV shows no significant changes of the film composition.

supported by SMWK

Collaboration: TU Dresden

M.F. Plass
W. Fukarek
A. Kolitsch

Growth and ex-situ characterization of boron nitride films

Boron nitride layers were deposited using ion beam assisted deposition with different ion to atom arrival (I/A) ratios, resulting in different cubic fractions. Additionally, some samples were post-deposition ion implanted to yield a phase modification. The BN films were examined with polarised infrared reflection (PIRR) spectroscopy. Three different BN modifications are identified, c-BN and two sp^2 bonded phases (amorphous and layered). The PIRR data were analysed with a multilayer model (c-BN on top of non-cubic BN) regarding the anisotropy of h-BN. The individual layer thicknesses, the cubic volume fraction of the toplayer, as well as a preferential orientation of the erected basal planes of the h-BN interlayer could be determined. Under conditions where a c-BN top-layer is formed, its cubic volume fraction (80 - 90 %) is independent of the deposition conditions, i.e. ion energy or I/A ratio. Even the use of an ion energy of 1.5 keV yields a toplayer with an almost pure cubic phase composition. However, the interlayer thickness decreases with increasing I/A ratio.

supported by SMWK

H.-U. Jäger

Molecular Dynamics studies of a-C:H film growth by energetic hydrocarbon molecule impact

Classical Molecular Dynamics calculations were performed to study the deposition of thin hydrogenated carbon films. A hydrogen-covered bulk-terminated diamond {111} surface was bombarded with energetic acetylene (C_2H_2) molecules. The impact energies ranged from 40 eV up to 160 eV. Brenner's hydro-carbon potential was used to model the atomic interactions. The structure of the growing amorphous films, especially the depth distributions of three- and fourfold coordinated carbon atoms were studied as a function of the substrate temperature.

M. Posselt
*C.S. Murthy **
*T. Feudel ***

Physically based modeling of 2D and 3D implantation profiles: Influence of damage accumulation

The dynamic binary collision code Crystal-TRIM was used in order to perform fundamental investigations on the change of the shape of the 2D and 3D range profiles with growing dose and on the formation of amorphous zones. As examples, 15 keV BF_2^+ and 30 keV P^+ implantations into (100)Si at normal and tilt incidence were considered. A simple geometry with a plane area irradiated by the ion beam and a surrounding impenetrable mask was employed. Comparison between results of Crystal-TRIM simulations for low (10^{13} cm^{-2}) and high dose implants (10^{16} cm^{-2}) shows that, although the shape of both the depth and the lateral profiles is affected by the defect evolution, the influence on depth distributions is higher. Due to increasing dechanneling the lateral straggling of the range distributions grows with dose. For high dose implantations the extension of the amorphous region in two and three dimensions was determined. Amorphous material is also formed beneath the mask. The simulated depth profiles of B and P and the predicted thickness of the amorphous layers are in good agreement with experimental data.

Collaboration: *IBM Semiconductor Research and Development Center, East Fishkill, USA, **ISE Integrated Systems Engineering AG, Zürich, CH

B. Schmidt
M. Posselt

Development of an efficient trajectory split algorithm for binary collision (BC) simulations of ion implantation

One of the major issues in BC simulations of ion implantation is the improvement of the statistical accuracy of the resulting range distributions especially in the so-called deep channeling tails of the profiles. Therefore, a method was developed and introduced into the Crystal-TRIM code which reduces the loss of statistical accuracy with increasing penetration depth. The algorithm is based on the idea of having a nearly constant number of pseudoparticle trajectories throughout all the interesting depth intervals of the target. This is achieved by duplicating the pseudoparticles at several points on their way. Additional variables were introduced which yield informations about the statistical accuracy of the range profiles at a certain depth. In typical ion implantation simulations the time needed for sufficiently good statistics is up to ten times shorter than in the case without using the trajectory split algorithm. In special cases this ratio can be even higher. The trajectory split method was introduced into the Crystal-TRIM version used in the 1D process simulator TESIM of ETH and ISE-AG Zürich.

supported by
ETH Zürich, CH

B. Schmidt
*N. Strecker**
M. Posselt

Introduction of Crystal-TRIM into the 2D process simulator DIOS

Process simulators provide a cheap and fast way of testing the effect of different conditions in semiconductor technologies. With DIOS this can be done for a wide variety of 2D target structures for different process steps like masking, etching, implantation, diffusion and activation of dopants. The correct modeling of ion implantation is crucial in order to obtain precise results. In 2D process simulations the number of possible target structures is much higher than in the 1D case. On the other hand, the number of available experimental data on 2D implantation profiles is much smaller

since 2D distributions are very difficult to measure. Both aspects require the simulation of the implantation step by a physically based binary collision (BC) code. Therefore, the BC code Crystal-TRIM was modified in a way which allows its use as a fully integrated part of DIOS. This has the advantage that the very general mesh generated by DIOS can be employed in order to describe ion implantation into complicated target structures like trenches. The trajectory split algorithm already introduced into 1D process simulations was extended to work with the 2D registration cells of DIOS.
Collaboration: *Institut für Integrierte Systeme der ETH Zürich, CH

supported by ETH Zürich, CH

T. Schwieger
*A. Anders**
M. Posselt
H. Reuther
R. Grötzschel

Simulation of depth profiles obtained by high dose tungsten implantation into silicon using a vacuum arc ion source

The vacuum arc ion source at the Lawrence Berkeley Laboratory allows efficient high dose implantations. The ions of the extracted beam have a certain charge state distribution, leading to multiple ion energies and therefore to specific implantation profiles. We studied the depth profiles of W ion implantations into silicon, at doses of 0.5, 1 and $2x10^{17}$ cm^{-2}, at an extraction voltage of 50 kV, where ions in six charge states have been observed with measurable intensity fractions. The process of high dose implantation was simulated by the TRIDYN code. It was assumed that WSi_2 with a density of 4.91 g/cm^3 (tetragonal phase) is immediately formed during implantation. Furthermore, a surface binding energy of 4.46 eV was assumed for both W and Si. The comparison of TRIDYN results with experimental depth profiles of W determined by AES and RBS shows that the assumption of WSi_2 formation is justified. The experimental profiles are mostly shallower than predicted by TRIDYN. This may be caused by an underestimation of sputtering and/or of the WSi_2 density in the simulations.
Collaboration: *Lawrence Berkeley Laboratory, USA

R. Kögler
M. Posselt
A. Mücklich
*A.B. Danilin**

Effect of ion channelling on the depth distribution of residual defects in silicon

The depth distribution of residual defects in silicon was determined after implantation of 3.5 MeV Si^+ ions and copper gettering at these defects after low temperature annealing at 700 °C. The Cu depth profile measured by SIMS shows two decorated defect bands in a depth of 2.5 µm and 3.6 µm. The deeper band extends up to about 4 µm. This is distinctly more than expected from a usual TRIM calculation giving a projected range (R_p) of the Si^+ ions of 2.7 µm and an extension of the atomic displacements to a maximum depth of 3 µm. Whereas an amorphous silicon target is assumed in the case of TRIM, the result of the TEM investigation of a cross sectional sample in the as-implanted state showed no amorphization. The latter is avoided by ion beam heating in the temperature range of 100 - 150 °C. A more realistic calculation is possible using Crystal-TRIM restricting the damage accumulation in the silicon crystal to 10^{20} displaced atoms per cm^3. In this way an *in situ* damage annealing is taken into account. This and ion channelling extend the ion range profile and the depth profile of the atomic displacements up to a depth of 4 µm which agrees reasonably with the measured copper distribution.
Collaboration: *Centre for Analysis of Substances, Moscow, Russia

F. Eichhorn
F. Prokert
A. Mücklich
R. Kögler

Determination of the strain depth profile induced by end-of-range defects in ion implanted silicon

The defect formation near buried ion implanted layers was investigated in Si(001) implanted with 5×10^{15} Ge^{+}/cm^{2} at an energy of 4 MeV. According to TRIM calculation the longitudinal ion range is 2.7 µm with a straggling of 0.42 µm. For the applied dose a buried amorphous layer is produced. With a double-crystal X-ray diffractometer the depth distribution of the strain $(\Delta d/d)_{\perp}$ was determined from the measurement of (004) rocking curves and their simulation.

In the as-implanted state a 0.9 µm thick layer exists from a depth of 1.4 µm with a tensional strain of 2.3×10^{-4}. By a thermal treatment at 650 °C for 1 h the amorphous layer is annealed and near the boundaries of this layer end-of-range defects are produced as it was observed by TEM. They cause a complex strained region in the depth range from 675 nm to 1155 nm consisting of a 25 nm thick range of compressive strain with a value of 4.2×10^{-3} and a 430 nm thick range of tensional strain of 2.0×10^{-4} immediately at the near-surface boundary of the former amorphous region.

*J.R. Kaschny**
*P.F.P. Fichtner***
A. Mücklich
U. Kreißig
R.A. Yankov
R. Kögler
*A.B. Danilin****
W. Skorupa

Formation, microstructure and gettering ability of helium induced cavities in silicon

Cavities in silicon produced by irradiation with He^{+}-ions were found to be very efficient in trapping metal contaminants such as Cu and Au. These findings have stimulated many explorations in this field with the aim of developing proximity gettering techniques for VLSI applications. In the present work the formation of cavitiy microstructures in silicon, following helium implantation (10 or 40 keV; $1x10^{15}$, $1x10^{16}$ and $5x10^{16}$ cm^{-2}) and annealing (800 °C, 10 min), is investigated by means of TEM, RBS/C and ERDA. The processes of cavity nucleation and growth are found to depend critically on the implanted He concentration. For a peak He concentration of $3.5x10^{20}$ cm^{-3} the resulting structures appear to contain large overpressurized bubbles whose formation cannot be accounted for by the conventional gas release model and bubble-coarsening mechanisms predicting empty cavities.

supported by National Research Council - CNPq, Brazil and AvH-Stiftung

Collaboration: *Instituto de Fisica and **Departamento de Metalurgi, Univ. Rio Grande do Sul, Porto Alegre, Brazil, ***Centre for Analysis of Substances, Moscow, Russia

B. Schmidt
*V. Eremin**
J. von Borany

Application of high energy ion implantation for silicon avalanche diodes

Alternatively to the mostly used deep diffusion and/or epitaxial layer deposition technique high energy ion implantation in the MeV-range has been applied to standard pin-diode technology to fabricate diodes with a high internal electric field region for charge carrier multiplication (avalanche effect). For the formation of the "low-high-low" n-type doping profile 10 MeV P^{+} ions with $D = 1.5\cdot10^{12}$ cm^{-2} were implanted through a suitable Al masking layer into <111>-oriented n-type high resistivity silicon ($\rho_n = 2000$ Ωcm) leading to a doping maximum of $N_D \approx 1.8\cdot10^{16} cm^{-3}$ in the depth of 3.75 µm. Electrical measurements have shown that up to the near breakdown region at (90...100) V the dark currents were smaller than 10 nA for diodes with an active area of 20 mm^2. A multiplication factor (gain) for photogenerated charge carriers up to $M = 3...10$ was obtained.

Collaboration: *Yoffe Physico-Technical Institute St. Petersburg, Russia

J. von Borany
R. Grötzschel
W. Jiang
W. Pilz
M. Posselt
B. Schmidt

Improved resolution of silicon detectors for heavy ion spectroscopy under channeling conditions

The energy resolution of different silicon detectors (made from (111)-oriented silicon) for the spectroscopy of 2.8 MeV oxygen ions has been investigated as a function of the angle of incidence.The detector was mounted on a two axis goniometer allowing a precise orientation of the detector against the incident ion beam with an accuracy of 0.05 °. Under [111] axial channeling conditions a significant improved detector resolution (FWHM) has been obtained compared to the random incidence case. Additionally, the peak is shifted by about 70 keV towards higher channels. These effects can be explained by the fact that due to nearly complete reduction of nuclear energy loss the electronic energy loss per particle is increased and distributed in a narrower zone. The results are confirmed by theoretical calculations using the Crystal-TRIM-Code. The best detector resolution of about 25 keV FWHM for 2.81 MeV oxygen ions have been obtained for special high field region detectors, which are characterized by a thin detector window and complete carrier collection from the depletion layer.

B. Schmidt
*V. Beyer**

Anisotropic selective wet chemical etching of silicon membranes using MeV-implanted doping layers

The electrochemical etch stop behaviour of buried MeV-implanted n-type layers has been investigated. (100)-oriented p-type Si wafers were implanted with 5, 10, and 15 MeV P^+ ions at doses of $1\cdot10^{13}$ and $1\cdot10^{14}$ cm^{-2}. The following annealing was performed at 800 °C for 30 min to prevent diffusion broadening of the deep implanted profile. The buried n^+-profiles have been electrically contacted via anisotropically etched, shallow P^+-implanted and Al-evaporated contact holes. A three-electrode potentiostatic configuration and a KOH/H_2O etch solution (c = 30 %, T = 80 °C) were used for the etching from the wafer back side. Thickness investigations using energy loss spectrometry of α-particles show, that the etch stop takes place at 1.0...1.5 µm before the pn-junction of the buried n^+-layer, which corresponds with the etch stop behaviour at shallow implanted n^+-layers. The membrane thicknesses have been measured as 4.7, 6.7 and 8.6 µm (± 0.1 µm) for implantation energies of 5, 10 and 15 MeV, respectively. The results show, that in the thickness range of (3...10) µm crystalline Si membranes with low thickness variation over the Si wafer can be prepared using MeV-ion implantation alternatively to deep diffused pn-junctions or to n^+-epitaxial layers on p-type substrates.

Collaboration: *TU Chemnitz-Zwickau

T. Henkel
V. Heera
R. Kögler
W. Skorupa

Optical in-situ study of the accumulation of damage in 6H-SiC during high energy ion irradiation

Single-crystalline 6H-SiC wafers (n-type, (0001) Si surface) were irradiated with 3 MeV I^{2+}-ions at temperatures between 110 K and 610 K in order to investigate the accumulation of damage in this material. The evolution of damage was studied in-situ by time resolved optical reflectivity measurements and ex-situ using RBS/C. The reflectivity measurements revealed that the amorphization of the bulk material is hampered during the ion irradiation to fluences below $6x10^{15}$ cm^{-2} at substrate temperatures above 530 K. At higher temperatures damaging of the crystalline lattice of the subsurface region was observed only. These results were confirmed by RBS/C.

V. Heera
N. Schell
F. Prokert
H. Seifarth
W. Skorupa

Density changes in amorphized silicon carbide

The amorphization of SiC by ion implantation leads to strong material swelling. Density reductions calculated from step height measurements on thin amorphous surface layers (100- 200 nm) vary between 10 and 20%. In order to get more precise results a thick amorphous layer (1.8 μm) was produced by 2 MeV 2×10^{16} Si^+/cm^2 implantation into single crystalline 6H-SiC (3.21 g/cm^3) at room temperature. The density was determined by X-ray reflectometry and step height measurements. Both methods provided in good agreement a density of (2.80±0.05) g/cm^3 for the as-amorphized SiC. Relaxation processes in the amorphous network after annealing at 500 °C were indicated by the decrease of the step height. The density of the material in relaxed amorphous state is about (2.95±0.05) g/cm^3.

H. Wirth
M. Voelskow
D. Panknin
W. Skorupa

Substitutional incorporation of implanted Ga- and Kr-ions in 6H-SiC

The influence of the chemical properties of the implanted ions on the incorporation behavior into the crystal lattice of 6H-SiC was investigated. Gallium and Krypton as elements with similar mass but different electron shell structure were implanted into this material. The RBS-technique was used to determine the incorporation fraction by comparing the channeled and random counts in the dopants peaks. There is a significant difference between the group-III element Gallium (90 % incorporation) and the rare gas Krypton (60 % incorporation), which points out the influence of the chemical properties on the crystal lattice location: Kr forms a high fraction of interstitials while Ga substitutes on lattice sites nearly completely.

supported by
Daimler-Benz AG, Frankfurt/M.

H. Weishart
W. Matz
W. Skorupa

Ion beam synthesis of conductive layers by high-dose tungsten implantation into 6H-SiC

We have investigated the influence of implantation and annealing temperature on W implanted 6H-silicon carbide. Tungsten implantation has been performed at 200 keV at temperatures between 60 °C and 500 °C. The samples have been subsequently annealed either at 950 °C or 1100 °C. RBS and XRD measurements have contributed to study structure and composition of the layer. Implantation temperatures up to 300 °C produce a typical Gaussian W distribution. The tungsten profile of the 400 °C implant is more confined. Two tungsten peaks arise during implantation at 500 °C; a first one located at a depth of 0.6 R_p and a second, higher one at R_p. Additional annealing at 950 °C leads to the crystallization of both W_5Si_3 and W_2C. After annealing at 1100 °C only crystalline W_5Si_3 is found. Implantation below 100 °C and annealing at a temperature above 700 °C leads to the crystallization of W_2C; tungsten silicide, however, remains amorphous.

H. Weishart
V. Heera
W. Matz
W. Skorupa

Ion beam assisted deposition of a tungsten compound layer on 6H-SiC

Ion beam assisted deposition (IBAD) as a means of synthesizing a tungsten carbide layer on top of SiC was investigated by RBS, XRD and four point probe measurements. Evaporation of tungsten and subsequent implantation of carbon leads to a crystalline layer of tungsten carbide whose resistivity is 1554 μΩcm. At an implantation dose of 5×10^{17} C^+ cm^{-2} enhanced surface erosion occurs. Simultaneous evaporation of tungsten and implantation of carbon produces a layer of crystalline W_2C mixed with tungsten. The resistivity of this layer is 400 μΩcm, i.e. only a factor of 5 higher than that of single crystal W_2C.

The formation of buried layers of $(SiC)_{1-x}(AlN)_x$ in 6H-SiC using ion beam synthesis

*R.A. Yankov**
N. Hatzopoulos
W. Fukarek
M. Voelskow
V. Heera,
*J. Pezoldt**
W. Skorupa

Solid solutions of SiC and III-V compound semiconductors are recognized as promising materials for novel semiconductor applications. Experiments were performed to explore the possibility of synthesizing thin buried layers of $(SiC)_{1-x}(AlN)_x$ having composition of about x = 0.2 by co-implanting N^+ and Al^+ ions into 6H-SiC wafers maintained at temperatures in the range 200 - 800 °C. Structural and compositional evaluation of as-implanted samples has been carried out using a combination of RBS/C and infrared reflectance spectroscopy. It has been shown that the structures are highly sensitive to the substrate temperature during implantation. The use of sufficiently high temperatures (400 - 800 °C) enables one to maintain in situ both the crystallinity of the host material and relatively low damage levels. The formation of Al-N bonds during implantation is also confirmed over the temperature range studied.

supported by DFG

Collaboration: *Institut für Festkörper-Elektronik, TU Ilmenau

Ion beam synthesis of SiC in silicon-on-insulator

R. Kögler
H. Reuther
M. Voelskow
W. Skorupa
*A. Romano-Rodriguez**
*A. Perez-Rodriguez**
*C. Serre**
*L. Calvo-Barrio**
*J.R. Morante**

Ion beam synthesis of ß-SiC in the silicon top layer of a SIMOX (Separation by Implantation of Oxygen) substrate was investigated by AES, RBS, XRD and TEM. This $Si/SiC/SiO_2$-system is of great interest for the fabrication of electronic devices operating at high temperatures. A SiC/SiO_2-heterojunction reduces significantly the leakage current in comparison to a SiC/Si one. It was found that the implantation into a SIMOX structure improves significantly the formation of a stochiometric SiC-layer and the strain release. The whole amount of implanted C is captured inside the 200 nm silicon top layer and preferentially accumulated at the Si/SiO_2-interface. The best crystal quality of the $Si/SiC/SiO_2$-structure is obtained by a C implantation at high temperature (T>500 °C) and a subsequent high temperature annealing treatment (T =1250 °C). It consists of a crystalline Si-overlayer, a Si-layer including a high density of perfectly aligned ß-SiC grains and the buried oxide layer. An implantation at high temperature is crucial for the quality of the SiC layer. But, the use of a high implantation temperature is limited due to the dissolution of the Si/SiO_2 interface of the buried oxide layer.

supported by DAAD-WTZ Spanien

Collaboration: *Department of Applied Physics and Electronics, University of Barcelona, Spain

Sensitization of silicon nitride surfaces for silver ions by ion implantation

D. Möller
M.T. Pham
J. Hüller
W. Matz
A. Mücklich
H. Reuther

Thin films of Si_3N_4 implanted with Ag^+ and S^+ ions have been studied by field effect measurements on electrolyte-insulator-semiconductor structures (EIS), AES, XPS, TEM, and XRD. Regardless of the sequence of the implantation, the resulting implanted layer is found to be predominantly composed of Ag clusters, mostly spherical in shape with diameters ranging from some nm to 100 nm, embedded within the Si_3N_4-matrix. In regions of overlapping Ag and S concentration profiles Ag_2S is observed to form a thin film enveloping the Ag spheres. Nominal ion doses according to a stoichiometric Ag_2S phase do not result in a complete conversion into the sulfide phase, suggesting that the Ag clustering is kinetically more favorable than the Ag to S bonding. Buried Ag and S, upon heating following implantation, are shown to favor the sulfide formation, compared to exposed implanted layers consistent with the thermally susceptible decomposition

supported by AiF

of Ag-sulfide. The composite material shows field effect sensitivity toward Ag ions. A linear relation between the surface potential and the logarithm of the electrolyte Ag ion concentration (ca.10^{-5} to 10^{-1} M/L Ag^+) was obtained.

J. Hüller
M.T. Pham
D. Möller
M. Mäder

Ion selective planar copper electrodes prepared by ion implantation

The electrodes were prepared on Si wafer substrates covered with a 100 nm SiO_2 layer. The SiO_2 was co-implanted with Cu and S to a fluence of $5 \cdot 10^{16}$ and $1 \cdot 10^{16}$ cm^{-2}, respectively, at three different energies of 16, 20 and 40 keV. AES and RBS analysis shows, deviating from the calculated Cu distribution, a Cu enrichment at the SiO_2 surface and a sulphur distribution correlating with the copper profile. The formed CuS layer can be ultrasonically bonded for electric contacting und shows a nearly Nernstian response of 28 mV/pCu between pCu 5 and 1 in nitrate and sulphate solutions. The main advantage of this implanted compound layer in comparison with CuS thin layers, which are chemically converted from Cu to CuS, is its incorporation in the SiO_2 near-surface layer and thus providing an improved adhesion and high resistance against cleaning and scratching of the chip electrode.

supported by AiF

F. Brenscheidt
*S. Oswald**
E. Wieser
A. Mücklich

Wear mechanisms in titanium implanted silicon nitride ceramics

Mechanisms to explain the wear reduction caused by titanium implantation ($1x10^{17}$ Ti^+/cm^2, 150 keV or 1 MeV) into silicon nitride ceramics were studied. XPS investigations show that silicon oxide is formed in the wear tracks. Titanium is not found at the bottom of the tracks. Therefore solid lubrication of titanium oxides as a mechanism for wear reduction can be excluded. TEM imaging shows that implantation results in an amorphous layer. In additon viscous flow of the intergranular glassy phase is observed. This flow, obviously caused by the compressive stress in the surface due to implantation, may close pre-existing surface cracks or diminish their severity thus leading to an improved wear behaviour.

Collaboration: *Institut für Festkörper- und Werkstofforschung, Dresden

F. Brenscheidt
W. Matz
E. Wieser

Annealing studies of chromium implanted silicon nitride ceramics

The effect of chromium implantation and subsequent annealing on the hardness and wear behaviour of a silicon nitride based ceramic was investigated. Implantation energies were 200, 400, 1000 and 2000 keV, the fluence was 10^{17} Cr^+/cm^2 in all cases. The implantation results in a partial amorphization of the near surface region. The recrystallization of this layer by tempering was examined with XRD. Annealing at 800 °C does not affect the crystal structure. At 1000 °C the α-Si_3N_4-phase is formed for 1 and 2 MeV implantation energy. At 1200 °C, Cristobalite and Keiviite is formed at the lower implantation energies, at higher energies α-Si_3N_4 is formed. Samples which show considerable formation of Cristobalite and Keiviite have a substantially lower hardness and increased wear after annealing compared with samples where also α-Si_3N_4 is preferentially formed. Samples implanted with MeV energies have a more or less reduced hardness compared with the starting material, this may be due to the different grain structure of the recrystallized region. The wear of these samples is improved due to a reduced influence of pre-existing flaws resulting from the recrystallized grain structure.

E. Wieser
D. Panknin
*N. P. Barradas**
M. Betzl
H. Reuther
*W. Henrion***
*H. Lange***

Formation of ternary $(Fe_{1-x}Co_x)Si_2$ structures by ion beam assisted deposition and ion implantation

The formation of ternary $(Fe_{1-x}Co_x)Si_2$ in the system Fe-Co-Si prepared by implantation of cobalt into a ß-$FeSi_2$ layer produced by ion beam assisted deposition (IBAD) of iron on (100) silicon substrates has been optimized. Cobalt implantation at room temperature and 250 °C results in a high amount of CoSi and FeSi in the as-implanted state. These monosilicides are dissolved by post-implantation annealing at 800 °C, but a remarkable contamination of $CoSi_2$ is formed thereby for the samples implanted at 250 °C. By implantation at 400 °C a nearly complete formation of ß-$(Co_xFe_{1-x})Si_2$ is observed already during implantation. A homogeneous depth distribution of cobalt is only obtained after annealing at 900 °C. Due to the cobalt incorporation, already at 900 °C the metallic α phase is formed. After a final retransformation into the semiconducting ß phase by annealing at 800 °C / 48h +750 °C / 48h a shift of the band gap energy from 0.89 eV to 0.73 eV is measured for ß-$(Fe_{0.85}Co_{0.15})Si_2$.

Collaboration: *Centro de Física Nuclear da Universidade de Lisboa, Portugal, **Hahn-Meitner Institut Berlin, Abteilung Photovoltaik

S. Parascandola
M. Betzl
E. Richter

Nitriding of austenitic stainless steel by low energy, high current ion implantation

Disks of DIN X6CrNiMoTi 17.12.2 stainless steel (corresponding to AISI 316Ti) were nitrided by low energy ion implantation of nitrogen (E = 1.2 keV). An ion current density of 1 mA/cm^2 and a substrate temperature of 400 °C has been applied. Process times up to 40 minutes result in fluxes between $7.5x10^{17}$ and $1.5x10^{19}$ $ions/cm^2$. A nitrogen enriched layer with thickness in the µm-range, which provides strongly improved tribological properties, is achieved. XRD analysis shows that the fcc crystal lattice is slightly expanded. Only small amounts of chromium nitride precipitates are found.

supported by SMWK

Collaboration: TU Dresden and TU Bergakademie Freiberg

E. Wieser
F. Prokert
R. Grötzschel
H. Reuther

Microstructure and wear improvement in Ni implanted Al

Ni was implanted at 200 keV and 1 MeV into a semihard aluminum (99.5 at.% Al) with the aim to improve the wear behavior by precipitation of the hard intermetallic phase $NiAl_3$. The doses were chosen in such a way that the maximum concentration in the Ni profile covers the range between 20 and 30 at.%. In the as-implanted state the strong broadening of the $NiAl_3$ XRD peaks indicates a nanocrystalline structure with a size of the precipitates between 5 and 10 nm. After annealing at 400 °C well crystallized $NiAl_3$ is formed. Annealing at 600 °C leads in the case of the 200 keV implantation to a strongly broadened depth distribution of the $NiAl_3$ precipitates and consequently to a decrease of the average Ni concentration from 25 to 5 - 3 at.%. The abraded volume in an oscillating ball on disc wear test decreases in the as-implanted state only by a factor 2 after 200 keV Ni implantation. A reduction factor 20 is obtained by the deeper 1 MeV implantation. 200 keV implantation and subsequent annealing at 600 °C also results in a wear reduction by a factor 20. This is explained by the formation of about 50 nm Al_2O_3 combined with the precipitation hardening of the subsurface region.

H. Reuther
M. Betzl
W. Matz
E. Richter

Investigation of Fe-Mg-alloys produced by ion implantation

Iron and magnesium are known as insoluble elements with each other and there is no phase diagram information. However, it is possible to produce artificial alloys by ion implantation. After iron implantation into magnesium ($1...60x10^{16}$ Fe/cm^2 at 200 keV) samples were characterized by conversion electron Mössbauer spectroscopy, AES and XRD. At low doses the iron depth profiles are Gaussian shaped and paramagnetic doublets appear in the Mössbauer spectra. These indicate that iron is included in the hexagonal magnesium host lattice non-statistically on at least two different lattice sites. At the highest dose the iron concentration reaches 90 at.% in a plateau and the Mössbauer spectrum shows a dominant ferromagnetic fraction. The X-ray pattern can be explained with a dilated α-iron lattice. Both results indicate the formation of an iron layer where the lattice dilation is caused by magnesium inclusions. Microhardness of all samples is clearly increased due to the implantation.

M.T. Pham
*I. Zyganow**
W. Matz
A. Mücklich
H. Reuther
*S. Oswald***
E. Richter
E. Wieser

Corrosion behavior and microstructures of titanium implanted with α and β stabilizing elements

Corrosion and microstructure aspects of implantation surface alloyed Ti were studied by anodic polarization in dilute electrolyte solutions, XRD and AES. Polished surfaces of pure Ti were alternatively implanted with Al (200 keV), V (200 keV) or Nb (100 keV) with doses ranging from $1x10^{17}$ to $3x10^{17}$ cm^{-2}. Ennoblement in the open circuit potential, by about 0.2 V (vs. SCE), was observed for all the implanted surfaces exposed to Hank' s electrolyte solutions. The anodic polarization reveals that the anodic current (active and passive dissolution) is reduced compared to the unimplanted surface. Spontaneous passivation occurs on both implanted and un-implanted surfaces, but the degree of passivation is greater for the former and increases in the order of the implanted additives Al, V, Nb. Implantation of Al, V, and Nb results in surface alloying which simulates a wide range of Ti alloys in composition and microstructure. The implanted additives reached up to 40 at.% at the profile maxima corresponding to depths of around 100 nm underneath the surface. Only α Ti was found after Al implantation, while a mixture of α and β Ti was formed after V or Nb implantation. Enhanced incorporation of oxygen was characteristic of all implanted surfaces examined, with decreasing tendency from Al via V to Nb. TiO_2 seems to dominate the outermost surface overlaying a subsurface region consisting of Ti suboxides and partially oxidized alloying additives. The improved corrosion resistance is assumed to be related to the perfection of the protective surface oxides.

Collaboration: *Technical University Lipezk, Russia, **Institut für Festkörper-analytik und Strukturforschung, Dresden

Nanoclusters

M.T. Pham
W. Matz
H. Seifarth

Surface roughness with nanometer-scale Ag particles generated by ion implantation

Surface roughness involving Ag features in nanometer dimensions has been produced by implantation of Ag ions into substrates of SiO_2, Si_3N_4, Ta_2O_5, and glass. The surface morphology has been explored by AFM and XRD. Ag particles, spherical or nearly spherical, are formed on or directly underneath the surface of SiO_2, Si_3N_4, Ta_2O_5, and glass as a result of Ag implantation. The medium particle size varies between some nanometers and some 100 nanometers in diameter depending on the ion doses from $2x10^{16}$ to $8x10^{16}$ cm^{-2} and dose rates between 0.6 and 2 $\mu A \cdot cm^{-2}$. The adjusting ion energy generates various degrees of submersion into the substrate. The particles are mechanically anchored by the matrix network. The implantation-induced surface morphology depends on the substrate material. For Ta_2O_5 and glass substrates, the Ag particles are more homogeneously dispersed, smaller in size, and more regularly shaped compared to Si_3N_4 and SiO_2 substrate systems. Si_3N_4 substrates or Si_3N_4 thin films on SiO_2 are shown to be efficient in shaping Ag features toward oblate spheroids. The ability is assumed to be related to the barrier against the Ag mobility. The preparation technique is considered applicable also to other metals, substrates, and their combination. Potential application refers to surface enhanced analytical techniques.

Collaboration: Institut für Analytische Chemie, TU Dresden

L. Rebohle
*I. Tyschenko***
R. Yankov
W. Skorupa
*H. Fröb**
*K. Leo**
*G. Kachurin***

Blue photoluminescence from high-dose Si- and Ge-implanted silicon dioxide layers

Thermally-grown, 500 nm thick SiO_2 films on (100) p-type Si wafers were implanted with Si^+, Ge^+ and Ar^+ at energies in the range of 100 keV to 350 keV to integral doses of $3.2x10^{16}$ cm^{-2} to $1x10^{17}$ cm^{-2} leading to a broad concentration profile in a depth region of 100-400 nm below the oxide surface. Post-implantation annealing procedures were performed in a N_2 atmosphere at different temperatures (300-1200°C) and times (30 min and 20 ms). The Si- and Ge-rich layers exhibit strong photoluminescence (PL) with maxima at 470 and 395 nm, respectively. Almost no PL was detected from the Ar-implanted material. The intensity of the Ge-rich layers is up to 5 times larger than the intensity of the Si-implanted material. The excitation spectra are dominated by a 250 nm peak for Si and a 240 nm peak for Ge. Annealing studies for Si-rich SiO_2 show a maximum PL at 500°C for 30 min and 900°C for 20 ms. The experimental results are well explained using a published model in which the energy levels of the $(HO)_3Si$-$Si(OH)_3$ defect were calculated. The PL can be explained by an excitation with 5.0 eV (248 nm) from the ground state to the triplet state, followed by a relaxation, and a radiative deexcitation of 2.7 eV (459 nm) with a further relaxation to the ground state minimum.

supported by SMWK

Collaboration: *TU Dresden, Institut für Angewandte Photophysik, **Institute of Semiconductor Physics, Nowosibirsk, Russia

H.Seifarth
L. Rebohle
B. Schmidt

Sputter deposition of Si-nanocluster containing SiO_2-layers

SiO_x compound layers with a predetermined composition x <2 have been deposited by reactive r.f. magnetron sputtering from a silicon target in an Ar/O_2 plasma. The optical emission line intensity of sputtered Si atoms at $\lambda = 251.9$ nm excited by the plasma was used to control the layer composition x. SiO_x layers with Si-nanoclusters embedded in an amorphous SiO_2-network were formed under proper conditions. The volume ratio of Si-clusters was estimated to (1...15) % in dependence on the layer composition x by application of the Bruggemann mixed medium model in connection with ellipsometrical measurements. The sputter deposited SiO_x layers with a mixed medium structure show pronounced photoluminescence with peaks at wavelengths between 450 nm and 800 nm depending on the mean Si nanocluster diameter.

*M. Palard**
K.-H. Heinig
M. Strobel
*M.-O. Ruault**
*H. Bernas**

In-situ TEM observation and computer simulation of $CoSi_2$ nanocluster formation and evolution during Co^+ implantation in Si

By a comparison of in-situ TEM observations and kinetic 3D lattice Monte Carlo simulations of 60 keV Co^+ implanted 70 nm thick Si membranes some specific features of the $CoSi_2$ nanocluster evolution could be understood: (i) the enhancement of Co diffusion in Si during implantation seems to be of secondary importance (factor 2..3 only); (ii) the growth of B-type precipitates is favored during Co^+ implantation, whereas A-type precipitates grow preferably during thermal annealing and/or Si ion assisted annealing. This could be explained by kinetically and energetically controlled growth during ion implantation and annealing, respectively; (iii) the growth rate of precipitates during Co^+ implantation is independent of the Co^+ flux. This behaviour has been also found by kinetic Monte Carlo simulations and can be used to adjust the effective Co-Co bond energy of the model.

Collaboration: * CSNSM-CNRS Orsay/Paris, France

M. Strobel
S. Reiss
K.-H. Heinig

Evolution of nanocluster ensembles: a unified treatment of diffusion and reaction controlled Ostwald ripening

The Ion Beam Synthesis (IBS) of nanoclusters can be controlled by the flux and fluence of ions and/or the implantation and annealing temperature. However, the evolution of nanoclusters is expected to behave different for systems like SiO_2 and $CoSi_2$ clusters in Si, because they are characterized by quite different ratios of diffusion constant to interface reaction constant. A unified model of Ostwald ripening of nanoclusters was developed, which describes for the first time simultaneously the pure diffusion and reaction controlled limits as well as all intermediate, mixed processes. Expressing the exact solution of the adiabatic diffusion equation by multipole moments we derive the governing equation for the evolution of an ensemble of nanoclusters in the leading monopole approximation. Computer simulations for ensembles of several thousands of nanoclusters demonstrate the evolution for typical cases.

K.-H. Heinig
M. Strobel

Computer simulations of nucleation, growth, ripening, and coalescence at ion beam synthesis

Our kinetic 3D lattice Monte Carlo program, which is based on a Cellular Automaton (CA), has been substantially improved: (i) systems with several 100 millions of sites of two fcc lattice (diamond structure, volume >(100 nm)^3) can now be treated; (ii) a program using a CA for a nearest neighbour pair of lattice sites was developed which accelerates the calculations considerably; (iii) the Borland-PASCAL program was translated into FORTRAN and runs now on UNIX based computers.

*A. Volkov**
K.-H. Heinig
M. Strobel
*A. Ryazanov**

Theory of the kinetics of nanocluster formation and growth during ion implantation

Starting with the Fokker-Planck equation, the governing equations for nucleation and growth of nanoclusters have been derived for a spatially homogeneous system supersaturated by a continuous supply of impurity atoms, which atoms could be assumed to be atoms deposited by ion implantation. The derived equations are too complex in order to be treated by easy numerical means. Justified by our kinetic 3D lattice Monte Carlo calculations we divide the ion beam synthesis of nanoclusters in 3 stages: (i) supersaturation at the beginning of ion implantation; (ii) nucleation of nanoclusters when supersaturation is highest; (iii) no further nucleation; growth of nanoclusters at the expense of ion deposition and decreasing supersaturation. Using these findings, in the governing equations specific approximations could be made for the different stages. The simplified equations allow a suitable description of the dependence of the formation and growth of nanoclusters on the ion flux and fluence as well as on the temperature.

supported by BMBF

Collaboration: *Kurchatov Institute, Moscow, Russia

*V.A. Borodin**
K.-H. Heinig
S. Reiss

Self-organization kinetics in finite precipitate ensembles during coarsening

A rate equation approach is applied for the description of the self-organization (layering) phenomena predicted by recent computer experiments. We demonstrate that the layering is triggered by local inhomogeneities in the spatial distribution of precipitate sizes. The change of the spatial profile of precipitate size starts from the boundary of the system and occurs within a "reaction shell" having a thickness of the order of the diffusional screening length. During annealing this "reaction shell" shifts progressively into the system, leaving behind layers of precipitates. The layering is shown to occur only in sufficiently large systems with characteristic dimensions of at least several diffusional screening lengths. The reason for the weak sensitivity of the interlayer distance to variations of system parameters is elucidated.

supported by BMBF

Collaboration: * Kurchatov Institute, Moscow, Russia

L. Bischoff
J. Teichert
B. Schmidt

Writing FIB implantation and subsequent anisotropic wet chemical etching for fabrication of 3D structures in silicon

Micromechanical test structures were implanted into (100) oriented silicon wafers at room temperature with 35 keV Ga^+ ions at a current of 1.5 nA. The implantation fluence was varied between $1 \cdot 10^{14}$ cm^{-2} and $3 \cdot 10^{16}$ cm^{-2}. The subsequent anisotropic wet chemical etching was carried out in an etchant of KOH / H_2O etch solution of 30 % concentration at two fixed temperatures of 40 and 80 °C. The corresponding etch rates $R_{<100>}$ of nonimplanted silicon were determined to be 100 nm/min and 1100 nm/min, respectively. Furthermore the influence of an additional annealing step to the etching process was investigated. After a heat treatment of 800 °C a reverse etch effect was observed. It may be caused by the precipitation of Ga in large clusters and a correlated defect formation during annealing due to the high Ga content exceeding the solubility concentration of $1.5 \cdot 10^{19}$ cm^{-3} at 800 °C. The Ga^+ FIB patterned and wet chemical etched test structures were characterized by scanning electron microscopy.

S. Hausmann
L. Bischoff
J. Teichert
*M. Marso**
*J. Schelten**

Production of metal-semiconductor-metal photodetectors by focused ion beam implantation

Metal-semiconductor-metal (MSM) photodiodes are very fast and sensitive detectors and their simple planar structure enables easy fabrication. They consist of a set of interdigitated metal fingers on a semiconductor substrate which allows large active areas. The Schottky barriers at the metal-semiconductor interfaces limit the dark current.

The metallic structures in Si(111) are formed by ion beam synthesis (IBS) using a focused cobalt ion beam. Due to the high current density of a focused ion beam (>1A/cm^2) the implantation parameters for the IBS to form $CoSi_2$ differ from conventional implanters ($\approx$10 µA/cm^2). To produce low dark currents new implantation parameters must be found. For implantation energy, dose and annealing conditions the same dependencies as in conventional implanters were determined. With increasing target temperature (up to 400 °C) decreasing dark currents have been found but a minimum is not yet reached.

Therefore, further experiments will be done at higher target temperature. Reducing the current density at fixed target temperature (400 °C) results in lower dark currents.

supported by DFG

Collaboration: *Institut für Schicht und Ionentechnik, Forschungszentrum Jülich

L. Bischoff
J. Teichert
*F. Machalett**
*P. Seidel**
*E. Steinbeiß***

Investigation of Josephson arrays fabricated by focused ion beam irradiation

In order to form single weak links as well as one dimensional arrays with a high long term stability of their electronic parameters, $YBa_2Cu_3O_{7}$-microbridges and meander like structures were irradiated with 35 keV Ga^+ and 70 keV Co^{2+}-ions, using the Rossendorf focused ion beam (FIB) equipment IMSA-100. The ion fluence was varied in the range from $1 \cdot 10^{14}$ cm^{-2} to $5 \cdot 10^{16}$ cm^{-2}. A change of the critical current due to the radiation damage was found for different doses at a fixed temperature of 77 K. So a lowering of the critical temperature in the irradiated areas and a reduction of the critical current density with increasing dose values was measured. After processing with a fluence of $2 \cdot 10^{14}$ cm^{-2} of 70 keV Co^{2+} ions into a 100 nm

thick $YBa_2Cu_3O_7$ - layer Shapiro steps could be observed in the temperature range from 65 - 73 K during microwave irradiation at a frequency of 18.45 GHz. The variation of the microwave power resulted in a modulation of the height of the Shapiro steps. A comparable behaviour was also found at other microwave frequencies.

Collaboration: *Institut für Festkörperphysik, FSU Jena, **Institut für Physikalische Hochtechnologie Jena

J. Teichert
L. Bischoff
*B. Köhler**

Evidence for acoustic waves induced by a focused ion beam

The ion-acoustic effect has been investigated using intensity-modulated focused ion beams. The aim of these investigations is the development of an ion-acoustic microscope which would allow to image surface as well as subsurface structures with high lateral resolution. The experiments have been carried out with a 3 nA gallium ion beam of 35 keV and 300 nm spot size. The acoustic response has been measured using a piezoelectric transducer with integrated pre-amplifier. Due to the low power of about 100 µW of the incident ion beam the measured acoustic signals are very low and the signal-to-noise ratio is bad. Acoustic wave signals were unambiguously distinguished from electrical cross-talk and other non-acoustic source signals by identifying the excitations of bending oscillations.

*Collaboration:**Fraunhofer-Institut für zerstörungsfreie Werkstoffprüfung, Dresden

*W. Driesel**
*C. Dietzsch**
E. Hesse
L. Bischoff
J. Teichert

In situ observation of the tip shape of liquid alloy ion sources

For *in situ* observation of the tip shape of the liquid metal emitter, CoNd and CoGe liquid alloy ion sources were operated in a 1 MeV TEM. The ion sources were mounted to special specimen holders. The formation of the field-stabilized liquid alloy cone, the change in the tip shape as a function of ion emission current, spatial shifts of the liquid alloy cone, and microdroplet emission have been revealed. Below the onset voltage the shape of the liquid alloy tip is spherical. At the onset voltage the Taylor cone is formed. At higher ion emission currents there is a jetlike protrusion at the Taylor cone vertex. The cone half-angle decreases and the jet length increases with increasing emission current.

Collaboration: *Max-Planck-Institut für Mikrostrukturphysik, Halle

Plasma Immersion Ion Implantation

S. Mändl
J. Brutscher
R. Günzel

Ion energy distribution in plasma immersion ion implantation

In plasma immersion ion implantation the ions are accelerated from the plasma to the target by applying negative high voltage pulses to the target. Direct time-resolved ion flux measurements during these pulses were performed using a spherical target with a small orifice between 0.5 and 2 mm. The ions were collected in the high vacuum region behind this orifice and their energy distribution was determined with a Faraday cup. For voltage pulses of 5, 10, and 15 kV and a length between 10 and 50 µs the measured ion energy distribution function exhibits a sharp peak at the nominal energy, whereas, for 20 kV an additional low energy tail was observed. The total current exhibits a sharp maximum at the beginning of the pulse and decreases very fast after a few microseconds.

These findings can be explained using a theoretical model describing the plasma sheath expansion during the voltage pulses. The sheath edge expansion, which is related to the ion current, changes from supersonic at the onset of the pulse to a stationary state around 5 µs. At the same time, the width of the positively charged sheath, accomodating the potential drop, is larger for higher voltages. For an applied voltage of 20 kV this results in collisions during the transit of the accelerated ions through the sheath which causes the observed low energy tail.

supported by BMBF

R. Günzel

Plasma immersion ion implantation (PSII) of stainless steel

Hardness and wear of stainless steels can be substantially improved with plasma nitriding. However, relatively high temperatures are needed in this process, leading to the formation of chromium nitrides at temperatures above 450°C, which bind chromium from the solid solution, and therewith degrade the corrosion resistance. Therefore, nitriding of stainless steel must occur below 400°C, which can be done with PSII.

Four different steels, 210Cr46, X5CrNi18.10, 42CrMo4, and X20C13 were treated with nitrogen PSII at 350 °C for one hour and a dose of 10^{18} cm^{-2}. All samples were treated with 5 µs pulses at a repetition rate of 1 kHz and 40 kV, and the temperature was checked with a pyrometer. A substantial hardness increase by a factor of two to three was observed for all samples for depth up to several micrometers, which is in contrast to the mean projected range for ions ($R_p \approx 20$ nm). The elevated treatment temperature of 350 °C is responsible for the enhanced diffusion. The observed hardness increase concurs with a substantial wear reduction of several orders of magnitude. Glancing angle XRD measurements show that in all samples only a small fraction of the chromium was bound as CrN. Therewith, in spite of the considerable improvement of the tribological properties, the high corrosion resistance of these steels remains.

supported by BMBF

J. Brückner
J. Brutscher
R. Günzel

Metal plasma immersion ion implantation and deposition

A new facility for metal plasma immersion ion implantation and deposition was set into operation. This method combines plasma immersion ion implantation and cathodic arc deposition by selecting the ion energy. Macroparticels are filtered using a curved magnetic filter (90° deflection, total length 50 cm, inner diameter 15 cm). The magnetic field is about 10mT at the filter axis and a wall bias of +20V is used. The cathodic arc source is operated in DC mode and the plasma at the probe location can be pulsed by pulsing the magnetic field and bias voltage of the filter (rise and fall time 3-5 ms). The maximum current density in the center of the generated metal plasma beam is in the order of 1 mA/cm². The homogeneity depends on the distance from the filter exit. The maximum area for implantation and deposition is several 100 cm².

Ion Beam Analysis

C. Neelmeijer
M. Mäder
*H.-P. Schramm**

COST-G1 : The "Paint layers" research program

The mobility of XRF, i.e. the possibility of analysis to take place directly in the museum, favours this method in principle. However, the detection of chromophoric low-Z elements like Al and Si (identification of ultramarine) is difficult owing to the low excitation cross sections. If depth dependent analysis is of interest XRF fails while the combination of external PIXE varying the proton energy and RBS is successful. The latter was proofed not only to distinguish single layer sequences, e.g. cinnabar on white lead (on chalk ground) from white lead on cinnabar or the corresponding pigment admixture, but also structures of higher complexity, e.g. the systems ultramarine / ochre / white lead on chalk ground. On the basis of special suppositions (the pigment to binder ratio, for example) PIXE allows the nondestructive estimation of paint layer thicknesses.

Collaboration: *Hochschule für Bildende Künste, Dresden

M. Mäder
C. Neelmeijer
*H.-P. Schramm**

Non-destructive pigment investigation of historic book paintings

Comparative characterization of the paint material of three coloured volumes of G. Agricola's "De re metallica" (museums of Freiberg, Zwickau, Glauchau) has been carried out using external PIXE. Generally, the identified pigments represent a historical palette. However, the various books show significant differences not only in the design but also in the pigments. Cinnabar and minium from red as well as copper blue and copper blue admixed with smalt were identified in the issues of Freiberg and Zwickau, respectively. In the book of Freiberg the copper green pigment was found to be atacamite.

Collaboration: *Hochschule für Bildende Künste, Dresden, Stadt- und Bergbaumuseum Freiberg, Städtisches Museum Zwickau, Stadtmuseum Glauchau

M. Friedrich
G. Sun
W. Bürger
R. Grötzschel
*R. Behrisch**
*C. García-Rosales**

supported by BMBF

Tritium depth profiling by accelerator mass spectrometry

Depth profiles of tritium in plasma-exposed samples from the Garching fusion experiment ASDEX-upgrade were measured by AMS at the 3 MV Tandetron. The measured tritium concentrations in a surface layer $\leq 25\ \mu m$ were in the range of 10^{11} to 5×10^{15} atoms/cm^3. The detection limit was about 10^{11} atoms/cm^3.

The distortion of the measured profiles due to edge effects from the side wall of the sputter crater was reduced by special shaping of the samples and by electronic gating.

Collaboration: *Max-Planck-Institut für Plasmaphysik Garching

P. Nitzsche
K. Lange
B. Schmidt
S. Grigull
U. Kreissig
*B. Thomas**
*K. Herzog**

Oxygen-, hydrogen- and sodium-drift in TEMPAX during anodic bonding to silicon or metals

The changes of near-surface hydrogen and oxygen depth profiles in TEMPAX glass were measured in situ by Heavy-Ion-ERDA using 35 MeV Cl ions at an incidence angle of 7° during several drift treatments. A shift of the oxygen profile edge into the metal or the silicon top layer (anode) was obtained at relatively low temperatures of 240 to 320 °C and a drift voltage of 250 V. As a consequence, the anodic bonding process cannot be explained as a purely thermally activated but mainly as an electric field assisted oxydation. The investigation of hydrogen shows that the initial profile redistributes only inside the Na-depleted glass layer. Besides the essential proton drift in the same direction as the Na drift a small shift of the

H profile edge into anode direction has been observed especially at the initial stage of the drift period. From NMR-measurements we conclude that the weakely bonded Na^+ ions are removed from the $[AlO_4]$- und $[BO_4]$-network groups and substituted by hydrogen. As a conclusion it can be established that the earlier supposed model of Na_2O dissociation and corresponding drift of Na and O toward the cathode and anode respectively does not describe correctly the bonding process. The absence of non-bridging oxygen in TEMPAX glass, which was also proved by NMR investigations, gives additional rise to suggest a new explanation of the oxydation path. In that case the H_2O dissociation inside the "leached" glass surface layer leads to H^+ and OH^-, and the drift of the hydroxid groups toward the anode will be the first step for the chemical interface bonding. After that the OH-groups together with the metal or silicon build up unstable complexes, which are transformed into metal oxide or silicon oxide and H_2O.

Collaboration: *TU Bergakademie Freiberg, Institut für Analytische Chemie

J. von Borany
D. Grambole
R. Grötzschel
F. Herrmann

Radiation damage investigations of silicon detectors during heavy ion spectroscopy using the nuclear microprobe

The radiation damage of silicon ion implanted detectors ($A=25\ mm^2$) for the spectroscopy of oxygen ions has been investigated using the Rossendorf nuclear microprobe. The irradiation of the detector was performed with 3.5 MeV oxygen ions under random incidence conditions. The area of the ion beam was varied between unfocused irradiation (some mm^2) and a minimum spot size of $20 \times 20\ \mu m^2$. The generally assumed letal fluence of heavy ion spectroscopy with silicon detectors of about $10^8 ... 10^9$ ions/cm^2 is related only to unfocused irradiation conditions. In this case, the enlarged electronic noise due to increased detector leakage current results in the reduced detector resolution. Under small spot incidence conditions the degradation of the detector resolution is caused by incomplete charge collection, which becomes significant only for very low local minority carrier lifetimes below 1 µs. Therefore, local fluences up to 10^{12} oxygen ions/cm^2 can be measured without significant peak broadening.

S. Hausmann
L. Bischoff
D. Grambole
F. Herrmann
J. Teichert

RBS investigations of focused ion beam implanted Co into Si(111) at the Rossendorf nuclear microprobe

The quality of $CoSi_2$-layers produced by ion beam synthesis depends on the damage production during implantation which is reduced by heating the silicon target. Focused ion beam (FIB) implantation means implantation with current densities higher than $1 A/cm^2$. Therefore, the optimum target temperature is different from that during conventional implantation. We implanted square areas with a size of $40 \times 40\ \mu m^2$ in channeling direction using a 70 keV Co^{2+} FIB and varied the target temperature from room temperature to 400 °C.

The implanted areas were analysed by RBS at the Rossendorf nuclear microprobe using a 3 MeV Li^+ beam with a spot size of about $5 \times 5\ \mu m^2$. Between 300 °C and 400 °C a significant increase of the mean projected range of the cobalt atoms was found. The increased range is interpreted by channeling during implantation due to continous damage annealing at elevated temperatures up to highest doses.

Equipment

M. Friedrich
S. Turuc
W. Bürger

Operation and development of the electrostatic accelerators

The *2 MV VdG* has been operated reliably exclusively for RBS measurements.

The ***5 MV Tandem*** has been applied to ion beam analysis, high energy implantation, surface modification, basic ion-solid interaction research and detector development. The reconstruction of the accelerator building including the electric power and heating system has improved the conditions for stable accelerator operation. Only a single opening of the pressure vessel was necessary for maintenance (exchange of a damaged ball bearing). The power supplies and the control scheme of the magnetic quadrupole lenses have been modernised. A prototype of a modular microprocessor based unit for common control purposes has been set into operation at the injector magnet power supply. At the central site of the accelerator a low inductance grounding system has been installed. The aim was to decrease the probability of critical electromagnetic interferences with respect to microprocessor controlled devices. A new compressor (Neumann & Esser) with low gas loss has been installed at the insulating gas handling system.

The ***3 MV Tandetron*** has been used for high energy ion implantation, ion beam synthesis and ion beam analysis. The facility proved to be very reliable at acceleration voltages from 0.1 to 3.0 MV. Earlier problems with the Li charge exchange channel for the production of negative He ions have been solved now with a new version of this device (HVEE Amersfoort).

W. Matz
F. Prokert
N. Schell
F. Eichhorn
M. Betzl

Synchrotron radiation beamline at the ESRF (Project ROBL)

The beamline structure, i.e. the lead shielded hutches and the control cabins were built and the installation of the communications was finished in 1996. The beam line optics was contracted and all technical specifications were written and agreed with the companies. For the materials research experiment the 6-circle-goniometer, a detector and a high temperature chamber were purchased. This equipment is under test in Rossendorf.

Collaboration: Institut für Radiochemie, Zentralabteilung Forschungs- und Informationstechnik, ESRF Grenoble

M. Weiler

Characterization of an ECWR-plasma beam

Mass spectroscopy, optical emission spectroscopy and faraday cup measurements have been carried out in order to characterize a plasma beam extracted from an inductively coupled, high frequency discharge with a superimposed perpendicular magnetic field (between 0.1 and 2 mT). The resonance of the electron cyclotron wave (ECWR) is used to optimize the ionization and dissociation degree of the plasma. The dissociation degree is strongly related to the residence time of the molecules in the plasma which is determined by the gas flow rate and the pumping speed. In the case of diatomic gases like oxygen and nitrogen as well as hydrogen, in a zero order resonance excited plasma, at flow rates above 20 sccm a dissociation degree of nearly 90% can be achieved. It is shown that the ECWR plasma excitation provides highly ionized plasma beams of H^+, N^+ and O^+ with well defined ion energies. The ion current density varies between 0.1 and 3 mA/cm^2 as a function of r.f. power and the ion energy varies between 10 and 300 eV as a function of the applied r.f. amplitude. The ion energy distribution always shows a sharp Gaussian distribution with a width of $\Delta E/E$ below 5 %.

Collaboration: CCR GmbH, Technologiezentrum ROTECH, Rossendorf

D. Panknin
R. Kliemann

High temperature chamber for Hall effect measurements

For investigations of the doping efficiency of SiC a high temperature chamber for Hall effect measurements at temperatures up to 500 °C was constructed. The chamber is used in combination with the commercial Hall effect measurement system HL 5500 (BIORAD Inc.) using an external electric magnet. The chamber can be evacuated and is water cooled. The heater is spiral and brazed on the backside of the sample holder. The temperature is measured using a thermocouple on SiC or on the sample holder. The Hall effect measurements using probes made of tungsten wire can be carried out in gas ambient or under vacuum. The step height and the rising time of the temperature rise are adjustable.

Other Activities

M. Jentschel
K.-H. Heinig
*H.-G. Börner**
*C. Doll***
*J. Jolie****

Crystal-GRID investigations on atomic collision cascades in ionic compounds

Crystal-GRID experiments with single-crystals of TiO_2 and NaCl have been carried out at the high-flux reactor of the ILL Grenoble. The energy of secondary γ-quanta emitted by recoiling atomic nuclei was measured with ultra-high resolution allowing to deduce information on the average velocity of atoms at the moment of γ-emission. The nuclei are excited by thermal neutron capture and recoiled by a primary γ quanta emission. The kinetic energies of the ^{49}Ti and ^{36}Cl are 261eV and 486eV, respectively. Contrary to disordered targets, for single-crystals a pronounced structure of Doppler-broadened γ-lineshapes is theoretically predicted and experimentally verified. The data of NaCl were analysed using different approximations in Molecular Dynamics simulations of the slowing down of recoils. In ionic compounds, first evidence for a very collective character of the slowing down was obtained even when the recoil energies were several hundreds of eV. It turns out that ionic compounds are no good candidates for the study of the repulsive interaction of atoms at small separations due to this collective character, which is caused mainly by the long-range Coulomb interaction.

supported by SWMK

Collaboration: *ILL Grenoble, F, **TU München, Physics Department, ***University Fribourg, CH

M. Jentschel
*H.-G. Börner**
*C. Doll***
*N. Stritt****
*J. Jolie****
K.-H. Heinig

Study of low-energy atomic motion after β-decay and neutrino emission

In Crystal-GRID experiments, the recoiling atoms have kinetic energies of several hundreds of eV. With much lower recoil energies in the range 0...40 eV, the β-decay of ^{24}Na to ^{24}Mg in NaCl and the K-shell capture of ^{152}Eu to ^{152}Sm in EuO single-crystals have been studied. The <100>and <110>crystal-to-spectrometer aligned line-shapes are clearly different for the β-decay, too. By Molecular Dynamics simulations this effect could not be explained, which is attributed to the bad understanding of the charge state of ^{24}Mg in NaCl. The K-shell capture leads to the emission of a neutrino, which induces a recoil energy of only 3eV to the produced ^{152}Sm nucleus. In this case the lineshapes are in good agreement with the simulations.

supported by SMWK

Collaboration: *ILL Grenoble, F, **TU München, Physics Department, ***University Fribourg, CH

F. Prokert
N. Schell
F. Eichhorn
*J. Sass**
*K. Masur**

X-ray reflectometry for determination of layer and interface parameters

Using the reflectometry set-up of the Siemens X-ray diffractometer D5000 and a Göbel mirror beam conditioner, reflectivity studies were performed on Ni/C and W/C gradient multilayers (ML) (50x Ni/C, 100x W/C) on Si** and on cleaned surfaces of $NdGaO_3$, Silicon and $A^{III}B^{V}$-type semiconductor wafers (GaAs, InAs, InP,GeP) to be used as substrates for HTSC films*. Due to the improved intensity conditions the ML reflections up to the 6th order could be used for the determination of the layer parameters (superlattice period and interface rms.-roughness σ) and their variations. For the substrate materials the values of the rms.-roughness for the surfaces were found to be strongly dependent on the wafer preparation technology. For the Si(111) surface e.g. a reduction of the rms.-value σ from (0.45 ± 0.03) nm to (0.05 ± 0.03) nm was determined after tempering in vacuum at 1100 °C for 15 min. The surface roughness for $NdGaO_3$ surprisingly was found to be extremely low ($\sigma \sim 0.23$ nm).

Collaboration: *Institute of Electronic Materials Technology ,Warsaw, P, **FhG-IWS Dresden

F. Prokert
W. Matz

XRD studies of uranium compounds and geological samples

Crystal structure investigations by XRD was performed to support the development of new preparation techniques of pure calcium uranate, sodium uranyle acetates, and uranylmalonates in the Institute of Radiochemistry. The X-ray data were used to judge the purity of samples. While calcium uranate can be prepared as pure phase there are phase contamination problems with the uranyles. The confirmation of crystallographic data is essential for EXAFS studies to be performed at the uranium compound. Different samples from natural rocks have been analysed for phase composition. All materials were used to study chemical degradation or transport processes of heavy metal compounds in geological formations. XRD analysis is used to detect structural changes after different treatments.

Collaboration: Institute of Radiochemistry of the FZR

T. Gehring,
*S. Howitz**

New microfluidic components for a miniature chemical analysis system

A nozzle-diffusor-pump and a flow sensor as two new elements for use in a silicon integrated miniature chemical analysis system were developed and tested.

The ***nozzle-diffuser-pump*** is a valveless, silicon-based micropump with a piezo-actuated mem-brane. The layout of this pump was optimized concerning the fluidic efficiency using a finite element program with the result of an optimized inlet/outlet opening angle of the pump chamber of about 8°. A modified version of the nozzle-diffuser-micro-pump with pumping rates up to 100 µl/ min at moderate driving voltages up to 80 V was realized.

For the detection of low flow rates less then 100 µl/min a ***thermal flow sensor*** based on a thin film heater on a SiN bridge surrounded by thin film thermistors was developed. The fluid temperature difference on two thermistors situated along a fluidic microchannel in silicon correlates to the flow rate. A first application of this new sensor has been realized for failure diagnostics of silicon micropumps in a fluidic microsystem.

supported by SMWA

Collaboration: *GeSiM mbH, Technology Center Rossendorf, Institut für Physikalische Hochtechnologie, Jena

Statistics

Publications

Bender, H, Brutscher, J., Ensinger, W., Günzel, R., Halder, J., Klein, J., Rauschenbach, B., Schäfer, J., Seiler, B., Thomae, R.,
Influence of plasma density and plasma sheath dynamics on the ion implantation by plasma immersion technique,
Nucl. Instr. Meth. B113 (1996) 266

Bischoff, L., Heinig, K.-H., Teichert, J., Skorupa, W.,
Submicron $CoSi_2$-structures fabricated by focused ion beam implantation and local flash lamp melting,
Nucl. Instr. Meth. B112 (1996) 201

Bischoff, L., Teichert, J., Hesse, E., Panknin, D., Skorupa, W.,
Ion beam synthesis of $CoSi_2$-microstructures by means of a high current focused ion beam,
"Ion Beam Modification of Materials" J.S.Williams, R.G. Elliman, M.C. Ridgway (eds.), Elsevier Science B.V. 1996, p. 933

Bischoff, L., Teichert, J., Hesse, E., Prewett, P.D., Wilson, J.G.,
Cluster beams from a Co-Nd liquid alloy ion source,
Microelectronic Engineering 30 (1996) 245

Borany, J. von, Schmidt, B., Grötzschel, R.,
The application of high energy ion implantation for silicon radiation detectors,
Nucl. Instr. Meth. A377 (1996) 514

Brauer, G., Anwand, W., Pacaud, Y., Skorupa, W., Plazaola, F., Coleman, P.G., Knights, A.P., Stoermer, J., Willutzki, P.,
Positron studies of defects in ion implanted SiC,
in "Silicon carbide and related materials", S.Nakashima, H.Matsunami, S.Yoshida, H.Harima (eds.), Inst.Phys.Conf.Ser.142 (1996) 457

Brauer, G., Anwand, W., Pacaud, Y., Skorupa, W., Plazaola, F., Coleman, P.G., Stoermer, J., Willutzki, P.,
Positron studies of defects in ion implanted SiC,
Phys. Rev. B54 (1996) 3084

Brauer, G., Kolitsch, A., Schut, A., van Veen, A.,
Variable energy positron measurements at nitrogen ion bombarded steel surfaces,
Effects of Radiation on Materials, ed. D.S.Gelles, R.K. Nanstad, A.S. Kumar, E.A. Little (eds.), ASTM 04-012700-35, p. 1134

Brenscheidt, F., Fischer, W., Matz, W., Wieser, E. ,
The influence of ion energy on the wear behaviour of titanium-implanted silicon nitride ceramics,
Surf. Coat. Technol. 83 (1996) 317

Brutscher, J., Günzel, R., Möller, W.,
Sheath dynamics in plasma immersion ion implantation,
Plasma Sources Sci. Technol. 5 (1996) 54

Brutscher, J.,
A 100kV 10A high-voltage pulse generator for plasma immersion ion implantation,
Rev. Sci. Instrum. 67 (1996) 2621

Chudoba, T., Richter, E., Schneider, M.,
Improvement of hardness, wear and corrosion behaviour of magnesium by ion implantation,
Proc. of the Ion Beam Modification of Materials (1996) 1008

Dobler, M., Reuther, H., Barradas, N.P.,
Conversion electron Mössbauer spectroscopy studies of FeSi and $FeSi_2$,
Hyperfine Interactions C1 (1996) 266

Dobler, M., Reuther, H., Betzl, M., Mäder, M.,
Investigation of ion beam synthesized iron silicide layers by conversion electron Mössbauer spectroscopy,
SIF Conf. Proc. Vol. 50, ICAME'95, I. Ortalli (ed.), Bologna 1996, p. 687

Dobler, M., Reuther, H., Betzl, M., Mäder, M., Möller, W.,
Investigations of ion implanted iron silicide layers after annealing and irradiation,
Nucl. Instr. Meth. B117 (1996) 117

Driesel, W., Dietzsch, C., Hesse, E., Bischoff, L., Teichert, J.,
In situ observation of the tip shape of Co-Ge liquid alloy ion sources in a high voltage transmission electron microscope,
J. Vac. Sci. Technol. B14 (1996) 1621

Eremin, V.K., Ilyashenko, I.N., Strokan, N.B., Schmidt, B.,
Recombination of Nonequilibrium charge carriers in heavy ion tracks in silicon,
Nucl. Instr. Meth. A377 (1996) 184

Friedrich, M., Bürger, W., Henke, D., Turuc, S.,
The Rossendorf 3 MV Tandetron: a new generation of high energy implanters,
Nucl. Instr. Meth. A382 (1996) 357

Fukarek, W., Yankow, R.A., Skorupa, W.,
Comparative study of SIMOX structures using four analytical techniques,
Surface and Interface Analysis 24 (1996) 243

Garke, B., Edelmann, C., Günzel, R., Brutscher, J.,
Modifizierung der Gasabgabe von Edelstahloberflächen durch Ionenimplantation,
Vakuum in Forschung und Praxis (1996) 251

Grambole, D., Herrmann, F., Herrmann, B.,
Multielement analysis on bone structures of medieval human femur,
Nucl. Instr. Meth. B109/110 (1996) 667

Große, M., Hempel, A., Böhmer, J., Eichhorn, F., Riekel, C., Engström, P.,
SAXS investigation of the structural changes in the plastic one ahead of a crack tip in ductile metals,
J. Mol. Struct. 383 (1996)267

Grötzschel, R., Mäder, M., Kreißig, U., Grigull, S., Assmann, W., Parhofer, S.,
Composition analysis of Nd_xFe_yB thin films by RBS and heavy ion ERDA,
Nucl. Instr. Meth. B118 (1996) 139

Günzel, R., Brutscher, J.,
Sheath dynamics in plasma immersion ion implantation,
Surf. Coat. Technol. 85 (1996) 98

Harz, M., Brückner, W.,
Stress reduction in anodically bonded silicon and borosilicate glass by thermal treatment,
J. Electrochem. Soc. 143 (1996) 1409

Harz, M., Engelke, H.,
Curvature changing and flattening of anodically bonded silicon and borosilicate glass,
Sensors and Actuators 55 (1996) 201

Heera, V.,
Comment on 'Evidence of enhanced epitaxial crystallisation at low temperature by inelastic electronic scattering of mega-electron-volt heavy-ion-beam irradiation [J.Nakata, J. Appl. Phys. 79 (1996) 682],
J. Appl. Phys. 80 (1996) 4235

Heera, V., Kögler, R., Skorupa, W., Stoemenos, J.
Ion beam induced crystallization of 6H-SiC,
"Silicon carbide and related materials", S.Nakashima, H.Matsunami, S.Yoshida, H.Harima (eds.),
Inst.Phys.Conf.Ser.142 (1996) 533

Heera, V., Petzoldt, J., Ning, X.J., Pirouz, P.,
High dose Co implantation of Aluminum and Nitrogen in 6H-Silicon Carbide,
"Silicon carbide and related materials", S.Nakashima, H.Matsunami, S.Yoshida, H.Harima (eds.),
Inst.Phys.Conf.Ser.142 (1996) 509

Hempel, A., Eichhorn, F., Reichel, P., Boede, W.,
A neutron double-crystal diffractometer with a position sensitive detector for small-angle scattering studies,
Nucl. Instr. Meth. A381 (1996) 466

Henkel, T., Heera, V., Kögler, R., Skorupa, W., Seibt, M.,
The temperature dependence of the ion beam induced interfacial amorphization in silicon,
Appl. Phys. Lett. 68 (1996) 3425

Hermann, S., Mahnke, H.-E., Schumann, D., Spellmeyer, B., Sulzer, G., Bollmann, J., Reinhold, B., Röhrich, J., Wienecke, M., Yankov, R., Gumlich, H.-E.,
Palladium as impurity in ZnTe,
J. Cryst. Growth 161 (1996) 181

Hesse, E., Driesel, W., Dietzsch, C., Bischoff, L., Teichert, J.,
Shape of a Co-Nd liquid alloy ion source,
Jap. J. Appl. Phys. Part I 35 (1996) 5564

Hesse, E., Mair, G.L.R., Bischoff, L., Teichert, J.,
Parametric investigation of current pulses in a liquid metal ion emitter,
J. Phys. D: Appl. Phys. 29 (1996) 2193

Illyashenko, I.N., Strokan, N.B., Schmidt, B.,
Characteristic features of the lineshape in the spectrometry of ions using Si detectors,
Semiconductors 30 (1996) 1158

Jäger, H.-U. ,
An explanation of trap-limited self-interstitial diffusion and enhanced boron clustering in boron doped silicon superlattices,
"Process Physics and Modeling in Semiconductor Technology", G.R. Srinivasan, Murthy, C.S., S.T. Dunham (eds.), The Electrochemical Society, Inc., Proceedings Series, Pennington, NJ (1996), PV 96-4, p. 210

Kögler, R., Heera, V., Skorupa, W., Voelskow, M.,
Ion beam induced epitaxial crystallisation of SiC: Fluence and temperature dependence,
"Ion Beam Modification of Materials" J.S.Williams, R.G. Elliman, M.C. Ridgway
(eds.), Elsevier Science B.V. 1996, p. 912

Köhler, B., Teichert, J., Bischoff, L.,
Investigation of the ion acoustic effect during focused ion beam irradiation,
Nucl. Instr. Meth. B120 (1996) 311

Kolitsch, A., Richter, E., Drummer, H., Roland, U., Ullmann, J.,
Effects of post-treatment of amorphous carbon films with high energy ion beams,
Nucl. Instr. Meth. B106 (1996) 511

Kolitsch, A., Sümmchen, L., Ullmann, J., Falke, U., Heger, P.,
Post-ion-implantation into amorphous carbon films,
Surf. Coat. Technol. 84 (1996) 495

Kruijer, S.Reuther, H., Nikolov, O., Brand, R.A., Keune, W., Liljequist, D., Weber, S.,
Scherrer, S.,
CEMS and DCEMS investigations of aluminium implanted iron,
SIF Conf. Proc. Vol. 50, ICAME'95, I. Ortalli (ed.), Bologna 1996, p. 699

Mändl, S., Brutscher, J., Günzel, R., Möller, W.,
Design considerations for plasma immersion ion implantation systems,
Nucl. Instr. Meth. B112 (1996) 252

Mändl, S., Brutscher, J., Günzel, R., Möller, W.,
Inherent possibilities and restrictions of plasma immersion ion implantation systems,
J. Vac. Sci. Technol. B14 (1996) 2701

Mathar, R.,
Influence of the first-order polarization on the stopping power of bare charges in the jellium model,
Phys. Rev. A53 (1996) 2873

Moll, H., Geipel, G., Matz, W., Bernhard, G., Nitsche, H.,
Solubility and speciation of $(UO_2)_2SiO_4 \cdot 2H_2O$ in aqueous systems,
Radiochimica Acta 74 (1996) 3

Möller, D., Pham, M.T., Hüller, J.,
Sensitization of silicon nitride surfaces for Ag^+ ions by ion implantation,
Proc. of EUROSENSORS X, The 10th European Conference on Solid-State Transducers, R. Puers
(ed.), Leuven, Belgium (1996), p. 243

Möller, W., Richter, E.,
Praktische Anwendungen der Ionenimplantation,
Neue Schichtsysteme für die Industrie, 18. Ulmer Gespräch, Saulgau (1996)

Murthy, C.S., Posselt, M., Frei, T.,
Three-dimensional modeling of low-dose BF_2^+ implantation into single-crystalline silicon,
J. Vac. Sc. Technol. B14 (1996) 278

Neelmeijer, C., Wagner, W., Schramm, H.-P.,
Depth resolved ion beam analysis of objects of art,
Nucl. Instr. Meth. B118 (1996) 338

Nomura, K., Reuther, H., Richter, E., Ujihira, Y.,
Magnetic structure of Fe-Si-Al films implanted with Al and N ions,
SIF Conf. Proc. Vol. 50, ICAME'95, I. Ortalli (ed.), Bologna 1996, p. 703

Pacaud, Y., Brauer, G., Perez-Rodriguez, A., Stoemenos, J., Barklie, R.C., Voelskow, M., Skorupa, W.,
Study of the different stages of damage induced by 200 keV Ge^+ ion implantation in 6H-SiC,
"Silicon carbide and related materials", S.Nakashima, H.Matsunami, S.Yoshida, H.Harima (eds.),
Inst.Phys.Conf.Ser.142 (1996) 537

Pacaud, Y., Skorupa, W., Perez-Rodriguez, A., Brauer, G., Stoemenos, J., Barklie, R.C.,
Investigation of the damage induced by 200 keV Ge ion implantation in 6H-SiC
Nucl. Instr. Meth. B112 (1996) 321

Pacaud, Y., Skorupa, W., Stoemenos, J.,
Microstructural characterisation of amorphised and recrystallised 6H-SiC,
Nucl. Instr. Meth. B120 (1996) 181

Pacaud, Y., Stoemenos, J., Brauer, G., Yankov, R.A., Heera, V., Voelskow, M., Kögler, R., Skorupa, W.,
Radiation damage and annealing behaviour of Ge^+-implanted SiC,
Nucl. Instr. Meth. B120 (1996) 177

Palard, M., Ruault, M.-O., Kaitasov, O, Bernas, H., Heinig, K.-H.,
Irradiation induced growth of CoSi2 precipitates in Si at 650 °C: An in-situ study,
Nucl. Instr. Meth. B120 (1996) 212

Panknin, D., Wieser, E., Skorupa,W., Henrion,W., Lange, H.,
Buried $(Fe_{1-x}Co_x)Si_2$ layers with variable band gap formed by ion beam synthesis,
Appl. Phys. A62 (1996) 155

Perez-Rodriguez, A., Kögler, R., Calvo-Barrio, L., Serre, C., Romano-Rodriguez, A., Heera, V., Skorupa, W., Morante, J.R.,
Ion beam assisted recrystallisation of SiC/Si structures,
Nucl. Instr. Meth. B112 (1996) 334

Perez-Rodriguez, A., Pacaud, Y., Calvo-Barrio, L., Skorupa, W., Morante, J.R.,
Analysis of ion beam induced damage and amorphization of 6H-SiC by Raman scattering,
J. of Electr. Mat. 25 (1996) 541

Perez-Rodriguez, A., Romano-Rodriguez, A., Serre, C., Calvo-Barrio, L., Cabezas, R., Morante, J.R., Kögler, R., Skorupa, W., Rodriguez, A.,
High temperature high dose carbon implantation in epitaxial SiGe,
Nucl. Instr. Meth.B120 (1996) 173

Perez-Rodriguez, A., Romano-Rodriguez, A., Serre, C., Calvo-Barrio, L., Cabezas, R., Morante, J.R., Calderer, J., Reuther, H., Skorupa, W.,
Ion beam synthesis and recrystallisation of amorphous SiGe/SiC structures,
Nucl. Instr. Meth. B120 (1996) 151

Pham, M. T., Matz, W., Möller, D., Hüller, J.,
Ion beam sensitized SiO_2 surface for halide ions,
Analytica Chimica Acta 320 (1996) 289

Pham, M. T., Möller, D., Hüller, J., Albrecht, J.,
Coimplantation of silver and halogens in thin SiO_2 films,
J. Appl. Phys. 79 (1996) 3915

Plass, F.M., Fukarek, W., Mändl, S., Möller, W.,
Phase identification of boron nitride thin films by polarized infrared reflection spectroscopy,
Appl. Phys. Lett. 69 (1996) 46

Plass, F.M., Fukarek, W., Kolitsch, A., Mäder, M., Möller W.,
Evidence for layered structure of boron nitride films detected by Rutherford backscattering,
Phys. Stat. Sol (a) 155 (1996) K1

Plass, M.F., Fukarek, W., Kolitsch, A., Steffen, J., Kreißig, U., Möller, W.,
Growth and characterisation of boron nitride thin films,
Surf. Coat. Technol. 84 (1996) 383

Posselt, M., Schmidt, B., Murthy, C.S., Feudel, T.,
Modeling of damage accumulation during ion implantation into single-crystalline silicon,
in: Process Physics and Modeling in Semiconductor Technology, G.R. Srinivasan, Murthy, C.S., and S.T. Dunham (eds.),The Electrochemical Society, Inc., Proceedings Series, Pennington, NJ (1996), PV 96-4, p. 453

Prokert, F., Savenko, B.N., Balagurov, A.M.,
Neutron diffraction study of phase transitions in the mixed crystal $Sr_{0.7}Ba_{0.3}Nb_2O_6$
between 20 and 300 K,
Ferroelectrics 188 (1996) 187

Prokert, F., Savenko, B.N., Balagurov, A.M.,
Observation of ferroelelastic domain effects at a study of low-temperature phase transitions in
$Sr_{0.7}Ba_{0.3}Nb_2O_6$,
Proc.Int. Symp. on Ferroic Domains and Mesoscopic Structures, ISFD4,Vienna, 1996, p. 100

Reiss, S., Heinig, K.-H.,
Self-structuring of buried SiO_2 precipitate layers during IBS: A computer simulation,
Nucl. Instr. Meth. B112 (1996) 223

Reuther, H., Dobler, M.,
CEMS and AES investigations on iron silicides,
Surf. Interf. Analysis 24 (1996) 411

Reuther, H., Dobler, M.,
Implantation and growth of large β-$FeSi_2$ precipitates and α-$FeSi_2$ network structures in silicon,
Appl. Phys. Lett. 69 (1996) 3176

Reuther, H., Lange, H., Dobler, M., Schumann, J.,
CEMS studies on iron silicides,
SIF Conf. Proc. Vol. 50, ICAME'95, I. Ortalli (ed.), Bologna, 1996, p. 573

Richter, E.,
Verfahren der Ionenstrahlbearbeitung und ihre Anwendung bei Umformwerkzeugen,
Blech Rohre Profile 43 (1996) 191

Romano-Rodriguez, A., Perez-Rodriguez, A., Serre, C., Calvo-Barrio, L., Morante, J.R., Kögler, R., Skorupa, W.,
TEM characterisation of Beta-SiC synthesised by high dose carbon implantation into silicon,
Proc. 9. Int. Conf. on Microscopy of Semiconducting Materials, Oxford (UK),
"Microscopy of Semiconducting Materials 1995", A.G.Cullis, A.E.Staton-Bevan (eds.),
Inst.Phys.Conf.Ser.No.146 (1995), p. 477

Romano-Rodriguez, A., Serre, C., Calvo-Barrio, L., Perez-Rodriguez, A., Morante, J.R., Kögler, R., Skorupa, W.,
Detailed analysis of β-SiC formation by high dose carbon ion implantation in silicon,
Mat. Sc. Eng. B36 (1996) 282

Schell, N., Simmons, R.O., Burkel, E.,
Low energy exitations in condensed ^{4}He at 56 MPa and 5 K studied by high-resolution inelastic X-Ray scattering spectroscopy,
J. of Synchr. Rad. 3 (1996) 316

Schmidt, B., Bischoff, L., Teichert, J.,
Writing FIB implantation and subsequent anisotropic wet chemical etching for fabrication of 3D structures in silicon,
Proc. of EUROSENSORS X, The 10th European Conference on Solid-State Transducers, P. Puers (ed.), Leuven, Belgium, (1996), p. 279

Schneider, P., Bischoff, L., Teichert, J., Hesse, E.,
The sputtering yield of cobalt ions on silicon and related materials,
Nucl. Instr. Meth. B117 (1996) 77

Serre, C., Calvo-Barrio, A., Perez-Rodriguez, A., Romano-Rodriguez, A., Morante, J.R., Pacaud, Y., Kögler, R., Heera, V., Skorupa, W.,
Ion beam synthesis of a-SiC films: Structural analysis and recrystallisation,
J. Appl. Phys. 79 (1996) 6907

Serre, C., Perez-Rodriguez, A., Calvo-Barrio, L., Romano-Rodriguez, A., Morante, J.R., Esteve, J., Acero, M.C., Skorupa, W., Kögler, R.,
Synthesis of thin membranes in Si technology by carbon ion implantation,
Mat.Res.Soc.Symp.Proc. 396 (1996) 727

Simov, S., Kalitzova, M., Karpuzov, D., Yankov, R., Angelov, C., Faure, J., Bonhomme, P., Balossier, G.,
High-dose phenomena in zinc-implanted silicon crystals,
J. Appl. Phys. 79 (1996) 3470

Skorupa, W., Heera, V., Pacaud, Y., Weishart, H.,
Ion beam processing of single crystalline silicon carbide,
Nucl. Instr. Meth. B120 (1996) 114

Skorupa, W., Yankov, R.A.,
Carbon-mediated effects in silicon and in silicon-related materials,
Materials Chemistry and Physics, L.J.Chen, K.N.Tu, U.M.Gösele (eds.), Elsevier Sequoia, Lausanne, 44 (1996) 101

Skorupa, W., Yankov, R.A., Rebohle, L., Fröb, H., Böhme, T., Leo, K., Tyschenko, I.E., Kachurin, G.A.,
A study of the blue photoluminescence emission from thermally-grown, Si-implanted SiO_2 films after short-time annealing,
Nucl. Instr. Meth. B120 (1996) 106

Skorupa, W., Yankov, R.A., Tyschenko, I.E., Fröb, H., Böhme, T., Leo, K.,
Room-temperature, short wavelength (400-500 nm) photoluminescence from silicon-implanted silicon dioxide films,
Appl. Phys. Lett. 68 (1996) 2410

Strobel, M., Reiss, S., Heinig, K.-H.,
Evolution of nanocluster ensembles: Computer simulation of diffusion and reaction controlled Ostwald ripening,
Nucl. Instr. Meth. B120 (1996) 216

Teichert, J., Bischoff, L., Köhler, B.,
Evidence for acoustic waves induced by focused ion beams,
Appl. Phys. Lett. 69 (1996) 1544

Teichert, J., Bischoff, L., Hesse, E., Schneider, P., Panknin, D., Geßner, R., Löbner, B., Zichner, N.,
Cobalt disilicide interconnects for micromechanical devices,
J. of Micromechanics and Microengineering 6 (1996) 272

Weishart, H., Matz, W., Skorupa, W.,
Ion beam synthesis by high dose tungsten implantation into 6H-silicon carbide,
"Silicon carbide and related materials", S.Nakashima, H.Matsunami, S.Yoshida, H.Harima (eds.),
Inst.Phys.Conf.Ser.142 (1996) 541

Weishart, H., Matz, W., Skorupa, W.,
Ion beam synthesis by tungsten implantation into 6H-SiC at elevated temperatures,
Mat.Res.Soc.Symp.Proc.423 (1996) 112

Weishart, H., Steffen, H.J., Matz, W., Voelskow, M., Skorupa, W.,
Ion beam synthesis by tungsten implantation into 6H-silicon carbide,
Nucl. Instr. Meth. B112 (1996) 338

Wieser, E., Reuther, H., Richter, E.,
Improvement of the mechanical surface properties of aluminium by high dose oxygen implantation,
Nucl. Instr. Meth. B111 (1996) 271

Wieser, E., Schöneich, A., Richter, E.,
Influence of high dose and high energy oxygen implantation on the mechanical surface properties of aluminium,
Surf. Coat. Technol. 83 (1996) 290

Yankov, R.A., Hatzopoulos, N., Skorupa, W., Danilin, A.B.,
Proximity gettering of copper in separation-by-implanted-oxygen structures,
Nucl. Instr. Meth. B120 (1996) 60

Zahn, D., Werninghaus, T., Pezoldt, J., Heera, V.,
Raman spectroscopy investigation of Al/N high dose implantation in 6H-SiC,
Mat.Res.Soc.Symp.Proc.423 (1996) 237

Zorba, T.T., Mitsas, C.L.,Siapkas, I.D., Terzakis, G.Z., Siapkas, D.I., Pacaud, Y., Skorupa, W.,
An infrared study of Ge^+ implanted SiC,
Appl. Surf. Sc. 102 (1996) 120

Conference Contributions

Albe, K.,
Modeling boron nitride: An empirical interatomic potential,
Int. Workshop on "First principle, tight-binding and empirical methods for materials simulation",
Chemnitz, June 26-29, 1996

Albe, K., Möller, W., Heinig, K.-H.,
Computer simulation and Boron Nitride,
COSIRES '96, Guildford, UK, July 22-26, 1996

Albertini, G., Carsughi, F., Cernuschi, M., Eichhorn, F., Hempel, A., Magnani, M., Regis, V.,
Topography of a IN738 superalloy turbine blade by small-angle neutron scattering,
8th Int. Symp. on Superalloys, Seven Springs, U.S.A., Sept., 1996

Barradas, N.P., Maas, A.J.H., Mändl, S., Günzel, R.,
Short pulse plasma immersion ion implantation of oxygen into silicon: Determination of the energy distribution,
3rd Int. Workshop on Plasma Based Ion Implantation, Dresden, Germany, Sept. 16–18, 1996

Barradas, N.P., Panknin, D., Wieser, E., Schmidt, B., Betzl, M., Mücklich, A., Skorupa, W.,
Influence of the ion irradiation on the properties of β-$FeSi_2$ layers prepared by ion beam assisted deposition,
10. Int. Conf. "Ion Beam Modification of Materials", Albuquerque, USA, Sept. 1-6, 1996

Bischoff, L., Teichert, J., (invited)
Application of highly focused ion beams,
Int. Symp. on Materials Science Applications of Ion Beam Techniques, Seeheim, Germany,
Sept. 9-12, 1996

Bischoff, L., Teichert, J., (invited)
Application of highly focused ion beams,
14th Int .Conf. "Application of accelerators in research and industry", Denton, USA, Nov.6-9, 1996

Borodin, V.A., Reiss, S., Heinig, K.-H.,
Scaling laws for precipitate patterning due to post-implantation annealing,
10th Int. Conf. "Ion Beam Modification of Materials", Albuquerque, NM, USA, Sept. 1-6, 1996

Bottyan, L., Deak, L., Gerdau, E., Gittsovich, V.N., Grof, A., Korecki, J., Leupold,O., Nagy, D.L.,
Reuther, H., Szilagyi, E., Semenov, V.G., Uzdin, V.M.,
Synchrotron Mössbauer reflectometry: A novel depth-selective method,
Int. Conf. on New Opportunities for Research at Third Generation Light Sources, Lipica, Slovenia,
May 25-29, 1996

Brenscheidt, F., Matz, W., Wieser, E., Möller, W.,
Annealing studies of chromium implanted silicon nitride ceramics,
10th Int. Conf. "Ion Beam Modification of Materials", Albuquerque, USA, Sept. 1-6, 1996

Brenscheidt, F., Mändl, S., Günzel, R., Wieser, E., Möller, W., Fischer, W., Herrmann, M.,
Tribological properties of silicon nitride ceramics modified by titanium and subsequent oxygen implantation,
5th Int. Conf. on Plasma Surface Engineering, Garmisch-Partenkirchen, Germany, Sept. 9-13, 1996

Brutscher, J., Günzel, R., Möller, W.,
Plasma immersion ion implantation using pulsed plasma with DC and pulsed high voltages,
3rd Int. Workshop on Plasma Based Ion Implantation, Dresden, Sept. 16-19, 1996

Chudoba, T.,
Ein neues Modell für die Interpretation elastoplastischer Eindringkurven,
Workshop Mechanische Werkstoffcharakterisierung in der Mikrosystemtechnik,
Dresden, Sept. 26-27, 1996

Chudoba, T.,
Charakterisierung des Verschleißverhaltens mit einer vibrierenden Diamantnadel,
Workshop Mechanische Werkstoffcharakterisierung in der Mikrosystemtechnik,
Dresden, September 26-27, 1996

Deak, L., Bayreuther, G., Bottyan, L., Gerdau, E., Korecki, J., Kornilov, E.I., Lauter, H.J.,
Leupold, O., Nagy, D.L., Pasyuk-Lauter, V.V., Petrenko, A.V., Reuther, H., Röhlsberger, R.,
Szilagyi, E.,
Pure nuclear Bragg reflection of synchrotron radiation by a periodic $^{56}Fe/^{57}Fe$ multilayer,
Int. Conf. on New Opportunities for Research at Third Generation Light Sources, Lipica, Slovenia,
May 25-29, 1996

Dobler, M., Reuther, H.,
CEMS-Untersuchungen an Eisensiliziden,
DPG-Frühjahrstagung, Regensburg, March 25-29, 1996

Dobler, M., Reuther, H., Möller, W.,
Microdisperse iron silicide structures produced by implantation of iron ions in silicon,
Int. Symp. on the Industrial Applications of the Mössbauer Effect, Johannesburg, Nov. 4-8, 1996

Dvurechenskii, A.V., Grötzschel, R., Heinig, K.-H., Markov, V.A., Zinovyev, V.A., Zinovyeva, A.F.,
Effect of pulse action with low-energy noble gas ions on the (111)Si surface during MBE growth of Si,
9th Int. Conf. on Radiation Physics and Chemistry of inorganic materials, Tomsk, Russia,
April 23-25, 1996

Dvurechenskii, A.V., Markov, V.A, Zinovyev, V.A., Zinovyeva, A.F., Grötzschel, R., Heinig, K.-H. ,
Effect of pulse action with low-energy noble gas ions on the (111)Si surface during layer-by-layer MBE growth of Si,
23th Int. Conf. on the Physics of Semiconductors, Berlin, July 21-26, 1996

Eichhorn, F., Prokert, F., Kögler, R., Wolf, K.,
Double-crystal x-ray diffractometry studies of silicon-germanium layers on silicon substrates,
3rd European Symp."X-Ray Topography and High Resolution Diffraction",
Palermo, Italy, April 22-24, 1996

Eremin, V., Ivanov, A., Verbitskaya, E., Li, Z., Schmidt, B.,
Long term stabilities in the defect assambly in irradiated high resistivity silicon detectors,
IEEE Nuclear Science Symposium and Medical Imaging Conference, Mariott Hotel, Anaheim,
California, USA, Nov. 3-9, 1996

Feudel, T., Posselt, M.,
Simulation of arsenic channeling in crystalline silicon during ion implantation,
1996 Semiconductor Technology Workshop, Hsinchu, Taiwan, May 14-16, 1996

Friedrich, M., Sun, G., Grötzschel, R., Behrisch, R., Garcia-Rosales, C., Roberts, M.L.,
Tritium depth profiling in carbon by accelerator mass spectrometry,
7th Int. Conf. On Accelerator Mass Spectrometry, Tucson, Arizona, USA, May 20-24, 1996

Friedrich, M., Sun, G., Grötzschel, R., Behrisch, R., Garcia-Rosales, C., Roberts, M.L.,
Tritium depth profiling in carbon by accelerator mass spectrometry,
3rd Int. Workshop on Tritium Effects in Plasma Facing Components, Ispra Site, Italy,
May 15-17, 1996

Fukarek, W., von Keudell, A.,
Application of in-situ ellipsometry during plasma processing,
ICMCFT, San Diego, April 22-26, 1996

Große, M., Böhmert, J., Eichhorn, F., Brauer, G.,
Investigation of the development of the irradiation-induced precipitates in the nuclear pressure vessel steel 15Kh2MFA during irradiation and annealing,
18th Symp. on Effects of Radiation on Materials, Hyannis/Massachusetts, USA, June 25-27, 1996

Günzel, R., Brutscher, J., Mändl, S., Möller, W.,
Verschleißminderung durch Plasma-Immersions-Ionenimplantation,
Innomata'96, Dresden, May 7-9, 1996

Günzel, R.,
Utilization of plasma source ion implantation for tribological applications ,
IV. Conf. on modification of structural materials by charged particle beams, Tomsk, Russia,
May 13-17, 1996

Günzel, R.,
The use of plasma source ion implantation for wear protection,
NATO ARW on protective coatings and thin films, Portimao, Portugal, May 30 - June 6, 1996

Hatzopoulos, N., Suder, S., van den Berg, J., Donelly, S.E., Armour, D.G., Panknin, D., Fukarek, W.,
Frey, L., Foad, M.A., Moffat, S., Bailey, P., Naakes, C.T.Q.,
Range and damage distribution in ultra low energy boron ion implantation,
11. Int. Conf. "Ion Implantation Technology", Austin/Texas, USA, June 16-21, 1996

Heera, V., Skorupa, W., (invited)
Ion implantation and annealing effects in silicon carbide,
MRS Fall Meeting: Symp.A "Materials Modification and Synthesis by Ion Beam Processing", Boston,
USA, Dec.2-6, 1996

Heinig, K.-H., Reiss, S., Strobel, M., Palard, M., Ruault, M.-O., Bernas, H.,
Theory and modeling of the formation of buried nanocluster layers by high-dose ion implantation,
10th Int. Conf. "Ion Beam Modification of Materials", Albuquerque, NM, USA, Sept 1-6, 1996

Heinig, K.-H., Reiss, S., Strobel, M., (invited)
Ion beam synthesis of nanoclusters: Fundamentals of the formation process,
Int. Symp. on Materials Science Applications of Ion Beam Techniques, Seeheim, Sept 9-12, 1996

Heinig, K.-H., Bernas, H., Ruault, M.-O., Palard, M., Strobel, M., (invited)
In-situ observation and atomic-scale simulation of cluster formation in irradiation environment,
Workshop on Defect Production, Accumulation and Materials Performance in Irradiation Environmemnt, Davos, Switzerland, Oct 2-8, 1996

Hermann, S., Mahnke, H.-E., Spellmeyer, B., Reinhold, B., Wienecke, M., Yankov, R.A.,
Formation of Pd defects in ZnTe and CdTe doped with implanted N, P, or As,
Int. Symp. on Materials Science Applications of Ion Beam Techniques, Seeheim, Germany, Sept. 9-12, 1996

Huber, H., Assmann, W., Grötzschel, R., Mieskes, H.D., Mücklich, A., Prusseit, W.,
Void formation and surface rippling in Ge induced by high energetic Au irradiation,
E-MRS Spring Meeting, Strasbourg, France, June 4 - 7, 1996

Hüller, J., Pham, M. T., Möller, D.,
Ultra thin copper-ISE for fluidic microsystem,
The Sixth International Meeting on Chemical Sensors, Gaithersburg, USA, July 22-25, 1996

Jäger, H.-U. ,
An explanation of trap-limited self-interstitial diffusion and enhanced boron clustering in boron doped silicon superlattices,
4th Int. Symp. on Process Physics and Modeling in Semiconductor Technology, ECS 1996 Spring Meeting, Los Angeles, CA, USA, May 5-10, 1996

Jentschel, M., Börner, H.-G., Doll, C., (invited)
New applications of the GRID-technique in nuclear and solid state physics,
9th Int. Symp.on Capture Gamma-Ray Spectroscopy and Related Topics Budapest, Hungary, Oct 8-12, 1996

Jentschel, M., Heinig, K.-H., Börner, H.-G.,
Crystal-GRID investigation of atomic collision cascades in ionic compounds,
Int. Symp. on Materials Science Applications of Ion Beam Techniques, Seeheim, Germany, Sept. 9-12, 1996

Kachurin, G.A., Tyschenko, I.E., Zhuravlev, K.S., Pazdnikov, N.A., Skorupa, W., Yankov, R.A., Volodin, V.A.,
Correlation between photo-luminescence and structural changes for nanosized Si inclusions formed in SiO_2 layers by ion implantation and pulse annealing,
10. Int. Conf. "Ion Beam Modification of Materials", Albuquerque, USA, Sept. 1-6, 1996

Kachurin, G.A., Tyschenko, I.E., Zhuravlev, K.S., Pazdnikov, N.A., Volodin, V.A., Gutakovsky, A.K., Leier, A.F., Skorupa, W., Yankov, R.A.,
Visible and near-infrared luminescence from Si nanostructures formed by ion implantation and pulse annealing,
E-MRS Spring Meeting, Symp. K:"Nanometric Phenomena Induced by Laser, Ion and Cluster Beams", Strasbourg, France, June 4-7, 1996

Kachurin, G.A., Zhuravlev, K.S., Pazdnikov, N.A., Leier, A.F., Skorupa, W., Yankov, R.A., Tyschenko, I.E., Volodin, K.S., Gutakovsky, A.K.,
Reverse annealing of photoluminescence from Si nanostructures formed by implantation of Si^+ ions into SiO_2 and pulse preheating,
10. Int. Conf. "Ion Beam Modification of Materials", Albuquerque, USA, Sept. 1-6, 1996

Kaschny, J., Mücklich, A., Kreißig, U., Yankov, R.A., Skorupa, W., Fichtner, P.F.P., Danilin, A.B.,
High dose implantation of helium into silicon: Bubble formation and gettering effects,
32. Deutsches Punktdefekttreffen am MPI-FKF, Stuttgart, Nov. 27-28, 1996

Kögler, R., Kaschny, J., Posselt, M., Skorupa, W.,
Detection of defects in ion implanted Si by metal gettering,
32. Deutsches Punktdefekttreffen am MPI-IKF, Stuttgart, Nov. 27-28, 1996

Kögler, R., Skorupa, W., Panknin, D., Eichhorn, F.,
Impurity gettering in damaged regions of silicon produced by high energy ion implantation,
11. Int. Conf. "Ion Implantation Technology", Austin/Texas, USA, June 16-21, 1996

Kögler, R., Skorupa, W., Romano-Rodriguez, A., Perez-Rodriguez, A., Serre, C., Calvo-Barrio, L., Morante, J.R.,
Ion beam synthesis of SiC in Silicon-on-Insulator,
11. Int. Conf. "Ion Implantation Technology", Austin/Texas, USA, June 16-21, 1996

Kögler, R., Werner, P., Danilin, A.B., Skorupa, W.,
Detektion von Defekten in ionenimplantiertem Silicium mittels Metallgetterung,
32. Deutsches Punktdefekttreffen am MPI-FKF, Stuttgart, Nov. 27-28, 1996

Kögler, R., Reuther, H., Voelskow, M., Skorupa, W., Romano-Rodriguez, A., Perez-Rodriguez, A., Serre, C., Calvo-Barrio, L., Morante, J.R.,
Ion beam synthesis of SiC in silicon-on-insulator,
11. Int. Conf. "Ion Implantation Technology", Austin/Texas, USA, June 16-21, 1996

Kruijer, S., Nikolov, O., Reuther, H., Keune, W., Weber, S., Scherrer, S.,
Tiefenanalyse der Phasenbildung in α-Fe nach Al-Ionenimplantation,
DPG-Frühjahrstagung, Regensburg, March 25-29, 1996

Kruijer, S., Dobler, M., Reuther, H., Keune, W.,
DCEMS Investigations of the phase formation in iron ion implanted silicon,
Int. Symp. on the Industrial Applications of the Mössbauer Effect, Johannesburg, South Africa, Nov. 4- 8, 1996

Lehmann, H., Jolie, J., Börner, H.-G., Doll, C., Jentschel, M., Casten, R.F., Zamfir, N.V.,
Lifetime measurements of multiphonon states,
9th Int. Symp. on Capture Gamma-Ray Spectroscopy and Related Topics, Budapest, Hungary, Oct 8-12, 1996

Machalett, F., Scherbel, J., Seidel, P., Steinbeiß, E., Eick, T., Brodkorb, W., Ijsselsteijn, R.,
Untersuchungen zur Herstellung von Josephson-Arrays mittels Ionenfeinstrahl,
Tagung"Kryoelektronische Bauelemente KRYO'96", Jena, Oct. 6-8, 1996

Mändl, S., Brutscher, J., Günzel, R., Plass, M.F., Fukarek, W.,
Plasma immersion implantation and PIRR-charakterisation of BN thin films
3rd Workshop on Low Pressure Gas Discharges for Surface Treatment, Mühlleiten, Germany, March 5-7, 1996

Mändl, S., Barradas, N.P., Brutscher, J., Günzel, R., Möller, W.,
Comparison of measured and calculated dose for plasma source ion implantation in 3-D objects,
10. Int. Conf "Ion Beam Modification of Materials", Albuquerque, USA, Sept. 1-6, 1996

Mändl, S., Reuther, H., Brutscher, J., Günzel, R., Möller, W. ,
Measured and calculated dose distribution for 2D-plasma immersion ion implantation,
3rd Int. Workshop on Plasma Based Ion Implantation, Dresden, Germany, Sept. 16–18, 1996

Mändl, S., Brutscher, J., Günzel, R., Möller, W.,
Ion energy distribution in plasma immerion ion implantation,
3rd Int. Workshop on Plasma Based Ion Implantation, Dresden, Germany, Sept. 16–18, 1996

Matz, W.,
Status Report for the ROBL Project,
12th CRG Club Meeting, ESRF, Grenoble, France, May 6-7, 1996

Matz, W., Prokert, F., Schell, N., Bernhard, G., Reich, T., Claußner, J., Funke, H.,
BM20 - The Rossendorf Beamline,
ESRF User Meeting, Grenoble, France, Nov. 18-20, 1996

Mazur, K., Sass, J., Giersz, W., Reiche, P., Schell, N.,
X-ray diffraction investigations of $NdGaO_3$ single crystals,
Int. Conf. on Substrate Crystals and HTSC Films; Jaszowiec, Poland, Sept. 16-20, 1996

Möller, D., Pham, M.T., Hüller, J.,
Sensitization of silicon nitride surfaces for Ag^+ ions by ion implantation,
EUROSENSORS X, The 10th Europ. Conf. on Solid-State Transducers, Leuven, Belgium,
Sept. 8-11, 1996

Möller, W., (invited)
Physik und Anwendungen der Plasma-Immersions-Ionenimplantation,
Frühjahrstagung der DPG, Rostock, March 3, 1996

Möller, W., (invited)
Ion implantation in solids,
Int. Symp. on Particle Penetration and Collison Cascades, Odense, DK, April 4, 1996

Möller, W., (invited)
Ionenimplantation für praktische Anwendungen,
18. Ulmer Gespräch der DGO, May 5, 1996

Möller, W., (invited)
Computer simulation of ion-assisted thin film deposition,
Int. Conf. "Computer Simulation of Radiation Effects in Solids", Guildford, UK, July 7, 1996

Möller, W., Heinig, K.-H., Posselt, M., (invited)
New trends of computer simulation of ion implantation into solids,
10th Int. Conf. "Ion Beam Modification of Materials", Albuquerque, NM, USA, Sept. 1-6, 1996

Nakamura, K., Mändl, S., Brutscher, J., Günzel, R., Möller, W.,
Incident ion monitoring during plasma immersion ion implantation by direct measurements of high-energy secondary electrons,
3rd Int. Workshop on Plasma Based Ion Implantation, Dresden, Germany, Sept. 16–18, 1996

Neelmeijer, C.,
XRF and IBA - competitive methods in non-destructive analysis of paint layers?,
5th Int. Conf. on non-destructive testing, microanalytical methods and environmental evaluation for study and conservation of works of art, Budapest, Hungary, Sept. 24 - 28, 1996

Neelmeijer, C., Mäder, M., Wagner, W., Schramm, H.-P.,
Layered artefacts: Non-destructive characterization by PIXE and RBS,
4th Int. Conf. on Optics Within Life Sciences, Münster, July 9 - 13, 1996

Pacaud, Y., Heera, V., Kögler, R., Skorupa, W.,
Damage behaviour and annealing of germanium implanted 6H-SiC,
11. Int. Conf. "Ion Implantation Technology", Austin/Texas, USA, June 16-21, 1996

Pacaud, Y., Perez-Rodriguez, A., Brauer, G., Stoemenos, J., Yankov, R.A., Heera, V., Kögler, R., Barklie, R., Skorupa, W.,
Defect annealing in germanium-implanted 6H-SiC wafers,
MRS Fall Meeting: Symp.A "Materials modification and synthesis by ion beam processing"
Boston, USA, Dec. 2-6, 1996

Pacaud, Y., Skorupa, W., Stoemenos, J.,
Mode of recrystallisation of implanted and annealed 6H-SiC,
E-MRS Spring Meeting, Symp.I:"New Trends in Ion Beam Processing of Materials", Strasbourg, France, June 4-7, 1996

Pacaud, Y., Stoemenos, J., Brauer, G., Yankov, R.A., Heera, V., Voelskow, M., Kögler, R., Skorupa, W.,
Radiation damage and annealing behaviour of Ge^{+}-implanted SiC,
E-MRS Spring Meeting, Symp.I:"New Trends in Ion Beam Processing of Materials", Strasbourg, France, June 4-7, 1996

Pacaud, Y., Weishart, H., Voelskow, M., Skorupa, W., Perez-Rodriguez, A., Brauer, G., Stoemenos, J.,
An annealing study of Ge-implanted 6H-SiC,
MRS Spring Meeting: Symp.E "III-V Nitride, SiC and Diamond materials for electronic devices", San Francisco, USA, April 8-13, 1996

Palard, M., Ruault, M.-O., Bernas, H., Heinig, K.-H.,
Evolution de nanoprecipites de $CoSi_2$ dans Si sous faisceau d'ions: Experience et Simulation,
NANOS96 - colloque Elaboration, caracterisation, proprietes et applications des nanomateriaux,
Fent-Romea, France, April 1-3, 1996

Palard, M., Ruault, M.-O., Bernas, H., Heinig, K.-H.,
Silicide nanocluster evolution in beam: Experiment and computer simulation,
9th Conf. on Semiconducting and Insulating Materials (IEEE SIMC-9), Toulouse, France,
April 29-May 3, 1996

Perez-Rodriguez, A., Romano-Rodriguez, A., Serre, C., Calvo-Barrio, L., Cabezas, R., Morante, J.R., Kögler, R., Skorupa, W., Rodriguez, A.,
High temperature high dose carbon implantation in epitaxial SiGe,
E-MRS Spring Meeting, Symp.I:"New Trends in Ion Beam Processing of Materials", Strasbourg, France, June 4-7, 1996

Perez-Rodriguez, A., Romano-Rodriguez, A., Serre, C., Calvo-Barrio, L., Cabezas, R., Morante, J.R., Calderer, J., Reuther, H., Skorupa, W.,
Ion beam synthesis and recrystallisation of amorphous SiGe/SiC structures,
E-MRS Spring Meeting, Symp.I:"New Trends in Ion Beam Processing of Materials", Strasbourg, France, June 4-7, 1996

Plass, M.F., Fukarek, W., Kolitsch, A., Möller, W.,
Layered structure diagnostic and optical modeling of c-BN films,
10. Int. Conf "Ion Beam Modification of Materials", Albuquerque, NM, USA, Sept. 1-6, 1996

Plass, M.F., Fukarek, W., Kolitsch, A., Möller, W.,
Growth and characterisation of boron nitride films: layer sequence and phase identification,
Diamond 1996, Tours, France, Sept. 8-13, 1996

Posselt, M., Schmidt, B., Murthy, C.S., Feudel, T., (invited)
Modeling of damage accumulation during ion implantation into single-crystalline silicon,
4th Int. Symp. on Process Physics and Modeling in Semiconductor Technology, ECS 1996 Spring Meeting, Los Angeles, CA, USA, May 5-10, 1996

Posselt, M.,
Modeling of damage accumulation in dynamic simulations of ion implantation into single-crystalline silicon,
11th Int. Conf. "Ion Implantation Technology", Austin, TX, USA, June 17-21, 1996

Rebohle, L., Tyschenko, I.E., Fröb, H., Leo, K., Yankov, R.A., Skorupa, W.,
Erzeugung blauer Lumineszenzzentren durch Ionenstrahlsynthese,
32. Deutsches Punktdefekttreffen am MPI-FKF, Stuttgart, Nov. 27-28, 1996

Reichert, W., Lossy, R., Gonzalez Sirgo, M., Obermeier, E., Skorupa, W.,
Investigation of the effects of high temperature implantation and post implantation annealing on the electrical behaviour of nitrogen implanted β-SiC films,
1.Europ. Conf. "Silicon carbide and related materials", Heraklion/Crete, Greece, Oct. 6 - 9, 1996

Reuther, H., Dobler, M., Kruijer, S., Keune, W.,
AES- und Mößbaueruntersuchungen an ionenimplantierten Fe-Si-Schichten,
8. Arbeitstagung Angewandte Oberflächenanalytik, Aachen, June 24-27, 1996

Reuther, H., (invited)
Structure, properties and applications of thin Fe-Al layers,
Int. Symp. on the Industrial Applications of the Mössbauer Effect, Johannesburg, South Africa, Nov. 4- 8, 1996

Reuther, H., Betzl, M., Richter, E.,
Investigation of Fe-Mg-alloys produced by ion implantation,
Int. Symp. on the Industrial Applications of the Mössbauer Effect, Johannesburg, South Africa, Nov. 4- 8, 1996

Richter, E.,
Radioaktive Verschleißmessungen ionenimplantierter Metalle,
13. Kolloquium Dünnschichtaktivierung, Rossendorf, Jan. 24-25, 1996

Richter, E.,
Möglichkeiten und Grenzen der Ionenstrahltechnik,
5. Gesprächskreis „Vakuum- und Schichttechnik", Rossendorf, March 7, 1996

Richter, E.,
Tribologische Eigenschaften ionenimplantierter meatllischer Werkstoffe,
„Oberfläche innovativ", Hannover Messe 96, Hannover, April 24, 1996

Richter, E., Günzel, R., Brutscher, J., Kreißig, U., Möller, W.,
Verschleißschutz durch Niederenergie-Ionenimplantation,
Innomata'96, Dresden, May 7-9, 1996

Richter, E., Günzel, R., Kolitsch, A., Möller, W.,
Ionenstrahltechnik - eine Möglichkeit zur Erzeugung von Funktionsschichten mit definierten Eigenschaften,
Innomata'96, Dresden, May 7-9, 1996

Schmidt, B., Bischoff, L., Teichert, J.,
Writing FIB implantation and subsequent anisotropic wet chemical etching for the fabrication of 3D structures in silicon,
10. Europ. Conf. on Solid State Transducers, Leuven, Belgium, Sept. 9-12, 1996

Schmidt, B., Posselt, M., Feudel, T.,
Simulation of channeling control in arsenic implantation into silicon,
11th Int. Conf. "Ion Implantation Technology", Austin, TX, USA, June 17-21, 1996

Schroer, E., Skorupa, W., Tong, Q.-Y., Hopfe, S., Gösele, U.,
Zum oxidationsinduzierten Wachstum vergrabener Oxidschichten von silicon-on-insulator (SOI) Strukturen,
Frühjahrstagung der Deutschen Physikalischen Gesellschaft, Halbleiterphysik, Regensburg, March 25-29, 1996

Simoen, E., Vanhellemont, J., Alaerts, A., Claeys, C., Gaubas, E., Kaniava, A., Ohyama, H., Sunaga,H., Nahsiyama,I., Skorupa, W.,
Proton irradiation effects in silicon devices,
7. Int. Symp. on "Recent progress in Accelerator Beam Application", Takasaki, Japan, March 18-20, 1996

Skorupa, W., (invited)
Damage processes in single crystalline 6H-SiC,
European IBOS-Meeting, Istituto LAMEL, Bologna, Italy, March 28-30, 1996

Skorupa, W., (invited)
Gettern in ionenimplantiertem Silicium,
Verbundtreffen "Nukl. Meth. Festkörperphysik", Univ.Konstanz, Oct. 1, 1996

Skorupa, W., Heera, V., Pacaud, Y., Weishart, H., (invited)
Ion beam processing of single crystalline silicon carbide,
E-MRS Spring Meeting, Symp.I:"New Trends in Ion Beam Processing of Materials", Strasbourg, France, June 4-7,1996

Skorupa, W., Yankov, R.A., Hatzopoulos, N., Kögler, R., Danilin, A.B.,
Proximity gettering of transition metals in SIMOX wafers,
11. Int. Conf. "Ion Implantation Technology", Austin/Texas, USA, June 16-21, 1996

Skorupa, W., Yankov, R.A., Rebohle, L., Fröb, H., Böhme, T., Leo, K., Tyschenko, I.E., Kachurin, G.A.,
A study of the blue photoluminescence emission from thermally-grown, Si-implanted SiO_2 films after short-time annealing,
E-MRS Spring Meeting, Symp.I:"New Trends in Ion Beam Processing of Materials", Strasbourg, France, June 4-7, 1996

Skorupa, W., Yankov, R.A., Tyschenko, I.E., Rebohle, L., Fröb, H., Böhme, T., Leo, K.,
Blue light emission from silicon nanostructures formed by the implantation of silicon into thermal silicon dioxide layers,
10. Int. Conf. "Ion Beam Modification of Materials", Albuquerque, USA, Sept. 1-6, 1996

Spieß, L., Nennewitz, O., Weishart, H., Lindner, J., Skorupa, W., Romanus, H., Erler, F., Pezoldt, J.,
Aluminium implantation of p-SiC for ohmic contacts,
1. Europ. Conf. "Silicon carbide and related materials", Heraklion/Crete, Greece, Oct. 6-9, 1996

Strobel, M., Reiss, S. Heinig, K.-H.,
Evolution of nanocluster ensemble: computer simulation of diffusion and reaction controlled Ostwald ripening,
E-MRS Spring Meeting, Symposium I: "New Trends in Ion Beam Processing of Materials",
Strasbourg, France, June 4-7, 1996

Strobel, M., Reiss, S. Heinig, K.-H., Möller, W.,
Computer simulation of precipitate coarsening: a unified treatment of diffusion and reaction controlled Ostwald ripening,
COSIRES '96, Guildford, UK, July 22 -26, 1996

Strobel, M., Reiss, S., Heinig, K.-H., Möller, W.,
Evolution of nanocluster ensembles: Computer simulation of diffusion and reaction controlled Ostwald ripening,
10th Int. Conf. "Ion Beam Modification of Materials", Albuquerque, NM, USA, Sept 1-6, 1996

Sümmchen, L., Drummer, H., Roland, U., Salzer, R., Kolitsch, A., Drescher, D.,
Characterisation of thin amorphous carbon and carbon nitride films by Raman spectroscopy,
ICORS, XVth Int. Conf. on Raman Spectroscopy, Pittsburgh, PA, USA, Aug. 11-16, 1996

Sümmchen, L., Roland, U., Salzer, R., Kolitsch, A.,
Surface mapping of thin carbon films by fourier transform raman spectroscopy,
Euroanalysis IX, Bologna, Italy, Sept. 1-7, 1996

Teichert, J., Bischoff, L., Hausmann, S.,
Fabrication of MSM detector structures on silicon by focused ion beam implantation,
Int. Conf. on Micro-and Nanoengineering MNE'96, Glasgow, UK, Sept.23-25, 1996

Teichert, J., Bischoff, L., Köhler, B.,
Investigation of the ion acoustic effect during focused ion beam irradiation,
E-MRS Spring Meeting, Symp.I:"New Trends in Ion Beam Processing of Materials", Strasbourg, France, June 4-7,1996

Teichert, J., Bischoff, L., Köhler, B.,
Study of the ion-acoustic effect of focused ion beams,
MRS Fall Meeting: Symp.A "Materials modification and synthesis by ion beam processing",
Boston, USA, Dec. 2-6, 1996

Tyschenko, I.E., Kachurin, G.A., Zhuravlev, K.S., Pazdnikov, N.A., Volodin, V.A., Gutakovsky, A.K., Leier, A.F., Fröb, H., Leo, K., Böhme, T., Rebohle, L., Yankov, R.A., Skorupa, W.,
Quantum-sized silicon precipitates in silicon-implanted and pulse-annealed silicon dioxide films: photoluminescence and structural transformations,
MRS Fall Meeting: Symp.A "Materials modification and synthesis by ion beam processing",
Boston, USA, Dec. 2-6, 1996

Weishart, H., Heera, V., Matz, W., Skorupa, W.,
Ion beam assisted deposition of a tungsten compound layer on 6H-SiC,
1.Europ. Conf. "Silicon carbide and related materials", Heraklion/Crete, Greece, Oct. 6-9, 1996

Weishart, H., Matz, W., Skorupa, W.,
Ion beam synthesis by tungsten implantation into 6H-SiC at elevated temperatures,
MRS Spring Meeting: Symp.E "III-V Nitride, SiC and Diamond materials for electronic devices, San Francisco, USA, April 8-13, 1996

Weishart, H., Schöneich, J., Voelskow, M., Skorupa, W.,
Ion beam synthesis by high dose tungsten implantation into 6H-SiC,
MRS Fall Meeting: Symp.A "Materials modification and synthesis by ion beam processing",
Boston, USA, Dec. 2-6, 1996

Werner, P., Kögler, R., Skorupa, W,.
TEM imaging of C-Si defects in carbon-implanted silicon,
11. Int. Conf. "Ion Implantation Technology", Austin/Texas, USA, June 16-21, 1996

Wieser, E., Richter, E.,
Oberflächenmodifizierungen zum Korrosionsverhalten von Titan-Werkstoffen für Bioanwendungen,
"Anwendungen moderner Oberflächentechnologien in der Medizintechnik", Dresden, May 5, 1996

Wirth, H., Panknin, D., Skorupa, W., Voelskow, M.,
Bor-Implantation in bulk-6H-SiC,
Frühjahrstagung der Deutschen Physikalischen Gesellschaft, Dünne Schichten, Regensburg, March 25-29, 1996

Yakimov, A.I., Stepina, N.P., Dvurechenskii, A.V., Scherbakova, L.A., Adkins, C.J., Dravin, V.A., Groetzschel., R.,
1D hopping conductivity in porous amorphous Si<Mn>,
4th Int. Conf. on Electrical Transport and Optical Properties of Inhomogeneos Media, Moscow, Russia, 23 - 30 July, 1996

Yankov, R.A., Hatzopoulos, N., Skorupa, W., Danilin, A.B.,
Proximity gettering of copper in separation-by-implanted-oxygen structures,
E-MRS Spring Meeting, Symp.I:"New Trends in Ion Beam Processing of Materials, Strasbourg, France, June 4-7, 1996

Yankov, R.A., Hatzopoulos, N., Fukarek, W., Heera, V., Voelskow, M., Pezoldt, J., Skorupa, W.,
Formation of buried layers of $(SiC)_{1-x}(AlN)_x$ in 6H-SiC using ion-beam synthesis,
MRS Fall Meeting: Symp.A "Materials modification and synthesis by ion beam processing"
Boston, USA, Dec. 2-6, 1996

Yankov, R.A., Kaschny, J., Kreißig, U., Mücklich, A., Fichtner, P.F.P., Danilin, A.B., Skorupa, W.,
Formation of bubbled layers by the implantation of helium into silicon and SIMOX substrates: annealing behaviour and gettering effects,
10. Int. Conf. "Ion Beam Modification of Materials", Albuquerque, USA, Sept. 1-6, 1996

Zahn, D., Werninghaus, T., Pezoldt, J., Heera, V.,
Raman spectroscopy investigation of high dose implantation in 6H-SiC,
MRS Spring Meeting: Symp.E "III-V Nitride, SiC and Diamond materials for electronic devices, San Francisco, USA, April 8-13, 1996

Lectures

Bischoff, L.,
Anwendung von feinfokussierten Ionenstrahlen,
Friedrich-Schiller-Universität Jena, April 19, 1996

Borany, J. von,
Ionenimplantation als partieller Verschleißschutz bei werkzeugen der Kunststoffverarbeitung,
Institutsseminar des Kunstoffinstituts Lüdenscheid, Lüdenscheid, June 11, 1996

Borany, J. von,
Materialveredelung mit Ionen,
Votrag zur Innovationsmesse Leipzig, Leipzig, Sept. 25, 1996

Brenscheidt, F.,
Ionenimplantation in Siliziumnitrid-Keramik,
Fraunhofer Institut für keramische Technologien und Sinterwerkstoffe (IKTS) Dresden, May 15, 1996

Dobler, M.,
CEMS-und AES-Untersuchungen an implantierten Fe-Eisendisiliziden,
VII. Mößbauerkolloquium Freiberg, Sept. 30 - Oct. 2, 1996

Eichhorn, F., Matz, W., Betzl, M.,
X-ray studies on implanted materials,
Seminar at the Institute of Electronic Materials Technology, Warsaw, Oct. 25, 1996

Grigull, S.,
Transport und Strukturmodifikation in Stickstoff-implantiertem amorphen Kohlenstoff,
Max-Planck-Institut für Plasmaphysik, Garching, Sept. 5, 1996

Grigull, S.,
Transport und Strukturmodifikation in Stickstoff-implantiertem amorphen Kohlenstoff,
TU Chemnitz-Zwickau, Nov. 8, 1996

Grötzschel, R.,
Grundlagen der Ionenstrahlanalytik,
Vortragsreihe, TU Chemnitz-Zwickau, Graduiertenkolleg "Dünne Schichten und nichtkristalline Materialien", 1. Vortrag Dec.10, 1996

Heinig, K.-H.,
Nucleation, growth and Ostwald ripening during ion beam synthesis,
FOM-Institute for Atomic and Molecular Physics, Amsterdam, The Netherlands, Feb 26, 1996

Heinig, K.-H.,
Keimbildung, -wachstum und -reifung von Präzipitaten und Defekten bei der Ionenimplantation,
Universität Augsburg (Physik), Augsburg, May 9, 1996

Heinig, K.-H.,
Application of high-resolution gamma-spectroscopy (GRID method) in solid state physics,
Institute Laue-Langevin, Grenoble, France, Oct. 9, 1996

Heinig, K.-H.,
Synthesis of layers and nanocrystals by ion implantation: Fundamentals of the formation process,
Centre de Spectrometrie Nucleaire et de Spectrometrie de Masse, Paris/Orsay, France, Oct. 24, 1996

Heinig, K.-H.,
Grundlagen der Nanocluster-Synthese durch Ionenimplantation,
Universität Freiburg (Physik), Freiburg, Oct. 25, 1996

Jentschel, M.,
Crystal-GRID Untersuchungen von atomaren Stoßkasskaden in Festkörpern,
TU München, Physik Department, E18, Jan. 10, 1996

Jentschel, M.,
Application of ultra high resolution gamma spectroscopy for the investigation of atomic motion in solids,
University of Prag, Institute of low temperature physics, Czech Republic, Dec 16, 1996

Kolitsch, A.,
Deposition of BN and CN_x films by ion beam assisted deposition,
TU Chemnitz-Zwickau, Jan. 26, 1996

Mändl, S.,
Plasma Immersion Ion Implantation,
Dept. of Solid State Physics, Byelorussian State University, Minsk, Byelorussia, Dec. 20, 1996

Matz, W.,
Dünnschichtuntersuchungen mit Synchrotronstrahlung - der neue Meßplatz in Grenoble,
TU Dresden, Institut für Angewandte Physik, June 18, 1996

Möller, W.,
Grundlagen und Anwendungen von Ionenstrahltechniken,
HMI Berlin, Jan. 22, 1996

Möller, W.,
Ionenbeschußeffekte an Festkörperoberflächen,
Institut für Werkstofforschung, Dresden, Jan. 24, 1996

Möller, W.,
Grundlagen und Anwendungen von Ionenstrahltechniken,
TU Braunschweig, Feb. 1, 1996

Möller, W.,
Neue Ansätze und Verfahren der Ionentechnik,
BMBF, Bonn, March 4, 1996

Möller, W.,
Ionenimplantation für neue Anwendungen,
Frühjahrssitzung des AK POT, Dresden, May 23, 1996

Möller, W.,
Anwendungen und Möglichkeiten der Plasma-Immersions-Ionenimplantation,
Seminar "Plasma-Immersions-Implantation in Deutschland", Rossendorf, Sept. 19, 1996

Möller, W.,
Ionenstrahlen in Forschung und Technik,
TU Dresden, Physikalisches Kolloquium, Oct. 29, 1996

Möller, W.,
Moderne Ionen- und Plasmentechniken zur Oberflächenbehandlung,
Universität Düsseldorf, Physikalisches Kolloquium, Dec. 5, 1996

Neelmeijer, C.,
Zerstörungsfreie Analyse von Kunstwerken am "Luft-Protonenstrahl",
TU Dresden, Institut für Strahlenschutzphysik, Jan. 1996

Neelmeijer, C.,
Zerstörungsfreie Diagnose von Unikaten am "Luft-Protonenstrahl",
Stiftung Institut für Werkstofftechnik Bremen, Jan. 1996

Neelmeijer, C.,
Zerstörungsfreie Diagnose von Kunstwerken am externen Protonenstrahl,
Universität Leipzig, Fakultät für Physik und Geowissenschaften, Jan. 1996

Neelmeijer, C.,
Zerstörungsfreie Analytik von Kunstwerken am "Luft-Protonenstrahl",
Heinrich-Heine-Universität Düsseldorf, Institut für Experimentalphysik, June 1996

Neelmeijer, C.,
Der "Luft-Protonenstrahl" als Instrument zur zerstörungsfreien Analyse an Kunstwerken,
Ruhr-Universität Bochum, Institut für Experimentalphysik, Sept. 1996

Richter, E.,
Ionenimplantation in Metalle,
TU Chemnitz-Zwickau, Graduiertenkolleg „Dünne Schichten und nichtkristalline Materialien",
Chemnitz, Jan. 16, 1996

Richter, E.,
Modifizierung von Werkstoffen mit Ionenstrahlen,
Institutsseminar Institut für Technologie der Polymere, Dresden, April 4, 1996

Scheffzük, Ch., Jansen. E.M., Betzl, M.,
Texture analysis by neutron diffraction of natural and experimetally triaxial deformed halite,
Vortrag auf der 74. Jahrestagung der Deutschen Mineralogischen Gesellschaft, Kiel, Sept. 9 - 12, 1996

Skorupa, W.,
Ionenstrahlprozesse für SiC,
Fakultät für Naturwissenschaften, Technische Hochschule Ilmenau, April 23, 1996

Skorupa, W.,
Ion beam processing of SiC,
Argonne National Lab., Argonne/IL, USA, June 24, 1996

Skorupa, W.,
Gettering and defect engineering in ion implanted silicon,
Dept. Electr. Eng. and Comp.Sc., Univ.of Berkeley, USA, Sept.9, 1996

Teichert, J.,
Erzeugung von fokussierten Ionenstrahlen und ihre Anwendung zur Ionenstrahlsynthese von
Kobaltdisilizid-Mikrostrukturen,
Ruhr-Universität, Bochum, June 13, 1996

Walther, K.,
Investigation of residual stresses by means of neutron diffraction,
Seminar at the Institute for Physics of Earth of the Russian Academy of Science, Moscow,
Feb. 7, 1996

Walther, K.,
The diffractometer "Epsilon" - Starting up and first results,
Frank Laboratory for Neutron Physics in the Joint Institute for Nuclear Research, Dubna, Russia,
Feb. 13, 1996

Walther, K., Frischbutter, A., Scheffzük, Ch.,
Bestimmung des vollständigen Deformationstensors eines quarzithaltigen Sedimentgesteines,
Informationstreffen "Spannungsmessung in der Geologie", FZ Rossendorf, Oct. 22, 1996

Weishart, H.,
Ionenstrahlsynthese von oberflächennahen leitfähigen Schichten durch Wolfram-Implantation in 6H-SiC,
Institut für Werkstoffwissenschaften, Univ. Erlangen-Nürnberg, Feb. 14, 1996

Wieser E.,
Ionenimplantation in Halbleiter,
TU Chemnitz-Zwickau, Graduiertenkolleg „Dünne Schichten und nichtkristalline Materialien",
Chemnitz, Jan. 9, 1996

Yankov, R.A.,
High-energy ion implantation in silicon processing - buried layers and impurity gettering,
Hahn-Meitner-Institut, Berlin, Nov. 19, 1996

Reports

Aldridge, L.P., Sabine, T.M., Eichhorn, F., Hempel, A., Ioffe, A.,
SANS spectra from hydrated cement pastes,
BENSC Experimental Reports 1995,
Berichte des HMI Berlin, HMI-B 536, June 1996, 298

Chudoba, T.,
Modifizierung mechanischer und korrosiver Oberflächeneigenschaften von Magnesium durch Ionenimplantation,
FZR-Report 143, July 1996

Eichhorn, F.,
Modernisierung eines Doppelkristalldiffraktometers (das mit zylindrisch gekrümmten perfekten Kristallen arbeitet, für Neutronenkleinwinkelstreuuntersuchungen mittels ortsauflösendem Detektor),
Erforschung kondensierter Materie im Verbund mit Großgeräten (Physik - Chemie - Biologie):
Ergebnisberichte 1992 - 1995 - Kurzdarstellung. Gefördert vom BMBF, June 1996, 780

Feudel, T., Posselt, M.,
Simulation of arsenic channeling in crystalline silicon during ion implantation,
Swiss Federal Institute of Technology Zürich, Integrated Systems Laboratory,
Technical Report No.2/96

Gehring, T., von Borany, J.,
Modellrechnungen zur Optimierung einer Düse-Diffusor-Pumpe,
Zwischenbericht zum SMWA-Verbundprojekt: Miniaturisiertes Analysesystem für die Gewässerüberwachung, Teilthema: Entwicklung eines Mikrofluidik-Handlingsystems für die chemische Analytik und Biotechnologie, PT-Nr.: 1677/355

Gehring, T., von Borany, J.,
Ausfallerkennung von Mikroaktoren in mikrofluidischen Systemen mittels Strömungsmessung,
Zwischenbericht zum SMWA-Verbundprojekt: Mikrofluidik-Handlingsystem für die chemische Analytik und Biotechnologie, PT-Nr.: 2114

Große, M., Böhmert, J., Eichhorn, F., Hempel, A.,
SAXS investigation of void nucleation and growth in the plastic zone ahead of a crack tip in ductile metals,
European Synchrotron Radiation Facility (ESRF) Annual Report 1994/1995, Grenoble 1995, R18

Häußler, F., Schreiber, J., Hempel, A., Eichhorn, F., Ioffe, A.,
SANS studies as a contribution to structural characterization of industrial materials,
BENSC Experimental Reports 1995,
Berichte des HMI Berlin, HMI-B 536, June 1996, 307

Hempel, A., Eichhorn, F.,
SANS investigations of hydrating cement,
BENSC Experimental Reports 1995,
Berichte des HMI Berlin, HMI-B 536, June 1996, 302

Kachurin, G.A.,
Zusammenfassung bisheriger Untersuchungen zum Mechanismus der Photolumineszenz in Si-reichen SiO_2-Schichten,
Abschlußbericht zum Gastaufenthalt, gefördert durch SMWK, May 7- June 15, 1996

Kolitsch, A. Uhlmann, J.,
Herstellung, Charakterisierung und Ionenstrahlmodifizierung amorpher Kohlenstoffschichten,
FZR-Report 127, Feb. 1996

Lange, K., Nitzsche, P., Schmidt, B., Harz, M.,
Abschlußbericht: Anwendungsgerechte Systemintegration und Zuverlässigkeit für die intelligente mikromechanische Sensorik (AN-SYS), Teilvorhaben: Silizium-Glas-Bonden
BMBF-Verbundprojekt, Förderkennzeichen 13 MV 0266

Lange, K., Schmidt, B., Grigull, S., Kreissig, U.,
In situ ERDA der Ionendrift in Technischen Gläsern,
Bericht zum Gesamtprojekttreffen, BMBF-Verbundprojekt AN-SyS,
Förderkennzeichen 13MV0266, Thyracont GmbH Passau, July 4, 1996

Matz, W., Prokert, F., Schlenk, R., Claußner, J., Schell, N., Eichhorn, F., Bernhard, G.,
The Rossendorf Beamline at the ESRF (Projekt ROBL), part 1,
FZR-Report 158, Rossendorf, Nov. 1996

Moll, H., Geipel, G., Matz, W., Bernhard, G., Nitsche, H.,
Solubility and Speciation of $(UO_2)_2SiO_4.2H_2O$ in aqueous systems,
Annual Report 1995, Institute of Radiochemistry, FZR-123, Rossendorf, Feb. 15, 1996

Podurets, K.M., Hempel, A., Eichhorn, F.,
Observation of the effect of adiabatic spin flip of neutrons at glancing passage through the domain walls in the bulk of silicon iron,
BENSC Experimental Reports 1995,
Berichte des HMI Berlin, HMI-B 536, June 1996, 309

Rustichelli, F., Cernuschi, F., Fiori, F., Eichhorn, F., Hempel, A.,
SANS topography of IN738 Ni-based superalloy turbine blade,
BENSC Experimental Reports 1995,
Berichte des HMI Berlin, HMI-B 536, June 1996, 306

Saroun, J., Mikula, P., Hempel, A., Eichhorn, F.,
Investigation of porosity in plasma-sprayed materials,
BENSC Experimental Reports 1995
Berichte des HMI Berlin, HMI-B 536, June 1996, 311

Schmidt, B., Nitzsche, P., Lange, K., Grigull, S., Kreissig, U.,
Sauerstoff- und Wasserstoffdrift in TEMPAX beim anodischen Bonden,
Bericht zum Gesamtprojekttreffen, BMBF-Verbundprojekt AN-SyS,
Förderkennzeichen 13MV0266, DESAG Grünenplan, Oct. 24, 1996

Uebele, P., Hermann, H., Wiedenmann, A., Hempel, A., Eichhorn, F., Herrmann, M.,
SANS study of silicon nitride ceramics,
BENSC Experimental Reports 1995,
Berichte des HMI Berlin, HMI-B 536, June 1996, 228

Laboratory Visits

Albe, K.,
Centre de Spectrometrie Nucleaire et de Spectrometrie de Masse, Paris/Orsay,
France, Jan. 25, 1996

Betzl, M.,
JINR Dubna, Nov. 4 - 15, 1996

Boede, W.,
JINR Dubna, Nov. 4 - 15, 1996

Eichhorn, F.,
Institute of Electronic Materials Technology, Warsaw, Poland, March 4 -7, Oct. 21 - 25, 1996

Eichhorn, F.,
European Synchrotron Radiation Facility, Grenoble, France, Nov. 17 - 21, 1996

Friedrich, M.,
University of North Texas, Ion Beam Modification and Analysis Laboratory, Denton, Texas, USA,
May 30-31, 1996

Grambole, D.,
Max-Planck-Institut für Kernphysik, Heidelberg, June 19 - 20, 1996

Grötzschel, R.,
Institute "Demokritos", Athen, Greece, April 29 - May 3, 1996

Grötzschel, R.,
Ludwig-Maximilians-Universität München, Beschleunigerlabor, Garching, Nov. 11 -14, 1996

Günzel, R.,
Soltan Institute for Nuclear Research Studies, Swierk, Poland, Dec.3 - 9, 1996

Hausmann, S.,
Institut für Ionentechnik, Forschungszentrum Jülich, Sept. 9-13, 1996

Heinig, K.-H.,
Centre de Spectrometrie Nucleaire et de Spectrometrie de Masse, Paris/Orsay, France, Feb. 3-7, July 2-7, Oct. 21-24, 1996

Heinig, K.-H.,
FOM-Institute for Atomic and Molecular Physics, Amsterdam, The Netherlands, Feb. 24-27, 1996

Heinig, K.-H.,
Centre de Spectrometrie Nucleaire et de Spectrometrie de Masse, Paris/Orsay, France, Feb. 3-7, July 4-11, Oct. 18-24, 1996

Heinig, K.-H.,
Universität Augsburg, May 9-10, 1996

Heinig, K.-H.,
ILL Grenoble, France, July 2-4, Oct. 9-18, 1996

Heinig, K.-H.,
Universität Freiburg, Oct. 24-26, 1996

Kögler, R.,
Dept. of Physics, Univ. of Barcelona, Spain, May 13-20, 1996

Kruse, O.,
Ludwig-Maximilians-Universität München, Beschleunigerlabor, Garching, Jan.11 – 14, 1996

Mäder, M.,
Hochschule für Bildende Künste, Vienna, Austria, Dec. 9 - 13, 1996

Mändl, S.,
Dept. of Solid State Physics, Byelorussian State University, Minsk, Byelorussia, Dec. 16 – 23, 1996

Matz, W.,
European Synchrotron Radiation Facility, Grenoble, France, March 25 - 27, May 6 - 8, August 6 - 7, Oct. 23 - 25, Nov. 17 - 21, 1996

Matz, W.,
Oxford Instruments, Accelerator Technology Group, Oxford, UK, March 14 - 15, July 9 - 10, Sept. 10 - 11, 1996

Mücklich, A.,
Philips Electron Optics, Eindhoven, Netherlands, March 10 - 15, 1996

Neelmeijer, C.,
Max-Planck-Institut für Kernphysik, Heidelberg, June 19 - 20, 1996

Posselt, M.,
Institut für Integrierte Systeme der ETH Zürich, Oct. 14-25, 1996

Prokert, F.,
Oxford Instruments, Accelerator Technology Group, Oxford, UK, March 14 - 15, July 9 - 10, Sept. 10 - 11, 1996

Prokert, F.,
Institut f. Kristallographie, Universität Tübingen, March 18 - 23, 1996

Reichel, P.,
JINR Dubna, Nov. 4 - 15, 1996

Schmidt, B.,
Institut für Integrierte Systeme der ETH Zürich, Oct. 14 - Nov. 1, 1996

Skorupa, W.,
Materials Science Division, Argonne National Lab., Argonne, IL, USA, June 23-25, 1996

Skorupa, W.,
Dept. Electr. Eng. and Comp.Sc., Univ.of Berkeley, Sept.8 - 10, 1996

Skorupa, W.,
Fakultät für Naturwissenschaften, Technische Hochschule Ilmenau, April 23 - 24, 1996

Spalthoff, P.,
JINR Dubna, Jan. 29 - Feb., Nov. 11 - 30, 1996

Walther, K.,
JINR Dubna, Jan. 10 - Feb. 16, March 22 - April 19, May 14 - 24, Nov. 4 - 15, Nov. 25 - Dec. 5, 1996

Wirth, H.,
Dept. of Physics, Univ. of Barcelona, Spain, June 16-23, 1996

Guests

Dr.D. Alexander,
Materials Science Division, Argonne National Lab., Argonne, IL, USA, Sept.11-13, 1996

M. Altmeyer,
Institut für Physikalische Chemie der Universität des Saarlandes, Saarbrücken, Nov. 25-29, 1996

Dr. D. Avasthi,
Nucl.Science Centre, New Delhi, India, Nov. 14 - 16, 1996

Dr. R. Behrisch,
Max-Planck-Institut für Plasmaphysik, Garching, Sept. 15 - 17, 1996

V. Belko,
University of Minsk, Belarus, Nov. 4-30, 1996

Dr. V. Borodin,
Russian Research Center, Kurchatov Institute of Atomic Energy, Moscow Russia,
April 4-May 18, 1996, Nov 11-Dec. 12, 1996

L.Calvo-Barrio,
Dept. of Physics, Univ. of Barcelona, Spain, Feb.12-25, 1996

Prof. Dr. J.A. Davies,
Mc Master University, Hamilton, Canada, Sept. 21-24, 1996

Dr. A. A. Deshkovskaya,
Belorussian State Universität of Informatic and Electronics, Minsk, Belarus, Aug. 8 - Sept. 10, 1996

Dr. V. Eremin,
Yoffe-Physico-Technical Institute, St. Petersburg, Russia, Nov. 16 - Dec. 9, 1996

Dr. J. Eschenbaum,
Institut für Physikalische Chemie der Universität des Saarlandes, Saarbrücken, March 25-29, 1996

Prof. P. Fichtner,
Dept.of Metallurgy, Univ.of Porto Alegre, Brazil, March 10-April 4, 1996

B. Groß,
Institut für Physikalische Chemie der Universität des Saarlandes, Saarbrücken, Nov. 25-29, 1996

Dr.N.Hatzopoulos,
Dept.of Electronic and Electr.Eng., Univ.of Surrey, UK, Nov.1-Dec.18, 1996

H. Huber,
Ludwig-Maximilians-Universität München, Beschleunigerlabor, Garching, March 18-22,
Aug. 19 - 23, 1996

Dr.G.A.Kachurin,
Institute for Semiconductor Physics, Novosibirsk, Russia, May 5-June 15, 1996

Dr. J. Kaschny,
Dept.of Physics, Univ.of Porto Alegre, Brazil, March 15-Dec.31, 1996

Dr. D. V. Karpov,
Efremov Scientific Research Institute of Electrophysical Apparatus, St. Petersburg, Russia,
Feb. 12 - 22, 1996

M. Kokkoris,
University of Athens, Greece, July 15 - 20, 1996

Dr. J. Krynicki,
Institute of Nuclear Chemistry and Technology, Warsaw, Poland, June 10 -12, 1996, Sept. 19 - 21,
1996, Nov. 21 - 23, 1996

Dr. F.Machalett,
Dept. of Physics, Friedrich-Schiller-Univ. Jena, April 2-4, 1996

Prof. V. Magula,
Welding Research Institute, Bratislava, Slovak Republik, June 10 - 18, 1996

M. Marik,
Nuclear Research Institute Rez, CR, Oct. 14 - 18, 1996

Dr. K. Mazur, Institut of Electronic Materials Technology, Warsaw, April 15 - 19,
Sept. 23 - 28, 1996

I. G. Mrotschek,
Belarussian State University, Minsk, Belarus, April 4 - May 31, 1996

S. Mukherjee,
Institut for Plasma Research, Gandhinagar, India, Sept. 18 - Dec. 2, 1996

Prof. D.L. Nagy,
KFKI Budapest, Sept. 16 - 29, 1996

Dr. K. Nakamura,
University of Nagoya, Japan, March 1 - Aug. 31, 1996

S. Netcheva,
Inst. of Electronics, Bulg. Acad. of Science, Sofia, Bulgaria, Jan.31-Feb.14, 1996

Prof. K. Obara,
University of Tokyo, Japan, March 1 - Oct. 15, 1996

M. Palard,
CSNSM - IN2P3 Orsay, Paris, France, Oct. 28-Dec. 10, 1996

Dr. J. Pezoldt,
Inst. für Festkörperelektronik, Techn.Univ.Ilmenau, June 27-28, Sept.11-13, Nov.6-8, 1996

Prof. Dr. J. Piekoszewski,
Soltan Institute for Nuclear Studies, Swierk, Poland, Dec. 14-21, 1996

Dr. V. Prozesky,
National Accelerator Lab., Faure, RSA, Sept.15 - 20, 1996

M. Roth,
Institut für Physikalische Chemie der Universität des Saarlandes, Saarbrücken, March 25-29, 1996

J. Rozinek,
Nuclear Research Institute Rez, CR, Oct. 14 - 18, 1996

Dr. A. Ryazanov,
Russian Research Center - Kurchatov Institute of Atomic Energy, Moscow Russia, Nov 21-27, 1996

J. Sass,
Institut of Electronic Materials Technology, Warsaw, April 15 - 19, Sept. 23 - 28, 1996

Prof. J. Schelten,
Inst. für Ionentechnik, Forschungszentrum Jülich, Feb.8-9, 1996

Dr. M. Schreiner,
Akademie der Wissenschaften Wien, March 5 - 9, 1996

Prof. A. M. Tolopa,
Academy of Science, Sumy, Ukraina, April 1 - May 31, 1996

Prof. Y. V. Trushin,
A.F. Ioffe Physicotechnical Institute, St. Petersburg, Russia, Nov. 18 - Dec. 12, 1996

T.Tsvetkov,
Inst. of Electronics, Bulg. Acad. of Science, Sofia, Bulgaria, Jan.31-Feb.14, 1996

Prof. A.Turos,
Inst. for Technology of Electronic Materials,Warsaw, Poland, Feb. 27- March 6, Dec. 11 -14, 1996

Dr. I. E.Tyschenko,
Institute for Semiconductor Physics, Novosibirsk, Russia, Jan.1-Feb.29/Oct.3-Dec.31, 1996

Dr. P. Vladimirov,
Russian Research Center - Kurchatov Institute of Atomic Energy, Moscow, Russia,
Aug. 2 -Nov. 26, 1996

Dr. A. E. Volkov,
Russian Research Center - Kurchatov Institute of Atomic Energy, Moscow Russia,
Nov. 11-Dec. 12, 1996

Dr. S. Wachol,
Inst. of Nuclear Chemistry and Technology, Warsaw, Poland, June 10 -12, Sept. 19 - 21,
Nov. 21 - 23, 1996

Dr. X. Wang,
Academy of Science, Institute of Metallurgy, Shanghai, China, from Aug. 24, 1996

Dr. R.Yankov,
Technische Univ. Ilmenau and Bulg.Acad.of Sciences, Sofia, Feb.6-July 31, Sept.1-Dec.20, 1996

Dr. I. Zyganov,
TU Lipezk, Russia, Oct. 1995 - July 1996

Awards

Drummer, H., (Professor-Schwabe-Preis)
„Anwendung moderner Methoden der Ramanspektroskopie für die Charakterisierung von dünnen Feststoffschichten“ (Diplomarbeit)
im Rahmen des SMWK-Projektes „Haftfeste dünne Kohlenstoffschichten“ des Instituts für Ionenstrahlphysik und Materialforschung

Jentschel, M., Heinig, K.-H. Börner, H.-G., (Award: Best Poster Contribution)
Crystal-GRID investigation of atomic collision cascades in ionic compounds,
Int. Symp. Materials Science Application of Ion Beam Techniques, Seeheim, Sept 9-12, 1996

PhD Theses

Chudoba, T.,
Modifizierung mechanischer und korrosiver Oberflächeneigenschaften von Magnesium durch Ionenimplantation
TU Dresden, June 1996

Harz, M.,
Untersuchung Thermo-mechanischer Spannungen beim Anodischen Bonden von TEMPAX-Glas und Silizium,
TU Dresden, July 1996

Hempel, A.,
Untersuchung des Einflußes von Temperatur und Luftfeuchtigkeit auf die Mesostruktur von Zementstein mittels Neutronenkleinwinkelstreuung
TU Chemnitz, July 1996

Reiss, S.,
Theorie und Computersimulation der Ostwald-Reifung bei der Ionenstrahlsynthese,
TU Dresden, March 1996

Diploma Thesis

Beyer, V.,
Anisotropes selektives naßchemisches Ätzen von monokristallinen Siliziummembranen unter Verwendung MeV-implantierter Strukturen,
TU Chemnitz-Zwickau, June 1996

Meetings organized by the institute

3rd Workshop on Plasma Based Ion Implantation, Sept. 15 - 18, 1996, FZ Rossendorf
Chairman: Prof. W. Möller (FZ Rossendorf)
Local Organizers: R. Günzel, I. Heidel, E. Richter, E. Wieser

3rd User Seminar of DANFYSIK 1090 Implanters, 19-20 September 1996, FZ Rossendorf
Chairmen: W. Möller (FZ Rossendorf), B. Nielsen (Jyllinge/DK)
Local Organizer: A. Kolitsch

COST-G1 Workshop, Rossendorf, Germany, June 3 - 4, 1996
Chairman: C. Neelmeijer (FZ Rossendorf),
Local Organizers: M. Mäder, I. Heidel, C. Neelmeijer

Patents

Köhler, B., Teichert, J., Bischoff, L.,
Vorrichtung und Verfahren zur gezielten Probenbearbeitung, vorzugsweise von Halbleiterbauelementen, mittels einer Ionenfeinstrahlanlage,
Deutsches Patentamt, Aktenzeichen P 196 06 478.3, eingereicht am 21.2.1996

Lauer, V., Wondrack, W., Pensl, G., Dalibor, T., Skorupa, W., Wirth, H.
Halbleiterbauelement mit durch Ionenimplantation eingebrachten Fremdatomen und Verfahren zu dessen Herstellung,
Deutsches Patentamt, Aktenzeichen P 196 33 183.8, eingereicht am 17.8.1996

Research Center Rossendorf

Institute of Ion Beam Physics and Materials Research (FWI)

Postfach 510119
D-01314 Dresden

Tel. 0351-260-2245
Fax 0351-260-3285

DIRECTOR: **Prof. Dr. W. Möller** 2245
DEPUTEE: **Prof. Dr. E. Wieser** 3096

NEW MATERIALS (FWIM)
Dr. W. Skorupa 3612
- Semiconductors
- Optical Applications
- Defect Engineering
- Submicron Ion Beam

INDUSTRIAL CONTACTS (FWIK)
Dr. J. von Borany 3378

ION IMPLANTATION (FWII)
Dr. E. Richter 3326
- Surface Properties
- Ion Beam Assisted Deposition
- Plasma Immersion Implantation
- Operation of Implanters

MEV ACCELERATORS (FWIB)
Dr. M. Friedrich 3284
- Operation of MeV Accelerators
- Accelerator Mass Spectrometry

ION BEAM ANALYSIS (FWIA)
Dr. R. Grötzschel 2802
- High-Energy Ion Beam Analysis
- Elementary Processes of Ion-Surface-Interaction

STRUCTURAL DIAGNOSTICS
Dr. W. Matz 3122 (FWIS)
- Transmission Electron Microscopy
- X-ray Diagnostics
- Electron Spectroscopies
- Rossendorf Beamline at ESRF

THEORY (FWIT)
Dr. M. Posselt 3279
- Computer Simulation
- Reaction-Diffusion-Calculations
- Defects
- Precipitation

PREPARATION (FWIP)
Dr. B. Schmidt 2726
- PVD Coatings
- Reactive Ion Etching
- Wet Chemical Processing
- Annealing

Experimental Equipment

1. Accelerators, Ion Implanters and Ion-Assisted-Deposition

o	van de Graaf accelerator	*1,8 MeV*
o	Tandem accelerator	*5 MV, Russian*
o	Tandetron accelerator	*3 MV, HIGH VOLTAGE, NL*
o	Ion implanter	*80 kV (Own construction)*
o	Ion implanter	*180 kV, medium current, SCANIBAL, FL*
o	High current ion implanter	*200 kV, high current, DANFYSIK, DK*
o	High energy ion implanter	*500 kV, HIGH VOLTAGE, NL*
o	Plasmaimmersion implantation	*5-60 keV*
o	Fine focused ion beam	*50 keV, 100 nm, 10 A/cm*^{2}
o	Ion beam assisted deposition	
o	Plasma enhanced chemical vapour deposition	

2. Particle and Photon Based Analytical Techniques

o	RBS	Rutherford backscattering	*p,*α*: 1-6 MeV*
o	ERDA	Elastic recoil detection analysis	*35 MeV,* ^{35}Cl
o	PIXE	Proton induced X-ray analysis	*+ PIGE-option, external beam*
o		Nuclear microprobe	*MeV, > 2* μm
o	NRA	Nuclear reaction analysis	$^{1}H(^{15}N,\alpha\gamma)^{12}C$
o	TEM	Transmission electron microscope	*300 kV, PHILIPS, NL*
o	STM	Scanning tunneling microscope	*+ AFM-option, DME, DK*
o	AES	Auger electron spectroscopy	*+ XPS-option, FISIONS, GB*
o		Mössbauer spectroscopy	
o	XRD	X-ray diffraction	
o		Spectroscopic ellipsometry	*250-1700 nm, WOOLLAM, USA*
o	FTIR	Fourier transform infrared spectrometry	*600-7000 cm*$^{-1}$*, NICOLET, USA*

3. Other Analytical Techniques

o	Surface profilometer	*Dektak, VEECO, USA*
o	Micro indenter	*SHIMATSU, J*
o	Scratch tester	*SHIMATSU, J*
o	Spreading resistance measuring station	*SENTECH, D*
o	Hall-effect equipment	*BIO-RAD, GB*
o	I-U and C-U- analyzer	*KEITHLEY, USA*

4. Preparation Techniques

o	Wet chemical etching and cleaning	*incl. anisotropic selective KOH-etching*
o	Photoliothographic patterning	*5* μm*-level*
o	Thermal treatment	*RT - 2000°C* *Furnace, Flash lamp unit, Rapid thermal annealing, RF-Heating (Vacuum)*
o	Physical deposition	*Sputtering DC / RF, Evaporation*
o	Dry etching	*Plasma and RIE mode*
o	Bonding techniques	*Anodic, Si-Si and WireBonding*

List of Personnel

Director: Prof. W. Möller

Deputy Director: Prof. E. Wieser

Scientific Staff: *Permanent:*

Dr. M. Betzl
Dr. L. Bischoff
Dr. J. von Borany
Dr. W. Bürger
Dr. F. Eichhorn
Dr. M. Friedrich
Dr. W. Fukarek
Dr. D. Grambole
Dr. R. Grötzschel
Dr. R. Günzel
Dr. V. Heera
Dr. K.-H. Heinig
Dr. H.-U. Jäger
Dr. A. Kolitsch
Dr. R. Kögler
Dr. U. Kreißig
Dr. W. Matz
Dr. A. Mücklich
Dr. C. Neelmeijer
Dr. D. Panknin
Dr. M.T. Pham
Dr. M. Posselt
Dr. F. Prokert
Dr. H. Reuther
Dr. E. Richter
Dr. B. Schmidt
Dr. J. Schöneich
Dr. H. Seifarth
Dr. W. Skorupa
Dr. J. Teichert
Dr. H. Tyrroff
Dr. M. Voelskow

Post Docs:

Dr. J. Brutscher
Dr. N. Schell
Dr. M. Weiler
Dr. H. Weishart

Projects:

T. Gehring
M. Harz
Dr. J. Hüller
Dr. O. Kruse
M. Mäder
P. Schneider
Dr. M. Seidel
Dr. K. Walther

PhD Students:

K. Albe
F. Brenscheidt
M. Dobler
S. Grigull
S. Hausmann
A. Hempel
M. Jentschel
W. Jiang
S. Mändl
D. Möller
S. Parascandola
M.F. Plass
L. Rebohle
Br. Schmidt
M. Strobel
G. Sun
H. Wirth

Diploma Students:

V. Beyer
T. Schwieger

Technical Staff:
Permanent:

J. Altmann
R. Aniol
G. Anwand
I. Beatus
W. Boede
K.-D. Butter
W. Gäßner
B. Gebauer
H.-J. Grahl
P. Hartmann
F. Herrmann
G. Hofmann
M. Iseke
S. Klare
R. Kliemann
L. Kumpf
A. Kunz
G. Küster
D. Maul
M. Mißbach
I. Morawitz
K. Müller
F. Nötzold
W. Probst
E. Quaritsch
P. Reichel
B. Richter
M. Roch
E. Rost
B. Scheumann
H. Schluttig
E. Schmidt
G. Schnabel
J. Schneider
A. Scholz
C. Schulenberg
K. Sommerfeld
U. Strauch
K. Thiemig
S. Turuc
A. Vetter
A. Weise
I. Winkler

Projects:

S. Scharfe
A. Schneider
H. Seifert
G. Winkler